National Library of Canada
Bibliothèque nationale du Canada

Canadian Theses Service
Service des thèses canadiennes

Ottawa, Canada
K1A 0N4

NOTICE

The quality of this microform is heavily dependent upon the quality of the original thesis submitted for microfilming. Every effort has been made to ensure the highest quality of reproduction possible.

If pages are missing, contact the university which granted the degree.

Some pages may have indistinct print especially if the original pages were typed with a poor typewriter ribbon or if the university sent us an inferior photocopy.

Reproduction in full or in part of this microform is governed by the Canadian Copyright Act, R.S.C. 1970, c. C-30, and subsequent amendments.

AVIS

La qualité de cette microforme dépend grandement de la qualité de la thèse soumise au microfilmage. Nous avons tout fait pour assurer une qualité supérieure de reproduction.

S'il manque des pages, veuillez communiquer avec l'université qui a conféré le grade.

La qualité d'impression de certaines pages peut laisser à désirer, surtout si les pages originales ont été dactylographiées à l'aide d'un ruban usé ou si l'université nous a fait parvenir une photocopie de qualité inférieure.

La reproduction, même partielle, de cette microforme est soumise à la Loi canadienne sur le droit d'auteur, SRC 1970, c. C-30, et ses amendements subséquents.

NL-339 (r. 88/04) c

Canada

Thermal Properties of Dianin's Compound and Its Adducts.

by

Marek Zakrzewski

Submitted in partial fulfillment of the requirements
for the degree of Doctor of Philosophy

at

Dalhousie University.
Halifax, Nova Scotia
October, 1990

© Copyright by Marek Zakrzewski, 1990

National Library of Canada
Bibliothèque nationale du Canada

Canadian Theses Service
Service des thèses canadiennes

Ottawa, Canada
K1A 0N4

The author has granted an irrevocable non-exclusive licence allowing the National Library of Canada to reproduce, loan, distribute or sell copies of his/her thesis by any means and in any form or format, making this thesis available to interested persons.

L'auteur a accordé une licence irrévocable et non exclusive permettant à la Bibliothèque nationale du Canada de reproduire, prêter, distribuer ou vendre des copies de sa thèse de quelque manière et sous quelque forme que ce soit pour mettre des exemplaires de cette thèse à la disposition des personnes intéressées.

The author retains ownership of the copyright in his/her thesis. Neither the thesis nor substantial extracts from it may be printed or otherwise reproduced without his/her permission.

L'auteur conserve la propriété du droit d'auteur qui protège sa thèse. Ni la thèse ni des extraits substantiels de celle-ci ne doivent être imprimés ou autrement reproduits sans son autorisation.

ISBN 0-315-64551-2

Canada

Moim Rodzicom

"It seemed to me ridiculous to worry about whether you spelled something wrong or not, because English spelling is just a human convention - it has nothing to do with anything *real*, anything from nature. Any word can be spelled just as well a different way."

Richard P. Feynman

Table of Contents

Table of Contents.....v

Figure Captions.....viii

List of Tables.....xiv

Abstract.....xvi

Symbols.....xvii

Acknowledgements.....xxii

Chapter 1: General Introduction.....1

Chapter 2: Introduction to Thermal Conductivity Theory.....5

Chapter 3: Dianin's Compound: Background.....16

Chapter 4: Dianin's Compound: Sample Preparation.....30

4.1 Preparation of Ethanol Adduct of Dianin's Compound.....30

4.2 Preparation of Unsolvated Dianin's Compound.....33

4.3 Preparation of Carbon Tetrachloride Adduct of Dianin's Compound.....35

Chapter 5: Heat Capacity Measurements.....36

5.1 Introduction (Theory).....36

5.2 Heat Capacity Measurements by Adiabatic Calorimetry.....39

5.3 Heat Capacity Measurement Procedure.....50

5.4 Heat Capacity Results.....52

5.5 Heat Capacity: Guests in The Cage Compared with Their Bulk Properties.....59

5.6 Contribution to The Proton Disorder.....66

Chapter 6: Thermal Expansion of Dianin's Adducts.....70

6.1 Introduction and Theory.....70

6.2 Results and Discussion.....74

Chapter 7: Brillouin Scattering.....91

7.1 Introduction and Theory.....91

7.2 Determination of Elastic Constants.....97

7.3 Sample Preparation.....99

7.4 Apparatus..... 102

7.5 Results and Discussion.....105

Chapter 8: Derived Thermodynamic Properties.....122

8.1. Theory.....122

8.1.a. Heat Capacity.....122

8.1.b. Effective Characteristic Temperatures.....123

8.1.c. Grüneisen Parameter.....126

8.2 Results and Discussion.....129

8.2.a. Heat capacity.....129

8.2.b. Effective Characteristic Temperatures.....136

8.2.c. Grüneisen Parameter.....144

Chapter 9: Thermal Conductivity.....151

9.1 Theory.....151

9.2 Thermal conductivity apparatus.....155

9.3 Crystal Preparation.....160

9.4 The Measurement Procedure.....162

9.5 Results.....163

9.6 Discussion.....170

9.6.a. Mean Free Path.....170

9.6.b. Universal Thermal Conductivity.....170

9.6.c. Einstein model.....176

9.6.d. Minimum Thermal Conductivity.....179

9.6.e. Guest-host Resonance Scattering Models.....180

Chapter 10: Summary.....194

References.....195

Figure Captions

		Page
Figure 2.1	Two-dimensional representation of three-phonon processes.	8
Figure 2.2	Thermal conductivity of a non-metallic crystal.	11
Figure 2.3	Thermal conductivity of crystalline quartz.	14
Figure 3.1	A schematic view of the structure of the Dianin host lattice.	17
Figure 3.2	The shape and size of the largest figure of revolution which can fit into the cage of Dianin's compound.	19
Figure 3.3	The orientation of the two ethanol molecules in the Dianin cage.	22
Figure 3.4	The ethanol molecule in Dianin's compound surrounded by the van der Waals radius of the cage atoms.	24
Figure 3.5	The crystal structure of the CCl_4 adduct of Dianin's compound.	27
Figure 5.1	Schematic of the adiabatic calorimeter.	42
Figure 5.2	The sample vessel and heater-thermometer assembly of the adiabatic calorimeter vessel.	45

Figure 5.3	Schematic of the computer system for the adiabatic calorimeter.	48
Figure 5.4	The molar heat capacity of a CCl_4 molecule in the CCl_4 adduct of Dianin's compound.	61
Figure 5.5	The molar heat capacity of an ethanol molecule in the ethanol adduct of Dianin's compound.	64
Figure 5.6	(a) The hexagons formed by the phenolic oxygens in Dianin's compound, in the a b plane. b) The positional potential of the phenolic hydrogens in Dianin's compound.	68
Figure 6.1	a) Linear monatomic chain at T=0 with lattice spacing a_0. b) Chain at temperature T with lattice spacing a(T). c) Interaction energy of two neighbouring atoms at positions r_ℓ and $r_{\ell-1}$.	72
Figure 6.2	The lattice parameter of the empty, ethanol and carbon tetrachloride adducts of Dianin's compound along the **a**-axis as a function of temperature.	77
Figure 6.3	The lattice parameter of the empty, ethanol and carbon tetrachloride adducts of Dianin's compound along the **c**-axis as a function of temperature.	79

Figure 6.4	The unit cell volume of the empty, ethanol and carbon tetrachloride adducts of Dianin's compound as a function of temperature.	81
Figure 6.5	Linear thermal expansion coefficients for unsolvated Dianin's compound and its ethanol and carbon tetrachloride adducts as a function of temperature in the a-direction.	84
Figure 6.6	Volume thermal expansion coefficients for Dianin's compound and its carbon tetrachloride and ethanol adducts as a function of temperature.	88
Figure 7.1	Brillouin scattering of a photon with emission (Stokes process) or absorption (Anti-Stokes process) of an acoustic phonon.	94
Figure 7.2	The hexagonal unit cell of Dianin's compound.	100
Figure 7.3	Block diagram of the experimental arrangement for Brillouin scattering.	103
Figure 7.4	A representative two-hour Brillouin scattering spectrum for the single crystal of the ethanol adduct of Dianin's compound.	106

Figure 7.5	The sample orientations for the 22 different phonon directions investigated by Brillouin scatteri in the single crystal of ethanol adduct of Dianin's compound.	108
Figure 8.1	The heat capacity at constant pressure and at constant volume for unsolvated Dianin's compound.	130
Figure 8.2	The heat capacity at constant pressure and at constant volume for the ethanol adduct of Dianin's compound.	132
Figure 8.3	The heat capacity at constant pressure and at constant volume for the carbon tetrachloride adduct of Dianin's compound.	134
Figure 8.4	The Debye temperatures for various numbers of subgroups (n) in Dianin's compound molecule as a function of temperature derived from the heat capacity of unsolvated Dianin's compound.	139

Figure 8.5	The Debye temperatures for various numbers of subgroups (n) in Dianin's compound molecule as a function of temperature derived from the heat capacity of ethanol adduct of Dianin's compound.	141
Figure 8.6	The results of the calculation of γ_a, γ_c γ and for the ethanol adduct of Dianin's compound.	145
Figure 8.7	The overall Grüneisen parameter of the unsolvated and ethanol and CCl_4 clathrates of Dianin's compound.	147
Figure 9.1	Thermal conductivity apparatus.	156
Figure 9.2	The thermal conductivity of single crystals of Dianin's compound.	164
Figure 9.3	The phonon mean free path in unsolvated Dianin's compound and its ethanol adduct.	171
Figure 9.4	Scaled thermal conductivities of THF clathrate hydrate and six amorphous solids in comparison with unsolvated Dianin's compound and its ethanol adduct.	174

Figure 9.5	The thermal conductivity of unsolvated Dianin's compound. comparison of experiment and the calculations for the Einstein and the Slack-Debye models.	177
Figure 9.6	The single resonance model fit to experimental data of thermal conductivity of single crystal of unsolvated Dianin's compound.	185
Figure 9.7	The two resonance model fit to experimental data of thermal conductivity of single crystal of ethanol adduct of Dianin's and unsolvated compound.	188
Figure 9.8	The thermal conductivity of single crystals of Dianin adducts: unsolvated , ethanol adduct, and carbon tetrachlorid.	191

List of Tables

Table 4.1. The Results of Chemical Analyses for Dianin's Compound, its Ethanol Adduct and its Carbon Tetrachloride Adduct. 32

Table 5.1. The experimental heat capacities of unsolvated Dianin's compound. 53

Table 5.2. The experimental heat capacities of the ethanol adduct of Dianin's compound. 55

Table 5.3. The experimental heat capacities of the CCl_4 adduct of Dianin's compound. 57

Table 6.1. The thermal expansion of the unsolvated Dianin's compound and its ethanol and carbon tetrachloride adducts along the **c**-axis at selected temperatures. 86

Table 7.1. The Brillouin scattering data for single crystals of the ethanol adduct of Dianin's compound at T=293 K. 115

Table 7.2 The (symmetrical) elastic stiffness tensor for the ethanol adduct of Dianin's compound at 20°C, as determined by Brillouin spectroscopy. 119

Table 7.3 The (symmetrical) elastic compliance tensor for the ethanol adduct of Dianin's compound at 20°C, as determined by Brillouin spectroscopy. 120

Table 9.1 The measured thermal conductivity κ of Dianin's compound. 166

Table 9.2 The measured thermal conductivity κ of ethanol adduct of Dianin compound. 168

Abstract

Clathrates are multicomponent materials in which one type of molecule forms a host lattice in which the guest molecules reside. In general, investigations of clathrates afford the opportunity to compare various properties of diluted guest molecules with their properties in their pure (bulk) form.

The origin of the unusual thermal conductivities of clathrate hydrates (which cannot exist without a guest) has been attributed recently to the interactions of low-frequency optic modes of the guest molecules with the lattice acoustic modes.

4-*p*-Hydroxyphenyl-2,2,4-trimethylchroman (Dianin's compound), forms many different clathrates by crystallization from appropriate solvent/guests. It is an unusual clathrate in that it also exists in its unsolvated form. The purpose of this work was to investigate the effect of the presence and type of guest on the thermal conductivity of Dianin's clathrate.

Unsolvated Dianin's compound and its ethanol and carbon tetrachloride adducts have been investigated.

The following properties have been measured for Dianin's compound and its ethanol and carbon tetrachloride adducts: heat capacity (by adiabatic calorimetry); lattice parameters (by variable-temperature x-ray powder diffraction); elastic constants (ethanol adduct only; by Brillouin spectroscopy); velocity of sound (unsolvated Dianin's compound and its ethanol adduct; by the ultrasonic pulse technique); thermal conductivity (unsolvated Dianin's compound and its ethanol adduct; by the steady state method). The thermal expansion and Grüneisen parameters derived from these measurements indicate the importance of the guest species in the anharmonicity of the interactions. The Debye temperatures for unsolvated Dianin's compound and its ethanol adduct were determined. Three different models for thermal conductivity are discussed. The results favour the guest-host resonance model but show the (unexpected) result that the unsolvated lattice has a similar (but less pronounced) resistance to heat flow. The thermal conductivity for the CCl_4 adduct of Dianin's compound was calculated.

Symbols

κ	thermal conductivity
C	heat capacity per unit volume
v	average particle (heat carrier) velocity
ℓ	mean free path of a particle
E	internal energy
n	a positive integer or zero
$\hbar$	Planck's constant divided by 2π
ω	angular frequency
q	wave vector
G	either a reciprocal lattice vector or zero
C_x	heat capacity measured under the constrain x
C_p	heat capacity measured under the constant pressure
C_v	heat capacity measured under the constant volume
dq	total heat added to the system
dT	differential in temperature
α_v	coefficient of volume expansion
V	molar volume
T	temperature
∂V	volume differential
∂T	temperature differential
χ^T	isothermal compressibility

∂P	pressure differential
dE	differential in the internal energy
dw	differential in work done by the system
k_B	Boltzmann constant
N	number of oscillators
ω_D	Debye frequency
a	lattice constant
v_g	phonon group velocity
$D(\omega)$	density of modes
θ_D	Debye temperature
U	voltage
q	Joule heat
R	heater resistance
t	duration of the heat
T_1	initial temperature
T_2	final temperature
ΔT	temperature change
T_{avg}	arithmetic average of T_1 and T_2
u_l	a displacement of an atom l
f, g, h	force constants
B	bulk modulus
γ	Grüneisen parameter
σ_{kl}	homogeneous stress
ϵ_{ij}	homogeneous strain
s_{ijkl}	crystal compliances

c_{ijkl}	stiffness constants
ρ	density
x_i	Cartesian coordinates
Γ_{il}	matrix element
q_k	direction cosine
δ_{ij}	the Kronecker delta
ω'	the photon frequency
Ω	frequency of created or destroyed phonon
k'	photon momentum
K	momentum of created or destroyed phonon
$\Delta\nu$	Brillouin shifts
ν_0	frequency of the laser radiation
c	velocity of light in vacuum
n_i	refractive index of the incident light
n_s	refractive index of the scattered light
θ	scattering angle
A	anisotropy factor
N_o	Avogadro's number
p	number of "atoms" in the molecule
M	molecular weight
v_m	average sound velocity
v_T	transverse velocity
v_L	longitudinal velocity
N	number of atoms per unit cell
γ_a	Grüneisen parameter parallel to the a-axis

γ_c	Grüneisen parameter parallel to the c-axis
χ_a^T	isothermal compressibility along the a-axis
χ_c^T	isothermal compressibility along the c-axis
h	total heat current
P(q)	number of phonons which form a wave packet
∇	the Nabla operator
P^o	the equilibrium value of the number of phonons which form a wave packet
τ	relaxation time
τ_{total}	total relaxation time
$\dot{q}$	power passed through a single crystal
A	cross-sectional area
n	density number
θ_E	Einstein temperature
τ_E	one half of a period of oscillation
l	interatomic spacing
λ	wavelength
τ_s	relaxation time related to a single resonance
G_0	concentration of the resonant scatterer
D	coefficient related to the strength of the acoustic-optic coupling
ω_0	optical vibrational frequency involved in resonant scattering
τ_u	relaxation time related to Umklapp process
B_u, α	empirical constants

τ_B	relaxation time for the boundary scattering
d	diameter of the cylinder
F	constant related to the nature of the scatterer
τ_R	relaxation time related to Rayleigh scattering

Acknowledgements

I would like to thank my supervisor, Prof. M. A. White for the guidance and assistance.

I would like to thank Prof. H. Kiefte and Dr. B. Mróz for their cooperation with respect to Brillouin scattering experiment performed at Memorial University of Newfoundland.

I would also like to thank Prof. T. S. Cameron and Dr. A. Linden for their help in single crystal x-ray work and crystallography related matters.

I would like to thank Prof. C. Warren for his help in computation and arranging the use of computers.

I would like to thank Prof. M. Jericho for his assistance in performing ultrasonic measurements.

I also, thank Prof. R. Wasylishen and Prof. R. Boyd for helpful discussions.

I thank B. Millier for technical assistance and company on the occasional skiing trips.

I would like to thank my friend, Dr. M. van Oort for help during my first year in Canada.

I would like to thank my fellow graduate students for their help during the time this work was done, especially: B. Borecka, M. MacIntosh, P. Hajigeorgiou, K. McMahon, J. Hilborn, N. Cann, G. Bednarz, B. Power, A. Perrot.

Finally, I would like to thank my girlfriend, Ewa, for her support and encouragement.

Chapter 1: General Introduction

Clathrates are multicomponent materials in which one type of molecule forms a host lattice in which the guest molecules reside. Clathrates are a subset of the larger class of materials called inclusion compounds; the distinguishing feature of clathrates is the cage structure of the host lattice. Indeed the word clathrate has its origins in the Latin *clathrus*, indicating the protection of the guest species by the grating provided by the host lattice.

Some inclusion compounds are of great importance to industry. For example, cyclodextrins are known to influence the rate of various reactions[1] including enzymatic reactions,[2,3] and cyclodextrin inclusion can affect the bioavailability (rate and extent of absorbtion) of drugs since this is controlled by the dissolution rate of the drug in the gastrointestinal fluid and the transfer of the dissolved compound across the absorption barrier (a combination of stagnant water layer, mucus and cellular membranes) to the blood.[4] One of the important characteristics of cyclodextrins is their formation of inclusion complexes with a large variety of drug molecules both in solution and in the solid state.[5] It is reported that they are particularly useful in the improvement of the

chemical lability and slow dissolution characteristics of some prostaglandin (long-chain fatty acids) through complex formation.[6,7,8] They were also found[9,10,11] to increase bioavailability of several drugs that are not very water soluble. Finally, cyclodextrins may be used to separate useful compounds in complicated samples such as coal tar and petroleum oil.[12]

The clathrate hydrates - inclusion compounds with an H_2O host lattice and molecular guest species - have an unusually long, about 180 years, scientific history.[13] They were commonly named the gas hydrates. The chlorine hydrate was discovered first in 1811 by Davy.[14] Its approximate composition was determined by Faraday[15] in 1823. The others followed later. In 1849 Wöhler[16] made the first quinol clathrate with hydrogen sulphide as a guest. However he and later Clemn[17] could not give a structural explanation. It took until 1886 for Mylius[18] to determine that there was no ordinary chemical combination between quinol and the other components. More than a half of century later the crystal structure was determined[19] by Palin and Powell.

The determination of two crystal structures for clathrate hydrates followed shortly.[20,21] In addition to research on their crystal structure these materials have been studied for their thermodynamic and elastic properties,[22,23,24,25,26,27,28,29,30,31,32,33] the motion of included molecules, and technological interest, (in natural gas pipe

lines, marine sediments, etc.[13]) These compounds also attract attention as an energy resource because vast deposits of the natural gas (CH_4, C_2H_6, etc.) hydrates were found recently to exist under the ocean bed and in the permafrost region.[34,35,36]

In general, investigations of clathrates afford the opportunity to compare various properties of diluted guest molecules with their properties in their pure (bulk) form. The other opportunity is to investigate guest-host interactions. One test of the proposed guest-host interaction model for thermal conductivity[29] (*vide infra*) would be the measurement of physical properties as a function of guest concentration but, alas, each clathrate hydrate is stable only for a narrow concentration range and removal of the guest collapses the lattice to the ice structure appropriate to the pressure-temperature conditions.

Another test of this model could be the measurement of other physical properties that indicate the degree of interaction anharmonicity in clathrate hydrates. One such measurement is thermal expansion. Again, since the "empty" clathrate hydrate is not stable, a true comparison of experimental results is not possible.

The origin of the unusual[37,38] thermal conductivities of clathrate hydrates has been attributed recently[29] to the

interactions of low-frequency optic modes of the guest molecules with the lattice acoustic modes. It has been proposed[29] that these guest-host interactions provide a further resistance to heat flow and therefore are responsible for the greatly reduced thermal conduction and opposite temperature dependence in clathrate hydrates, in comparison with ice.[22,23,27,28,29,37,39,40] Of course, such phonon-phonon scattering is a manifestation of anharmonic interactions since a perfectly harmonic crystal would have no phonon-phonon collision mechanism, and therefore infinite thermal conductivity.

Another appropriate test of the guest-host interaction theory is the extension of experimental studies to other clathrates. To date, only one such thermal conductivity study has been reported, the urea/hexadecane system,[41] showing again relatively low thermal conductivity and a temperature dependence intermediate between that of ice and clathrate hydrates. However, again no comparable experimental data can exist for the empty host lattice, due to its instability.

All of the above suggests that it would be highly desirable to examine the thermal conductivity of a clathrate which can exist in both its "occupied" and "empty" form.

Chapter 2: Introduction to Thermal Conductivity Theory

From the kinetic theory of gases Debye derived[42] the following expression for thermal conductivity:

$$\kappa = C\, v\, \ell/3 \qquad (2.1)$$

where C is the heat capacity per unit volume, v is the average particle (heat carrier), velocity and ℓ is the mean free path of the particle.

Electrons can play the role of heat carriers in metallic solids, but it is somewhat more difficult to identify the heat carriers in non-metallic crystals. The energy in a lattice vibration or elastic wave is quantized and the quantum energy in an elastic wave is called a <u>phonon</u>.[43] Thermal vibrations in a crystal lattice are thermally-excited phonons and they the play role of the heat carriers in metals. Using a simple harmonic oscillator model, it is found that the energy of an elastic mode of angular frequency ω is given by:

$$E = (n+1/2)\hbar\omega \qquad (2.2)$$

where $\hbar\omega/2$ is the zero point energy, n is a positive integer or zero, and $\hbar$ is Planck's constant divided by 2π.

Furthermore, phonons interact with other particles and fields as if they had momentum $\hbar q$, where q is their wave vector (2π/wavelength). Taking into account anharmonicity in the potential energy of a displaced atom produces results describing three-phonon interactions (cubic term with respect to displacement in the equation of motion) and four-phonon interactions (quartic term). It is sufficient to use the squared term to describe vibrational energy and heat capacity, but the cubic term is required to describe heat conductivity (with the exception of very high temperatures).[43]

Two-phonon interactions may occur if two conditions are fulfilled:

$$\omega_1+\omega_2=\omega_3 \qquad (2.3)$$

where ω_1, ω_2, ω_3 are phonon frequencies associated with wavevectors q_1, q_2 and q_3 respectively, and:

$$q_1+q_2 = q_3+G \qquad (2.4)$$

where G is either a reciprocal lattice vector or zero. Equation (2.3) represents the energy conservation in a three-phonon process and equation (2.4) is a pseudomomentum conservation for G=0. An interaction for which G=0 is called a Normal (N) process, and the interaction for which G is

non-zero is called an Umklapp (U) process. The difference between N- and U-processes is illustrated in Figure 2.1. This shows a two-dimensional interpretation of these processes in the first Brillouin zone in a square two-dimensional lattice. Since the thermal energy is carried in the direction of the phonon group velocity, in N-processes the direction of the energy flow carried by mode q_3 is similar to the direction of flow carried by modes q_1 and q_2 and there is no thermal resistance. In U-processes the thermal energy is transported in a quite different direction, so the U-processes are directly responsible for thermal resistance. There are some cases however when scattering rates may be frequency-dependent and the N-processes may transfer energy from a mode which would be little-scattered to another more easily scattered mode, indirectly causing thermal resistivity. Therefore the role of N-processes cannot be ignored in thermal conduction.

At normal and high temperatures ℓ, the phonon mean free path, is limited by interactions among the phonons themselves, and at sufficiently high temperatures ℓ is inversely proportional to T.[44] As the temperature decreases, interactions among the phonons become rapidly less effective in restricting ℓ, and ℓ thus increases more rapidly than T^{-1}. At low temperatures ℓ may reach several millimetres and be comparable with the dimensions of samples investigated. It eventually reaches a constant value as the

Figure 2.1 Two-dimensional representation of three-phonon processes: a) resultant q_3 falls within the Brillouin zone (N process); b) resultant q'_3 falls outside the Brillouin zone so it is shifted by $2\pi/a$ vector to give q_3 (U process).[44]

NORMAL AND UMKLAPP PROCESSES

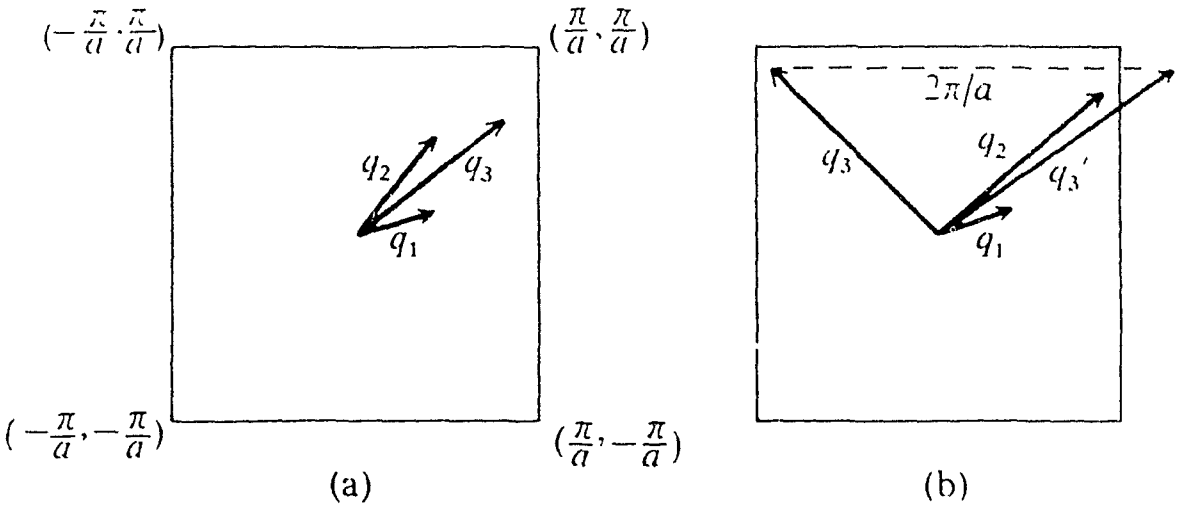

Figure 2.1

temperature is lowered. Considering the temperature dependence of the heat capacity, C, after Debye,[42,45] one can say that at temperatures which are high enough for $\ell \propto T^{-1}$, C is nearly constant. Regarding the mean velocity as independent of temperature makes $\kappa \propto T^{-1}$. When the temperature becomes low enough for the mean free path to become constant, the temperature dependence of the thermal conductivity follows the low-temperature T^3 behaviour of the heat capacity. A typical thermal conductivity curve for a non-metallic crystal is shown in Figure 2.2.

There is a class of solids in which there is no long-range order in the structure. Glasses belong to this category. The thermal conductivity and heat capacity for these materials differ from corresponding quantities for crystals. In an amorphous solid the mean free path is limited to the dimension of the structural units. At high temperatures this causes the thermal conductivity to follow the heat capacity and decrease with decreasing temperature.[44] There is not much difference between the thermal conductivity of a glass and a crystal at very high temperatures since the phonon mean free path for crystals is also limited to the order of the lattice constant. The difference occurs at lower temperatures where the thermal

Figure 2.2 Thermal conductivity of a non-metallic crystal. The dominant phonon scattering mechanisms are indicated along the temperature axis. The upper curve is for a crystal of larger diameter than the lower curve.[44]

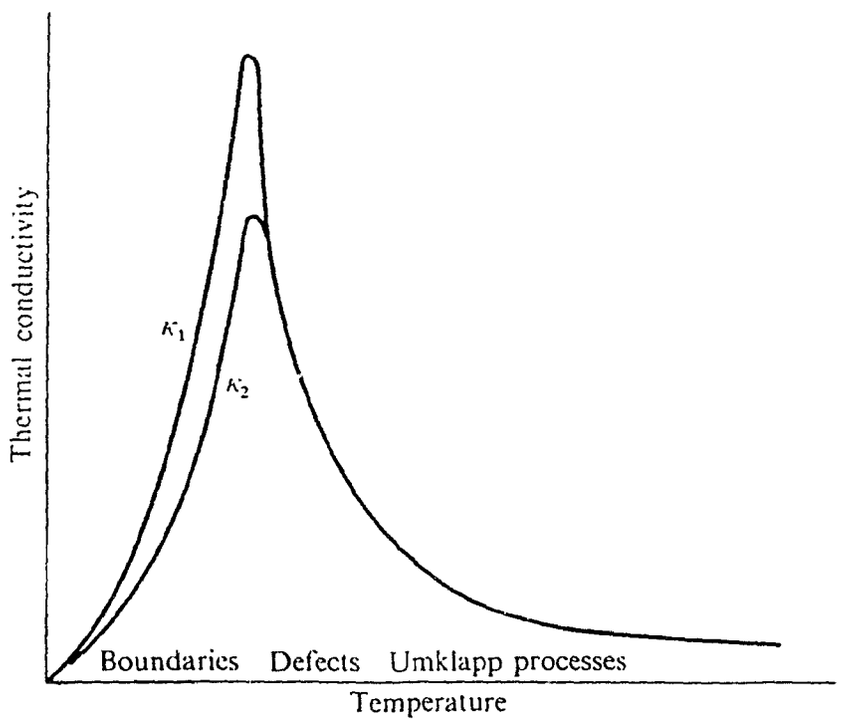
Thermal conductivity
κ_1
κ_2
Boundaries
Defects
Umklapp processes
Temperature

Figure 2.2

conductivity reaches a maximum for crystals, but not for glasses. The difference is illustrated in Figure 2.3.

Orientational disorder in a molecular solid should affect the thermal conductivity by limiting ℓ.[46] Some substances exhibiting this effect have been studied[47,48,49,50] and it was found that the thermal resistivity increased significantly due to order-disorder phase transitions.

The measured thermal conductivities of clathrate hydrates resemble those of glasses[29,37,38] despite the fact that clathrates exhibit long-range structural order. It would be very interesting to see if the thermal conductivity of an "empty" clathrate behaves more like a crystal or glassy material.

Figure 2.3 Thermal conductivity of crystalline quartz parallel to the c-axis (curve A) and of vitreous (glassy) silica (curve B).[44]

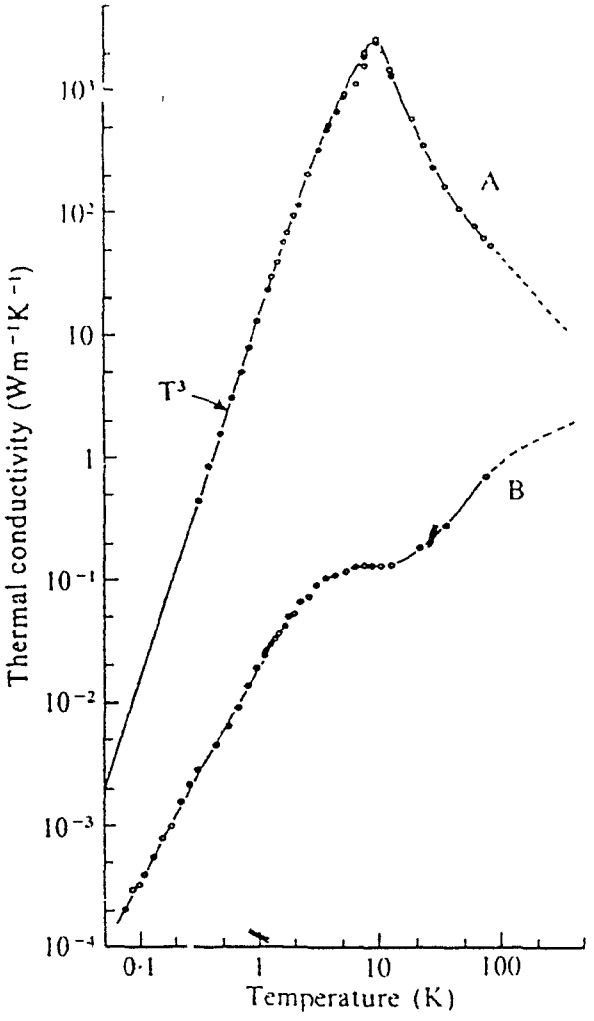
Thermal conductivity (Wm⁻¹K⁻¹)
10³
10²
10
1
10⁻¹
10⁻²
10⁻³
10⁻⁴
0·1
1
10
100
Temperature (K)
A
B
T³

Figure 2.3

Chapter 3: Dianin's Compound: Background

4-*p*-Hydroxyphenyl-2,2,4-trimethylchroman, **1**, was first reported[51] in 1914, and is commonly called after Dianin, its discoverer. Dianin's compound forms many different clathrates by crystallization from appropriate solvent/guests.[52,53] The parent compound and its clathrates all appear to crystallize in the space group $R\bar{3}$.[54,55]

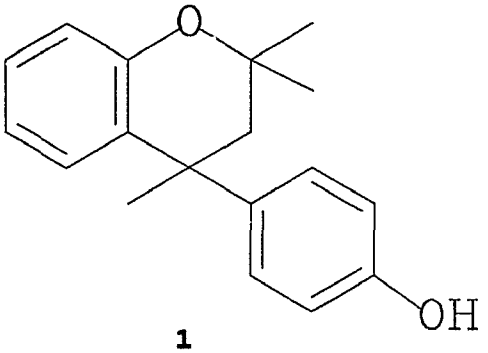

1

The general structure of the host lattice consists of hexamers of **1**, linked by a network of hydrogen bonds involving the phenolic hydroxy groups, as shown in Figure 3.1. Monomeric units of the hexamers alternately point up and down along the **c**-axis, and the binding force between hexamers is due to van der Waals interactions. There are 18 molecules of Dianin's compound per hexagonal unit cell, *i.e.* three six-molecule complexes, each of which is situated on a three-fold inversion center.[54] The structure is composed of hour-glass shaped cages capable of accommodating even bulky molecules.[52] The cages are quite large, each with free volume of about 180 $Å^3$.[54] Figure 3.2 represents the shape and size of the largest figure of revolution which can fit

Figure 3.1 A schematic view of the structure of the Dianin host lattice.[54,55] The phenolic oxygens are shown as open circles and the phenolic protons are omitted for clarity.

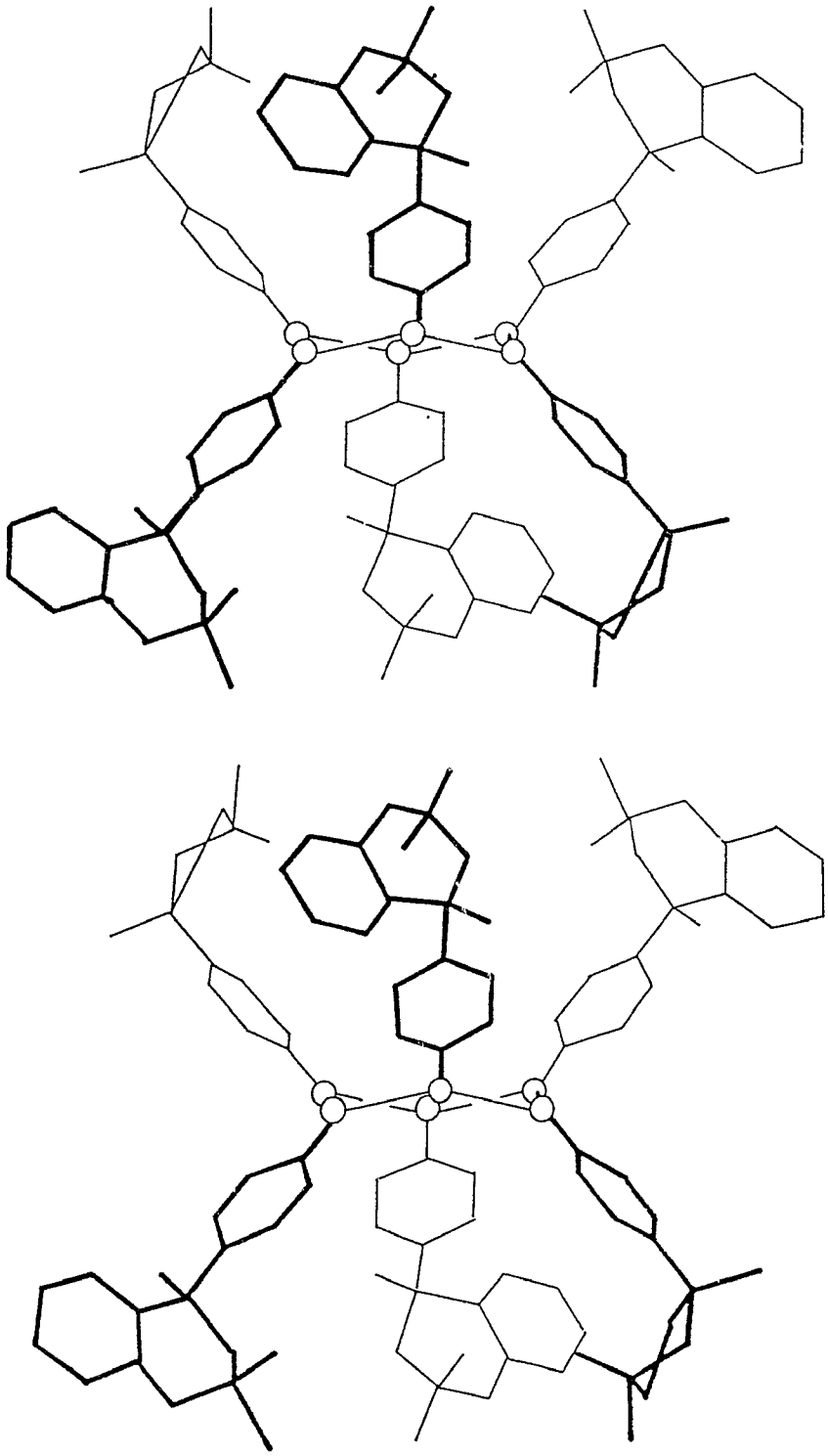

Figure 3.1

Figure 3.2 The shape and size of the largest figure of revolution which can fit into the cage of Dianin's compound.[54]

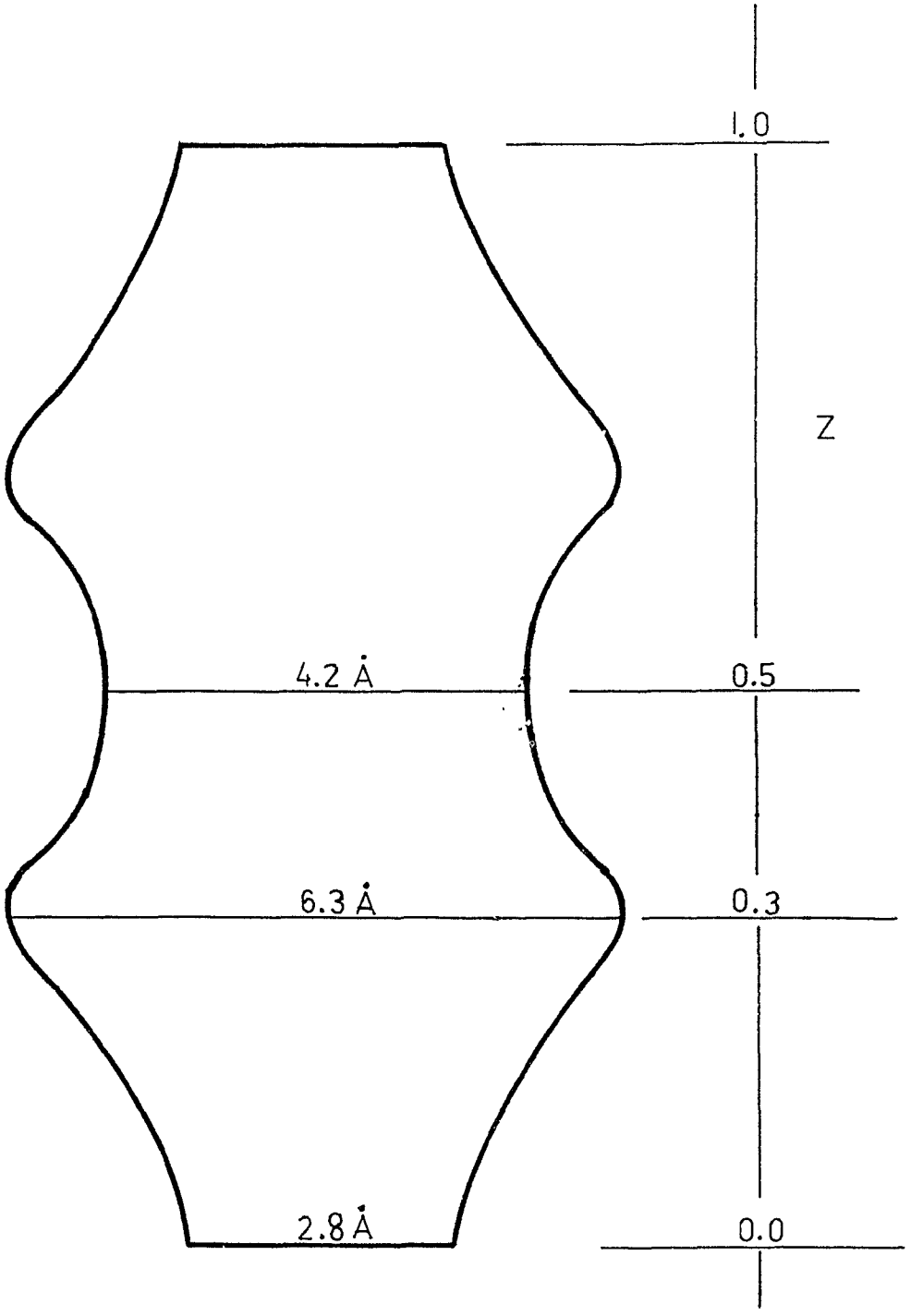

Figure 3.2

into the cage, but there is more space for shapes that vary from cylindrical symmetry.[54] The cage diameter is 2.8 Å at the narrowest (the hydrogen-bonding region), 4.2 Å at the waist and 6.3 Å at the broadest point.[54] The cage height is about 11 Å. Dianin's compound has been found to include more than fifty guest molecules.[52] The usual host:guest ratio is either 3:1 (two guests per hexamer host cage; small guest molecules) or 6:1 (one guest per hexamer host cage; larger guest molecules). However, other ratios such as 7:1 (one vacancy in every seventh cage) are observed also.[53]

The ethanol adduct of Dianin's compound contains one hydrogen-bonded guest dimer within each hexamer host cage, as shown by X-ray crystallography[54] and infrared difference spectroscopy.[56] This is illustrated in Figure 3.3. The ethanol molecules use the largest cross-section in the cage, with the z coordinates between 0.25 and 0.35 for one ethanol molecule and between 0.65 and 0.75 for the other. The position of each ethanol molecule is triply degenerate as deduced from the three-fold rotational symmetry of the crystal. The large thermal parameters of the ethanol molecules in the X-ray study indicate disorder of the guest molecules and possibly occupational deficiencies.[54] The size of the ethanol molecule is considerably less than the size of the cage, as shown in Figure 3.4.

The structure of the CCl_4 adduct of Dianin's compound

Figure 3.3 The orientation of the two ethanol molecules in the Dianin cage (each ethanol molecule is triply-disordered since the crystal requires a three-fold rotation axis). The carbon and oxygen atoms of the ethanol molecules are shown by the closed circles.[54]

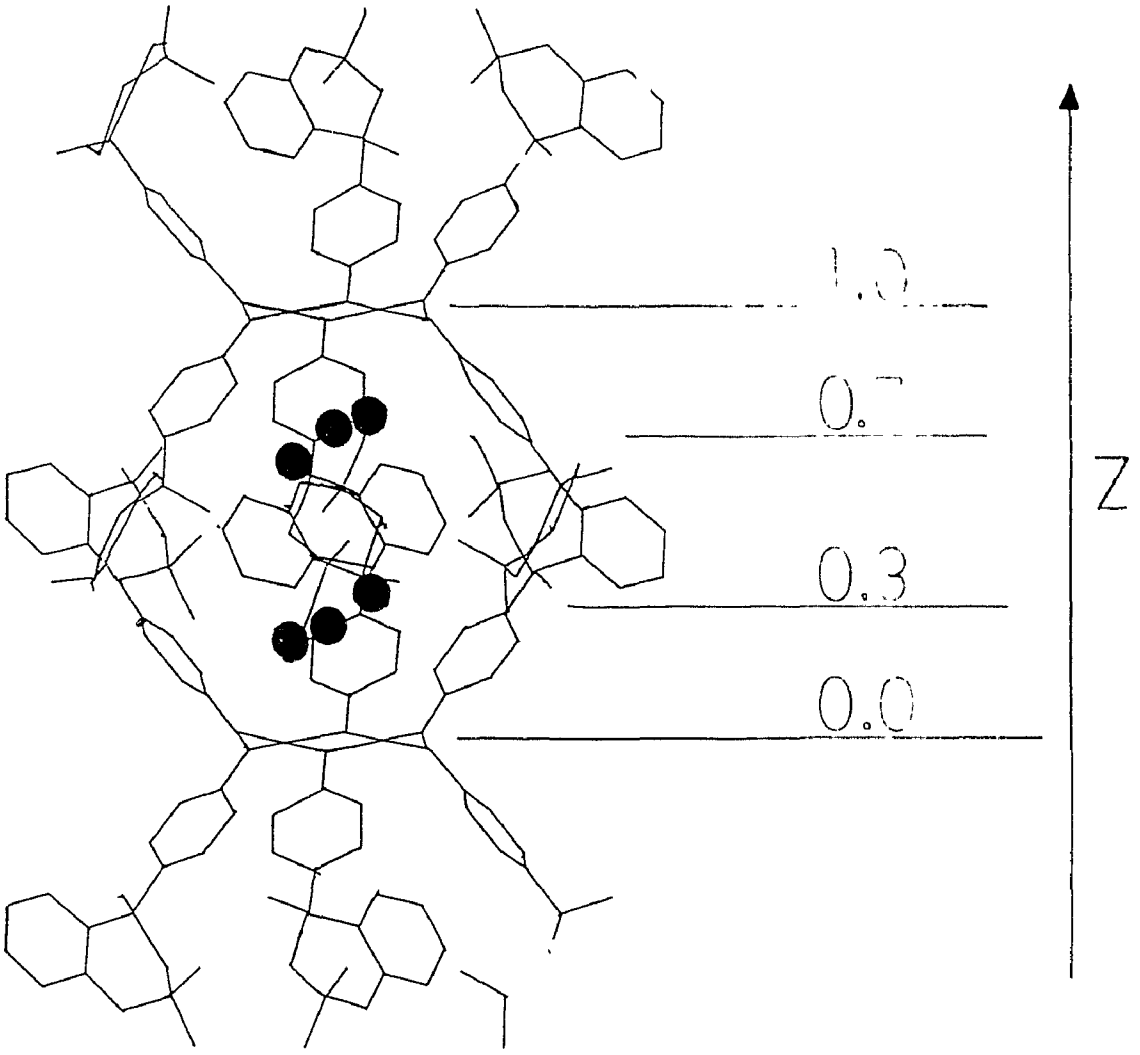

Figure 3.3

Figure 3.4 The ethanol molecule in Dianin's compound surrounded by the van der Waals radii of the cage atoms.[54]

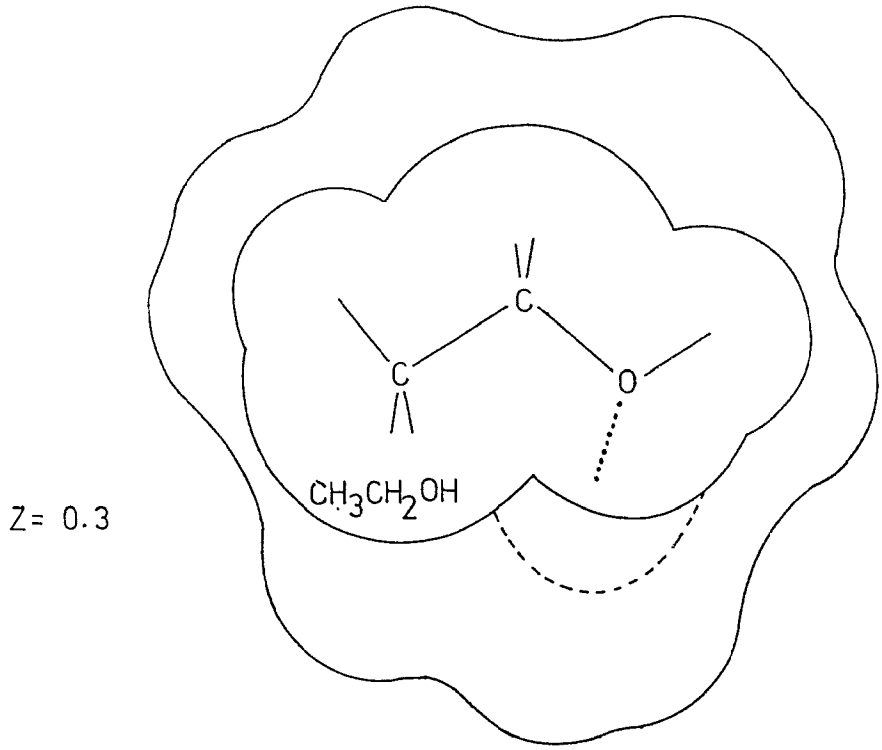

Figure 3.4

is $R\bar{3}$,[57] *i.e.* the same as that of the ethanol adduct[54] and the unsolvated Dianin's compound.[58] Until recently it had been believed that there were two CCl_4 molecules inside the cavity.[52] Now it is known that there is one CCl_4 molecule per host lattice cage.[57] The CCl_4 guest molecule is randomly distributed in the cage (Figure 3.5): one Cl atom occupies the center of the waist in the cage, and this position belongs to both guest molecules with a site occupancy factor of 100%. The occupation probability for the remaining C and three Cl atomic positions is 50%, for each half of the cage.

It is reported that Dianin's compound can be prepared guest-free.[52] The overall structure is substantially unchanged on removal of the guest, and the space group is still $R\bar{3}$.[59] Unlike most inclusion compounds, including clathrate hydrates, β-quinol and urea, it appears that the guest is not essential to "prop open" the structure of Dianin's compound.

Another particularly important feature of the adducts of Dianin's compound is that there is a relatively narrow range of unit cell parameters amongst the Dianin inclusion compounds, compared to, for example, β-quinol, indicating rigidity of the Dianin host lattice.[55]

The existence of a rigid host lattice capable of accommodating a variety of guest molecules and capable of being prepared guest-free allows investigation of the

Figure 3.5 The crystal structure of the CCl_4 adduct of Dianin's compound. The stacking of the host lattice along the c-axis; each hexamer cage contains one CCl_4 molecule.[57]

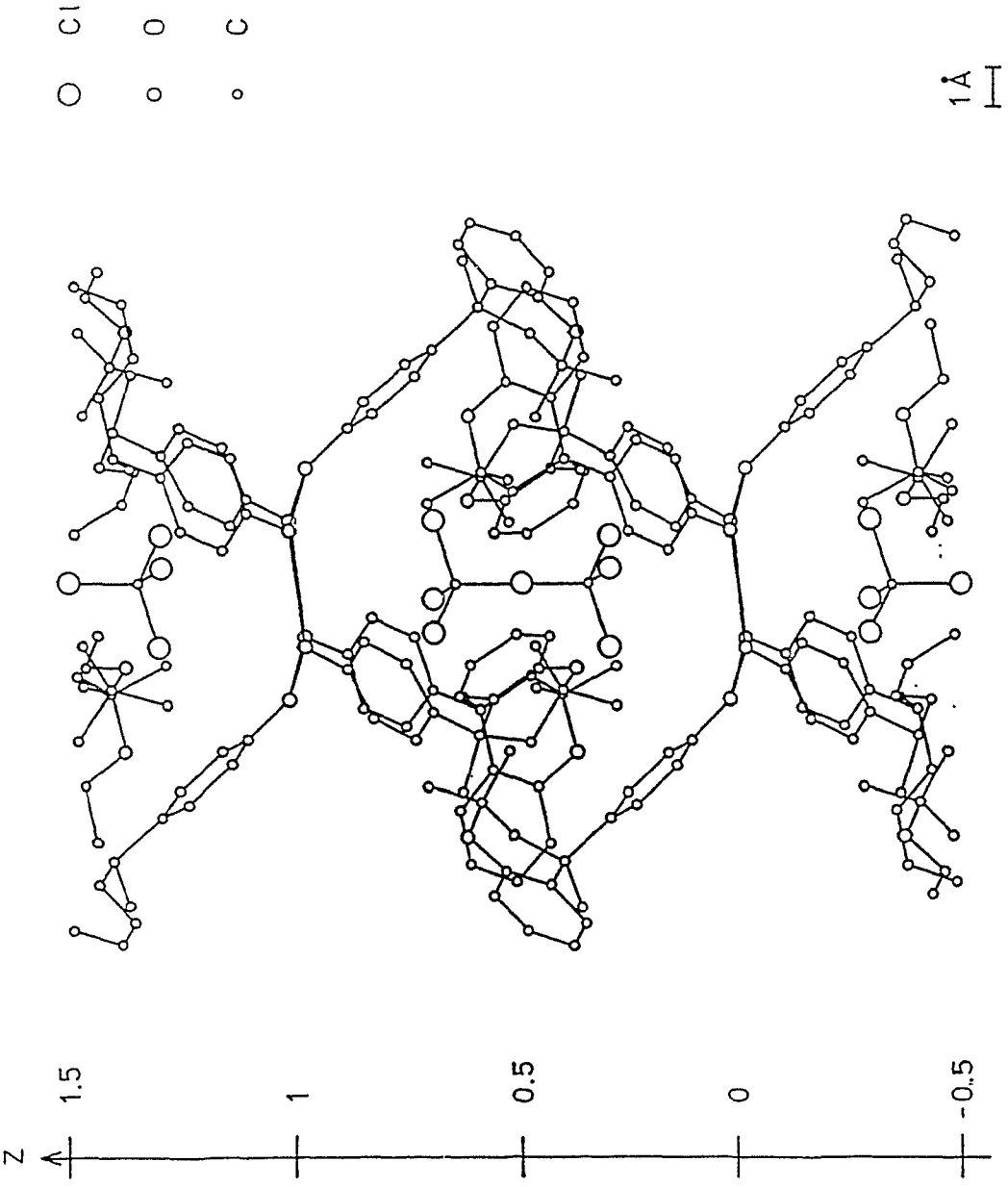

Figure 3.5

following: the additivity of the guest and host properties; the effect of the presence and type of guest on anharmonicity of the crystal lattice; the effect of the presence and type of guest on thermal conductivity.

However, it has to be kept in mind that prior to this work Dianin's compound was not a very extensively studied system and additional experiments to determine helpful quantities were necessary. For direct use in thermal conductivity theory there would be a need to measure velocity of sound. The Debye temperature is needed also and can be determined from heat capacity data under the constraint of constant volume, or from elastic constant measurements. To convert experimentally determined heat capacity (under the constraint of constant pressure) to isochoric heat capacity, thermal expansion and thermal compressibility data are necessary. All of the above suggest that elastic constant measurements should be performed in addition to heat capacity and thermal conductivity measurements, in order to answer questions concerning the role of the guest species in the thermal conductivity of these clathrates.

Chapter 4: Dianin's Compound: Sample Preparation

4.1 Preparation of Ethanol Adduct of Dianin's Compound

4-*p*-Hydroxyphenyl-2,2,4-trimethyl chroman (Dianin's compound) was prepared by the reaction of phenol and mesityl oxide .[52]

A mixture of phenol (analytical reagent, BDH Chemical) and mesityl oxide (practical Eastman) was saturated with a stream of anhydrous hydrogen chloride (8 hr.). The red viscous mixture was kept at about 38°C for four days, giving a red-brown crystalline mass. Boiling water was added and the mixture was shaken well and heated on a water-bath. The top aqueous layer was decanted and the procedure repeated. After being decanted, the damp, oily product was then shaken with hot ethanol, cooled and shaken. After a few hours the crystalline ethanol adduct that accumulated was filtered and twice stirred with cold ethanol and then filtered again. The product was recrystallized from ethanol, collected, washed well with cold ethanol and filtered, giving colourless hexagonal needles.

A single crystal of ethanol adduct was grown by slow evaporation at room temperature after placing a seed in the saturated ethanol solution of the Dianin compound. Vacuum thermal insulation was used during the crystal growth to

avoid temperature changes causing undesired precipitation.

In order to prepare a fine powder for the x-ray powder crystallographic study, precipitation from a hot saturated solution was carried out rapidly by quenching a hot saturated solution in an ice-water bath. This was preferable to grinding, as it was found that the latter method caused unusual and irreproducible characteristics in the diffractogram.[60] Thermogravimetric analysis showed a mass loss at the melting point (165°C) of 4.8%; if due entirely to loss of ethanol this would correspond to an average of 1.8 ethanol molecules per hexamer unit of the host lattice. The measured density of the crystals at 23°C, from determinations using a calibrated pycnometer matching the crystal density with aqueous KI solutions, was 1.223 ± 0.005 g cm^{-3}, which is in good agreement with 1.225 g cm^{-3}, the density calculated from X-ray diffraction data,[54,55] based on a 3:1 host-to-guest ratio. Results of chemical analyses are given in Table 4.1 for all adducts prepared.

Table 4.1. The Results of Chemical Analyses for Dianin's Compound (**1**), its Ethanol Adduct and its Carbon Tetrachloride Adduct. The values in parentheses are theoretical values based on 3:1 host:guest stoichiometry for the ethanol adduct and 6:1 host:guest stoichiometry for the CCl_4 adduct. All values are mass per cent. Errors quoted indicate the range of duplicate analyses.

	C	H	Cl
Unsolvated Dianin's compound	79.75±0.05 (80.6)	7.6±0.1 (7.51)	
Ethanol Adduct of Dianin's Compound	79.5±0.2 (79.1)	7.8±0.2 (7.76)	
CCl_4 Adduct of Dianin's Compound	73.45±0.2 (74.3)	7.1±0.1 (6.86)	9.5±0.1 (8.04)

4.2 Preparation of Unsolvated Dianin's Compound

The ethanol complex was dissolved in hot 2N-sodium hydroxide; this was refluxed while carbon dioxide gas was passed through the hot solution for 30 minutes.[52] The collected solid was boiled twice with water and dried in vacuum over phosphoric anhydride. This unsolvated Dianin's compound was a fine white powder. Chemical analysis results are given in Table 4.1.

To grow a single crystal of the unsolvated Dianin's compound the slow evaporation technique was used again but with a few modifications. Decanol was chosen as a solvent, as it does not form a clathrate with Dianin's compound.[61] This was confirmed by checking the melting point (158-159°C)[62] and by x-ray analysis.[58,60] Because of the high boiling point of decanol (229°C), to allow a reasonable rate of evaporation of the solvent from the saturated solution the temperature was kept at 65°C. To avoid temperature changes the vessel with the saturated solution was kept in liquid paraffin, chosen because of its high heat capacity and low vapour pressure.

Because of the importance of the guest content to the interpretation of the results, samples were examined carefully for the most likely included guests, N_2, O_2, CO_2 and H_2O. A Raman spectroscopic investigation showed no evidence of the CO_2 lines at 1288 and 1386 cm^{-1}, nor did it

show any evidence of N_2 (2330 cm^{-1}) or O_2 (1556 cm^{-1}). The CO_2 bands should be very intense due to Fermi resonance, and, in comparison with Raman investigations of the ethanol and CCl_4 adducts of Dianin's compound,[63] the detection limit on the CO_2 content was placed at one CO_2 molecule every 10 to 20 hexamer cages. Infrared spectroscopic measurements to detect H_2O showed a small broad line at 1625 cm^{-1} (the bend in pure H_2O is at 1640 cm^{-1}).[64] In comparison with the intensity of the line at 3300 cm^{-1} due to the R-O-H stretch, assuming similar absorbtivities and the usual 10:1 ratio for the stretch:bend intensities, this could be attributable to one water molecule every 20 cages. Thermogravimetric analysis showed a 0.22 % mass loss at the melting point (158-159°C) of the "empty" Dianin's clathrate, which, if due to loss of guest would correspond to the expulsion, on average, of a species of molecular mass of 3.5 g mol^{-1} from each hexamer cage; however, there is some evidence that mass loss on melting Dianin's compound is due to volatilization of the parent species.[65] Although it is difficult to prove that something is totally absent, it appears[66] that the samples prepared were substantially without guest. The density of single crystals was found, by matching the crystal density with aqueous KI solutions, to be 1.171±0.005 g cm^{-3} at 23°C. The density calculated from X-ray diffraction data[58] was found to be 1.165 g cm^{-3}. The discrepancy could be caused by a presence of one decanol

molecule every 100 Dianin's compound molecules which would result in a density of 1.172 g cm^{-3}. A similarly scarce occupancy ratio was found for n-decane in Dianin's compound (1:106).[53]

4.3 Preparation of Carbon Tetrachloride Adduct of Dianin's Compound

The unsolvated Dianin's compound was dissolved in gold label carbon tetrachloride (Aldrich) and its adduct obtained by slow evaporation. The carbon tetrachloride adduct was a fine white powder. The observed melting point was 159-160°C (159-160°C), where the parenthetic values are from the literature.[52] Chemical analysis results are given in Table 4.1.

For the X-ray powder diffraction experiments the powder sample was sieved to use particles less than 50 μm in size. This procedure was chosen because grinding larger crystals produced structural defects and decomposition, as shown by the high background scattering and line broadening in the diffraction diagram.[57]

The densities of single crystals were measured using a calibrated pycnometer and was determined to be 1.262±0.005 g cm^{-3} at 23°C. Using the lattice constants and thermal expansion determined here, this gives a ratio of host to guest molecules of (5.94±0.05):1.[57]

Chapter 5: Heat Capacity Measurements

5.1 Introduction (Theory)

Heat capacity, C, is defined as the quantity of heat required to raise the temperature of a system by one unit:

$$C_x=(dq/dT)_x \qquad (5.1.1)$$

where x denotes any one of several constraints that may be imposed, dq is the total heat added to the system and dT is the resulting differential in the temperature. Constant volume and constant pressure are the most common constraint conditions. The latter is usually used for solids. For isotropic materials C_p and C_v are related to each other by:[45]

$$C_p - C_v = \alpha_v^2 VT/\chi^T \qquad (5.1.2)$$

where V is the molar volume, α_v is the coefficient of volume expansion ($\alpha_v = (1/V)(\partial V/\partial T)_p$) and χ^T is the bulk isothermal compressibility ($\chi^T=-(1/V)(\partial V/\partial P)_T$). The difference between C_p and C_v at T=0 K is zero, and it is a small fraction of C_p for most solids at room temperature.

The first law of thermodynamics relates the heat capacity to the internal energy of the system, E:

$$dE = dq + dw \qquad (5.1.3)$$

where dE is the differential in the internal energy of the system and dw is the differential in work done by the system. For pressure-volume work dw can be expressed as:

$$dw = p \cdot dV \qquad (5.1.4)$$

where p is the external pressure and dV is the differential in volume. Under conditions of constant volume, dw is zero, so measurement of the differential increase in the energy through Joule heating is equivalent to dq at constant volume. With the concurrent measurement of the resultant temperature increase at constant volume the heat capacity can be determined.

On the other hand, the internal energy of the crystal lattice can be expressed as the sum of the energies of harmonic oscillators (in the harmonic oscillator approximation). This is connected to the heat capacity by the phonon frequencies. If one assumes that all oscillators have the same frequency then it will follow (this is the Einstein model) that in the high-temperature limit for a monatomic solid:

$$C_v = 3\ N\ k_B \qquad (5.1.5)$$

where k_B is the Boltzmann constant and N is the number of oscillators. This is in agreement with the experimental Petit-Dulong law. Although this model works quite well describing high-frequency modes (optical modes), it is not satisfactory at low temperatures.

Debye assumed[42] a continuous distribution of phonon frequencies up to the so called Debye frequency, ω_D, where the maximum allowed phonon frequency (ω_D) is limited by the lattice constant, a, and the phonon group velocity, v_g:

$$\omega_D = \left(\frac{6N\pi^2 v_g^{\ 3}}{V} \right)^{1/3} \qquad (5.1.6)$$

where V is the volume of the crystal. In terms of the Debye frequency, the Debye distribution function, $D(\omega)$, also called the density of modes, is given by:

$$D(\omega) = \frac{9\omega^2 N}{\omega_D^{\ 3}} \qquad (5.1.7)$$

The heat capacity expression obtained using the Debye model is in good agreement with the Petit-Dulong law at high temperature. In the low-temperature limit it gives the Debye T^3 law:

$$C_v = \frac{12\pi^4}{4} N \left(\frac{T}{\theta_D} \right)^3 \qquad (5.1.8)$$

where θ_D is the Debye temperature given by:

$$\theta_D = \frac{\hbar\omega_D}{k_B} \qquad (5.1.9)$$

and the T^3 temperature dependence is observed experimentally for $T \ll \theta_D$.

5.2 Heat Capacity Measurements by Adiabatic Calorimetry

Heat transport phenomena, including conduction, radiation, convection, and heat transfer, are of central importance in calorimetry. The occurrence of a temperature differential causes heat flow and this creates the possibility of heat losses (heat leaks), which are heat fluxes not detected by the measuring sensor. On the other hand, no heat exchange can take place in the absence of temperature gradients. In order to be measured, heat must flow, but a heat flux can be associated with temperature differences which create errors in calorimetric measurements.

One way out of this dilemma is the adiabatic calorimeter. Under ideal conditions, no heat exchange occurs between the measuring system and the surroundings. There are

three methods for fulfilling these requirements satisfactorily:[67] (1) the sample reaction takes place sufficiently rapidly so that no appreciable quantity of heat can leave or enter the system during the time the measurement is taken; (2) the measuring system is isolated from the surroundings by an infinite thermal resistance; (3) the temperature of the surroundings is controlled to be always equal to that of measuring system.

In most adiabatic calorimeters, a high vacuum, an adiabatic shield and a heat sink for the electrical leads are used to prevent unwanted heat exchange through method (3) above. Any heat exchange between the system and the surroundings brings about a change in the system temperature. The adiabatic shield must be adjusted so as to match this temperature change in order to ensure that the unknown heat exchange with the surroundings is reduced to a tolerable minimum. A completely isolated system is not possible in practice, but it is possible to obtain a sufficient approximation.

Adiabatic calorimeters are not available commercially, so each is usually specially designed. The adiabatic calorimeter used in this work consists of a calorimetric vessel with its electrical heater, platinum resistance thermometer and D.C. power supply, adiabatic shield and its controller, digital multimeter, vacuum system, cryostat, and computer system.[68,69] A schematic of the adiabatic calorimeter

is given in Figure 5.1.

To obtain low-temperature conditions cryogenic fluids were used. Large glass Dewars were used to submerge the enclosure can in either liquid nitrogen or liquid helium, depending on the temperature range. In the range from the boiling point of liquid nitrogen up to about 350 K, a single Dewar was used to contain liquid nitrogen. In the range from the boiling point of liquid helium to that of liquid nitrogen two Dewars were used, one inside the other. The outer Dewar contained liquid nitrogen. The inner Dewar contained liquid helium.

To obtain good insulation and maintain quasi-adiabatic conditions the enclosure can was evacuated. A cylindrical copper enclosure can surrounded the calorimeter vessel, adiabatic shield and heat sink assembly and was fastened to a flange. An indium vacuum seal was used between the flange and the enclosure can. The evacuation system consisted of a roughing pump and an oil diffusion pump which maintained a vacuum better than 10^{-5} Torr.

All electrical connections were made using thermal-free solder (Leeds and Northrup) to reduce thermal emf effects. A cylindrical copper adiabatic shield surrounding the vessel-heater-thermometer assembly was used to minimize the unknown heat exchange between the system and the surroundings. To control the temperature gradient between the shield and the vessel, a copper-constantan thermocouple

Figure 5.1 Schematic of the adiabatic calorimeter. 1. vacuum line, 2. Dewar, 3. flange, 4. indium seal, 5. heat sink, 6. nylon filaments, 7. adiabatic shield, 8. sample vessel, 9. enclosure can, 10. cryogen.

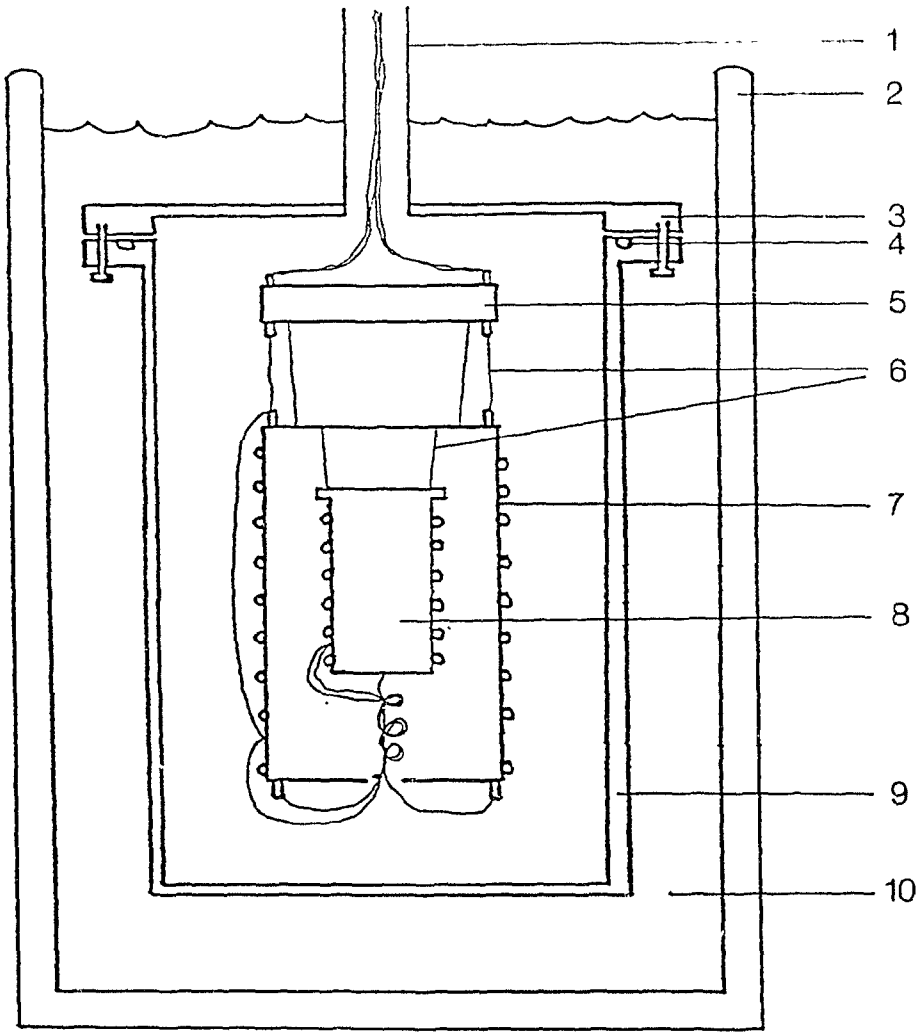

Figure 5.1

junction on the shield with a reference thermocouple junction on the bottom of the sample vessel assembly was used. A heater (15 m of manganin wire) was wound bifilarly on the outer surface of the shield.

To maintain adiabatic conditions the thermocouple was connected to an Artronix 5301-E shield controller which was the D.C. power supply for the shield heater. An acceptable set point gave a temperature drift in the calorimetric vessel less than 0.003 K/min. The calorimeter vessel and heater-thermometer assembly were suspended inside the shield by a nylon filament. These are shown in Figure 5.2.[69]

A calibrated miniaturized Pt resistance thermometer (Lake Shore Cryotronics Pt-103, 100 Ohms at T=273 K) was used. The sample vessel was gold-plated copper. An indium O-ring between its flange and lid guaranteed a hermetic seal. A thicker copper washer was used above the lid to increase compression. The total volume was about 5 cm^3 and the mass was about 11 g.

The heater-thermometer assembly also was constructed from thin copper sheet with the thermometer well placed inside. Approximately 2.6 m Karma wire (590 Ohms) was wound bifilarly around and varnished to the surface. The total mass of the sample vessel and heater thermometer assembly was about 19 g.

To maximize sensitivity the platinum resistance thermometer was connected in a circuit with a standard

Figure 5.2 The sample vessel and heater thermometer assembly of the adiabatic calorimeter vessel.[69]

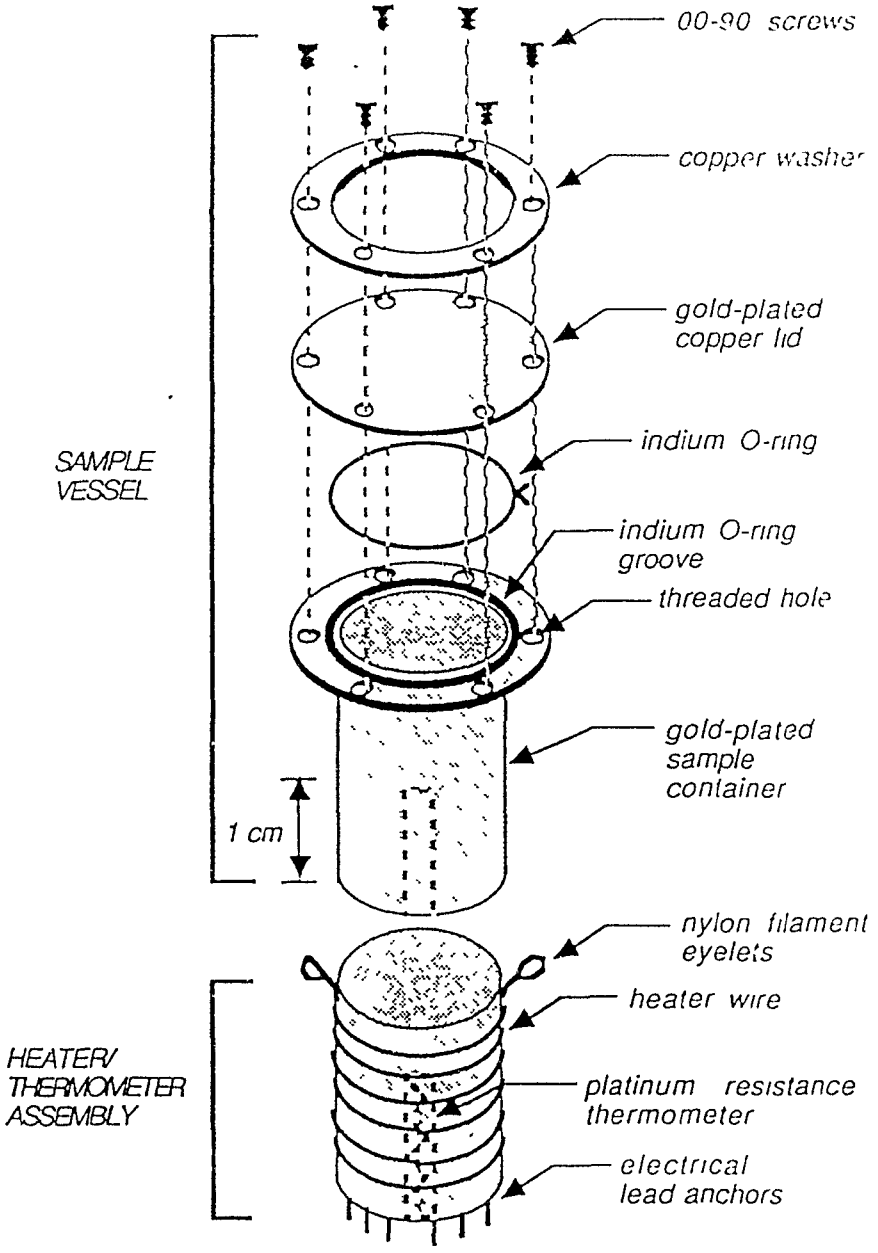
00-90 screws
copper washer
gold-plated copper lid
indium O-ring
indium O-ring groove
threaded hole
gold-plated sample container
SAMPLE VESSEL
1 cm
nylon filament eyelets
heater wire
platinum resistance thermometer
electrical lead anchors
HEATER/ THERMOMETER ASSEMBLY

Figure 5.2

resistor (100 Ohm) and a small D.C. current (1 mA) was passed through the circuit. The ratio of the voltage drop across the thermometer relative to the standard resistor was measured with a Hewlett-Packard 3456A digital multimeter. A schematic of the circuit is shown in Figure 5.3. Thermometer resistance ratio measurements were taken in both current directions to correct for thermal emf.

The platinum resistance thermometer was calibrated by the manufacturer from T=4 K to 380 K against a platinum resistance thermometer which had been calibrated based on the 1976 Provisional 0.5 to 30 K temperature scale (EPT-76)[70] below 30 K, and International Practical Temperature Scale of 1968 (IPTS-68)[71] above 30 K. Above 27 K the claimed calibration accuracy was ±10 mK and below 27 K the claimed accuracy was ±15 mK.[72]

A Hewlett-Packard 87A personal computer was interfaced to the Hewlett-Packard 3456A digital multimeter. All time measurements were made by the internal computer clock with accuracy of 0.02%. The software[72] provided the choice of heating by either timed pulses or heating by temperature increments; the time-range of data omitted from the temperature extrapolation due to thermal relaxation; the frequency of data collection; and the set point increments of the shield controller. A few of these variables had to be determined by semi-automated runs. The calculated heat capacity was printed and plotted as a function of

Figure 5.3 Schematic of the computer system for the adiabatic calorimeter where: V represents the constant voltage supply; R represents the standard 100 Ohm resistance; i represents the constant current supply for the thermometer measurement circuit; i↓↑ denotes the computer-controlled current direction relay; H/T represents the heater thermometer measurement relays; DVM represents the HP 3456A digital multimeter.[72]

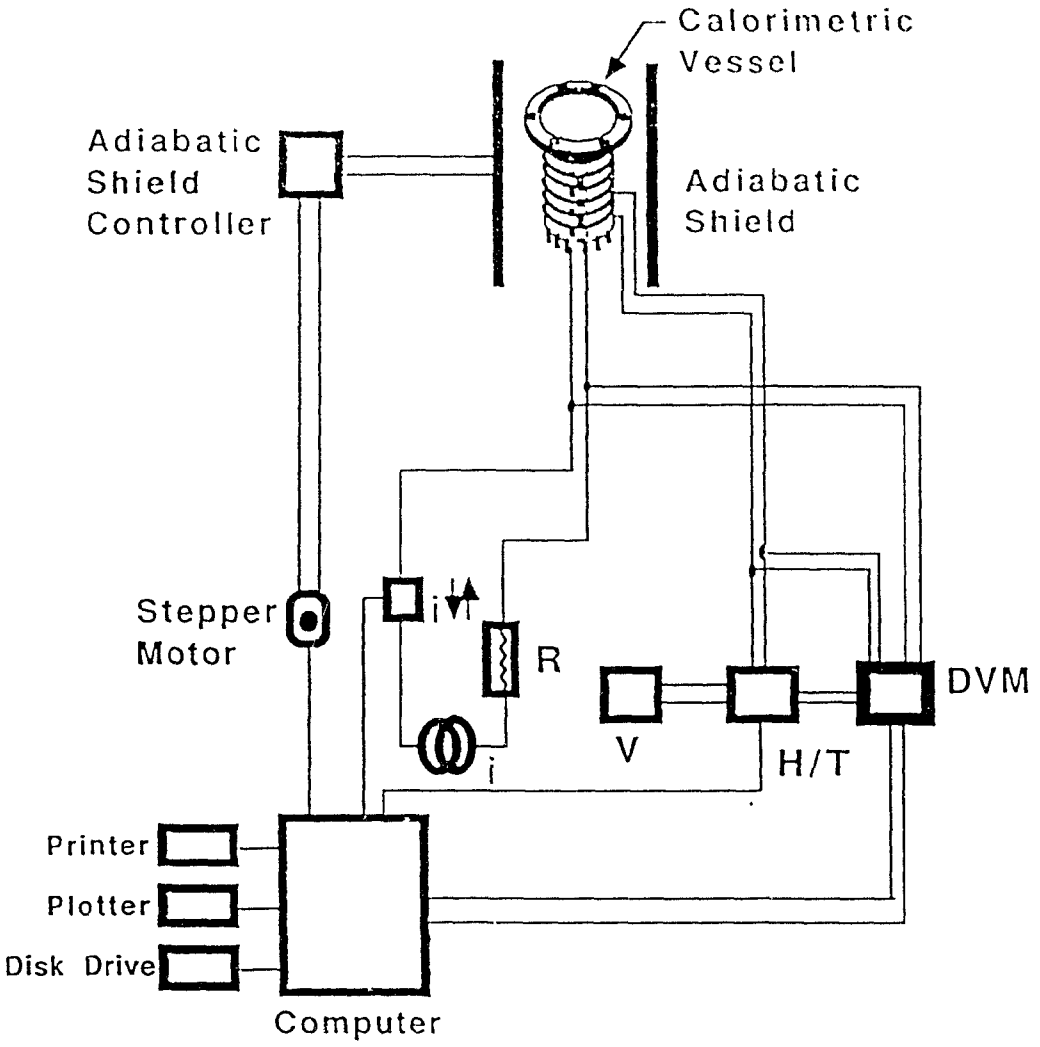
Calorimetric
Vessel
Adiabatic
Shield
Controller
Adiabatic
Shield
Stepper
Motor
i
R
i
V
H/T
DVM
Printer
Plotter
Disk Drive
Computer

Figure 5.3

temperature by an Hewlett-Packard plotter. All data was collected on diskette. The calorimeter had been tested with Calorimetry Conference (NBS-49) benzoic acid from 35 to 310 K. The results agreed with the literature to within 0.5%.[69]

5.3 Heat Capacity Measurement Procedure

When the starting temperature was reached the set point was found manually. An acceptable set point is one which produces a drift rate smaller than 3 mK/min. When that was obtained resistance ratio (RR) data were taken for an arbitrary time (typically 1 hour). Then the calorimetric vessel heater was heated electrically. The voltage (U) was measured three times and the heater resistance (R) twice (just before and just after the heat) and both quantities averaged. The duration of the heat (t) was measured by the internal clock of the computer. The quantity of (Joule) heat applied, q, is calculated as:

$$q = (U^2 / R) t \quad . \qquad (5.3.1)$$

The shield controller set point was usually changed during the heating to adjust to the new temperature and new temperature gradient between the vessel and the shield. When heating was finished resistance ratio data were taken again

as a function of time. The RR data from before the heat were extrapolated towards the middle of the heat time to determine T_1, the initial temperature. Similarly, T_2, the final temperature was determined from RR data following heating. The temperature change, ΔT, was calculated as:

$$\Delta T = T_2 - T_1 \quad . \qquad (5.3.2)$$

The total heat capacity (of the sample, calorimetric vessel, heater assembly, indium seal, grease) was calculated at T_{avg} as:

$$C_p = q \ / \ \Delta T \qquad (5.3.3)$$

where C_p is the heat capacity at constant pressure, and T_{avg} is the arithmetic average of T_1 and T_2. Because the contributing heat capacities are additive, correction values were subtracted from the total heat capacity in order to obtain the heat capacity of the sample. First the heat capacity of the empty calorimeter was measured and the experimental data were fitted using the spline method,[73,74,75,76,77] in order to know its value at an arbitrary temperature. The literature heat capacity data for Apiezon T grease[78] and for indium metal[79,80] also had been fitted with the spline method. All of these procedures were included

into the computer program.[69] Correction for the mass of Apiezon T (mass < than 0.01 g) and the indium seal (mass about 0.1 g) are not greater than 0.04% of the total heat capacity of the empty vessel.[72]

5.4 Heat Capacity Results

The heat capacities of each of the three compounds (unsolvated Dianin's compound, ethanol adduct of Dianin's compound, carbon tetrachloride adduct of Dianin's compound) were measured from about 30 K to above 300 K in the adiabatic heat-pulse calorimeter, described in the previous sections. The respective sample masses were 1.396 g, 3.269 g, and 1.700g.

The heat capacities for the three compounds investigated are given in Tables 5.1 to 5.3, respectively on a gram basis. No thermal history effects were noted, and the results are given in order of increasing temperature. The relaxation times following heating, which can sometimes indicate unusual thermal properties, were typical for well-behaved materials in this calorimeter, about 15 to 25 min. for the empty Dianin's compound, 15 to 20 min. for the ethanol adduct and 15 to 30 min. for the CCl_4 adduct. In each case the shortest relaxation time was observed at the lowest temperature.

Table 5.1. The experimental heat capacities of unsolvated Dianin's compound.

T/K	C_p/J K^{-1} g^{-1}	T/K	C_p/J K^{-1} g^{-1}
47.48	0.206	198.14	0.865
52.45	0.221	203.44	0.888
57.57	0.258	205.05	0.899
63.11	0.287	206.18	0.906
69.04	0.308	211.46	0.940
74.80	0.345	213.04	0.950
82.22	0.366	214.22	0.952
82.32	0.374	219.48	0.987
88.21	0.387	221.04	0.990
97.02	0.431	222.27	0.990
99.97	0.429	227.54	0.998
103.48	0.453	229.03	1.017
105.78	0.463	230.29	1.026
105.99	0.465	235.60	1.047
109.34	0.477	237.00	1.053
111.57	0.492	238.34	1.057
111.89	0.493	244.94	1.084
116.14	0.509	246.36	1.086
118.32	0.509	252.91	1.119
123.95	0.524	254.44	1.128
126.05	0.546	259.72	1.144
131.77	0.573	260.88	1.151
133.87	0.578	262.46	1.168
134.48	0.581	267.79	1.177
139.63	0.604	268.89	1.181
141.70	0.619	275.87	1.204
142.37	0.622	276.82	1.223
147.53	0.642	283.99	1.232
149.55	0.647	284.82	1.254
150.28	0.658	285.12	1.285
155.49	0.676	286.09	1.264
157.42	0.695	292.76	1.283
158.21	0.687	293.99	1.299
163.47	0.707	294.88	1.285
165.29	0.716	308.19	1.320
166.17	0.723	315.62	1.348
171.46	0.749	323.64	1.395
173.21	0.756	325.95	1.430
174.14	0.757	334.05	1.446
179.46	0.784	339.73	1.486

continued....

Table 5.1 continued:

T/K	C_p/J K^{-1} g^{-1}
181.16	0.794
182.14	0.797
187.46	0.822
189.10	0.825
190.15	0.829
195.44	0.857
197.05	0.869

Table 5.2. The experimental heat capacities of the ethanol adduct of Dianin's compound (**1**).

T/K	C_p/J K^{-1} g^{-1}	T/K	C_p/J K^{-1} g^{-1}
26.60	0.120	192.34	0.915
29.52	0.159	195.22	0.926
31.45	0.173	200.11	0.948
32.55	0.168	202.93	0.963
33.23	0.178	207.91	0.990
34.72	0.179	210.66	1.004
36.10	0.182	215.75	1.025
37.91	0.187	218.40	1.040
38.16	0.189	223.57	1.061
42.50	0.217	226.16	1.078
47.36	0.243	231.46	1.092
52.36	0.262	234.02	1.101
57.44	0.294	239.33	1.136
62.43	0.319	241.92	1.137
67.40	0.338	247.22	1.162
72.42	0.362	249.89	1.172
77.45	0.392	255.11	1.192
83.19	0.413	257.90	1.205
84.51	0.422	259.24	1.215
86.81	0.427	263.03	1.224
88.14	0.432	264.36	1.240
89.80	0.438	265.87	1.242
92.50	0.454	270.98	1.259
94.53	0.461	271.91	1.261
98.12	0.478	273.14	1.275
99.92	0.485	273.87	1.270
103.75	0.506	278.91	1.293
105.93	0.510	279.86	1.297
109.39	0.532	281.80	1.307
111.97	0.543	286.81	1.343
115.98	0.562	287.79	1.347
118.76	0.570	289.75	1.356
123.56	0.590	294.72	1.372
126.35	0.604	295.69	1.382
131.17	0.627	302.65	1.407
133.95	0.639	303.61	1.412
138.75	0.661	304.81	1.421
141.57	0.676	311.55	1.445
146.38	0.701	312.78	1.456
149.18	0.714	320.85	1.493
153.98	0.736	324.92	1.522
156.81	0.747	327.68	1.523

continued....

Table 5.2 continued:

T/K	C_p/J K^{-1} g^{-1}	T/K	C_p/J K^{-1} g^{-1}
161.61	0.767	332.97	1.549
164.44	0.784	337.28	1.574
169.27	0.804	341.02	1.586
172.12	0.816		
176.94	0.839		
179.81	0.851		
184.61	0.875		
187.52	0.888		

Table 5.3. The experimental heat capacities of the CCl_4 adduct of Dianin's compound.

T/K	C_p/J K^{-1} g^{-1}	T/K	C_p/J K^{-1} g^{-1}
33.62	0.139	164.66	0.701
35.74	0.160	165.20	0.704
38.79	0.171	168.44	0.721
46.53	0.206	172.61	0.734
48.18	0.204	173.15	0.737
51.53	0.227	176.36	0.755
56.63	0.254	180.58	0.768
61.67	0.282	181.10	0.772
66.59	0.298	184.29	0.791
71.40	0.313	188.56	0.808
76.00	0.338	189.09	0.808
80.76	0.371	192.24	0.826
82.22	0.368	196.57	0.837
85.46	0.381	197.10	0.842
85.97	0.386	200.25	0.855
88.12	0.384	204.67	0.872
90.15	0.394	205.17	0.878
92.69	0.408	208.28	0.900
92.93	0.406	212.73	0.919
93.97	0.412	216.32	0.939
94.84	0.416	220.79	0.955
99.60	0.435	224.36	0.972
99.76	0.433	228.84	0.985
105.28	0.462	232.41	1.003
105.55	0.462	236.90	1.016
107.12	0.472	240.46	1.034
111.01	0.488	244.97	1.049
111.36	0.488	248.50	1.065
113.84	0.498	253.05	1.088
117.71	0.507	256.61	1.099
118.12	0.508	261.14	1.116
121.53	0.524	264.71	1.131
125.41	0.538	269.28	1.148
125.89	0.541	272.85	1.165
129.27	0.554	277.47	1.178
133.19	0.570	277.78	1.180
133.70	0.572	281.12	1.194
133.04	0.591	286.14	1.224
141.00	0.607	294.25	1.247
141.53	0.609	297.32	1.285

continued...

Table 5.3 continued:

T/K	C_p/J K^{-1} g^{-1}	T/K	C_p/J K^{-1} g^{-1}
144.86	0.626	305.46	1.314
148.86	0.639	313.28	1.338
149.38	0.643	313.54	1.338
152.69	0.658		
156.75	0.670		
157.28	0.672		
160.54	0.687		

5.5 Heat Capacity: Guests in The Cage Compared with Their Bulk Properties

One of the aims of this investigation was to calculate the contribution of the guest species to the heat capacity and to compare this with C_p of the bulk guest species. As mentioned earlier, Dianin's compound and its adducts are particularly suited to this purpose because the empty host lattice exists and its heat capacity can be measured. By contrast, the β-quinol empty host lattice is unstable, but β-quinols are available at various guest occupancy levels.[55,81] Unsolvated clathrate hydrates are unstable, and furthermore, the adducts occur only at fixed guest compositions.[82]

In order to calculate the heat capacity of the guest species (CCl_4) or guest dimer (ethanol), it was assumed that the heat capacities of the guest(s) and the unsolvated host are additive. Although this may be too simplistic, the relatively large cage of the Dianin's compound, the rigidity of the host lattice and the relatively weak guest-host interactions work in favour of this assumption. The stoichiometries of the ethanol adduct and that of the CCl_4 adduct have been taken to be exactly 3:1 and 6:1, respectively, to calculate the molar heat capacities of the guest species. It can be noted that the very similar heat capacities per gram for the adducts and the unsolvated

Dianin's compound make the guest heat capacity rather insensitive to the occupancy of the cage, and therefore slight occupational deficiencies will not change results significantly. It can also be noted that the isochoric and isobaric heat capacities of the guest molecules will be the same if the guests are one per cage, and able to rotate freely;[24] in the ethanol adduct the first condition is not met, but both may be met in the CCl_4 adduct.

Figure 5.4 illustrates the single-molecule heat capacity of CCl_4 in the Dianin adduct as calculated from the experimental heat capacities of the unsolvated and CCl_4 adducts. The similarity between the single-molecule heat capacity and that of bulk CCl_4 (dashed curve)[83,84] is striking, particularly in the region from about 60 K to 260 K. However, the single-molecule heat capacity differs from that of bulk CCl_4 in several ways, *viz.* there is a heat capacity plateau from about 100 K to 200 K, and there are no first-order phase transitions as observed in bulk[83] CCl_4. The latter may reflect the decreased strength of orientational interactions in adjacent CCl_4 molecules in the clathrate; the average CCl_4 separation is 11 Å along the c-axis and 27 Å along the a-direction in the clathrate, compared with 5.8 Å in bulk CCl_4.[85,86] The source of the heat capacity plateau in the single-molecule heat capacity may be similar to that observed in the clathrate hydrate of tetrahydrofuran,[25] *i.e.* fully-excited hindered rotational

Figure 5.4 The molar heat capacity of a CCl_4 molecule in the CCl_4 adduct of Dianin's compound. The dashed line indicates the molar heat capacity[83,84] of bulk CCl_4, including its solid-solid transition at 226 K and its solid-liquid transition at 250 K. The error bar at T = 150 K represents the error in the molar heat capacity of the CCl_4 molecule in the clathrate, as propagated from an error of $\pm$0.5% in the heat capacity of unsolvated Dianin's compound and $\pm$0.5% in the CCl_4 adduct of Dianin's compound. R=8.314 J K^{-1} mol^{-1}.

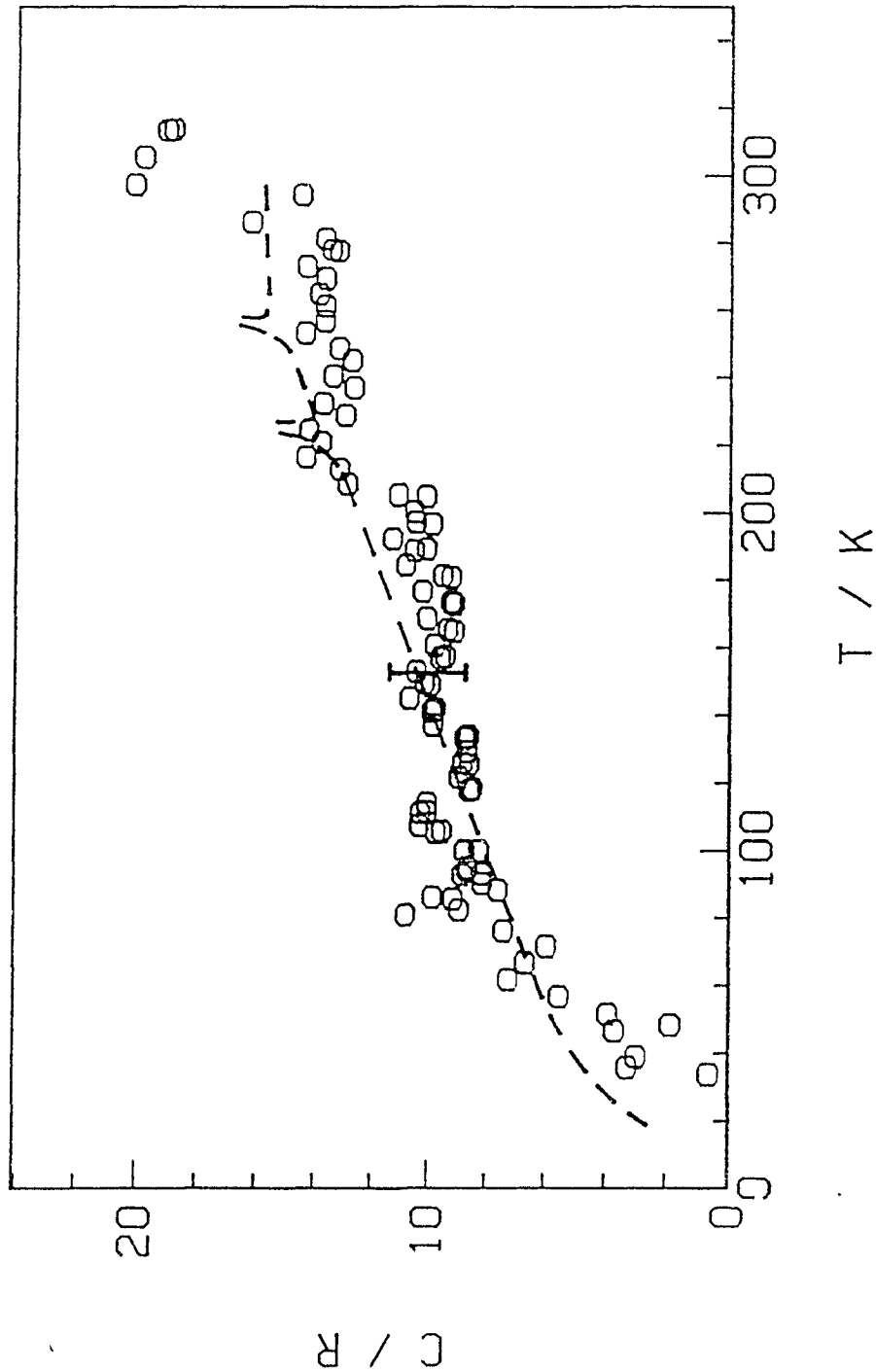

Figure 5.4

contributions. It is known from the NQR study of the CCl_4 clathrate of Dianin's compound that the librational frequencies of the CCl_4 molecule are very low (37 and 47 cm^{-1}),[87] consistent with full thermal excitation (heat capacity plateau) above about 100 K. At lower temperatures, the single-molecule heat capacity is considerably less than that of bulk CCl_4, indicating, within the constraints of the assumption of additivity of the guest and host contributions to the heat capacity, that there are fewer low-frequency modes associated with CCl_4 in the clathrate relative to bulk CCl_4.

The molar heat capacity of the ethanol dimer, again calculated assuming additivity of the guest and host contributions, is illustrated in Figure 5.5. For comparison, the heat capacity of bulk ethanol[88] is illustrated also (dashed curve). In contrast with the heat capacity of CCl_4, the heat capacity of the ethanol dimer is considerably different from the bulk solid. However, the match is closer above the melting point of pure ethanol. It appears that the heat capacity of the ethanol dimer is much more liquid-like than that of CCl_4 enclathrated in Dianin's compound. It is interesting to note here that the properties of the tetrahydrofuran molecules in the tetrahydrofuran clathrate hydrate have been described as "a glass in a crystalline matrix";[29] the investigation of the degrees of freedom of the ethanol dimer in the ethanol

Figure 5.5 The molar heat capacity of an ethanol molecule in the ethanol adduct of Dianin's compound. The dashed line indicates the molar heat capacity of bulk ethanol,[88] including its solid-liquid transition at T = 158.5 K. The error bar at T = 150 K represents the error in the molar heat capacity of the ethanol molecule in the clathrate, as propagated from an error of ±0.5% in the heat capacity of unsolvated Dianin's compound and ±0.5% in the ethanol adduct of Dianin's compound. R=8.314 J K^{-1} mol^{-1}.

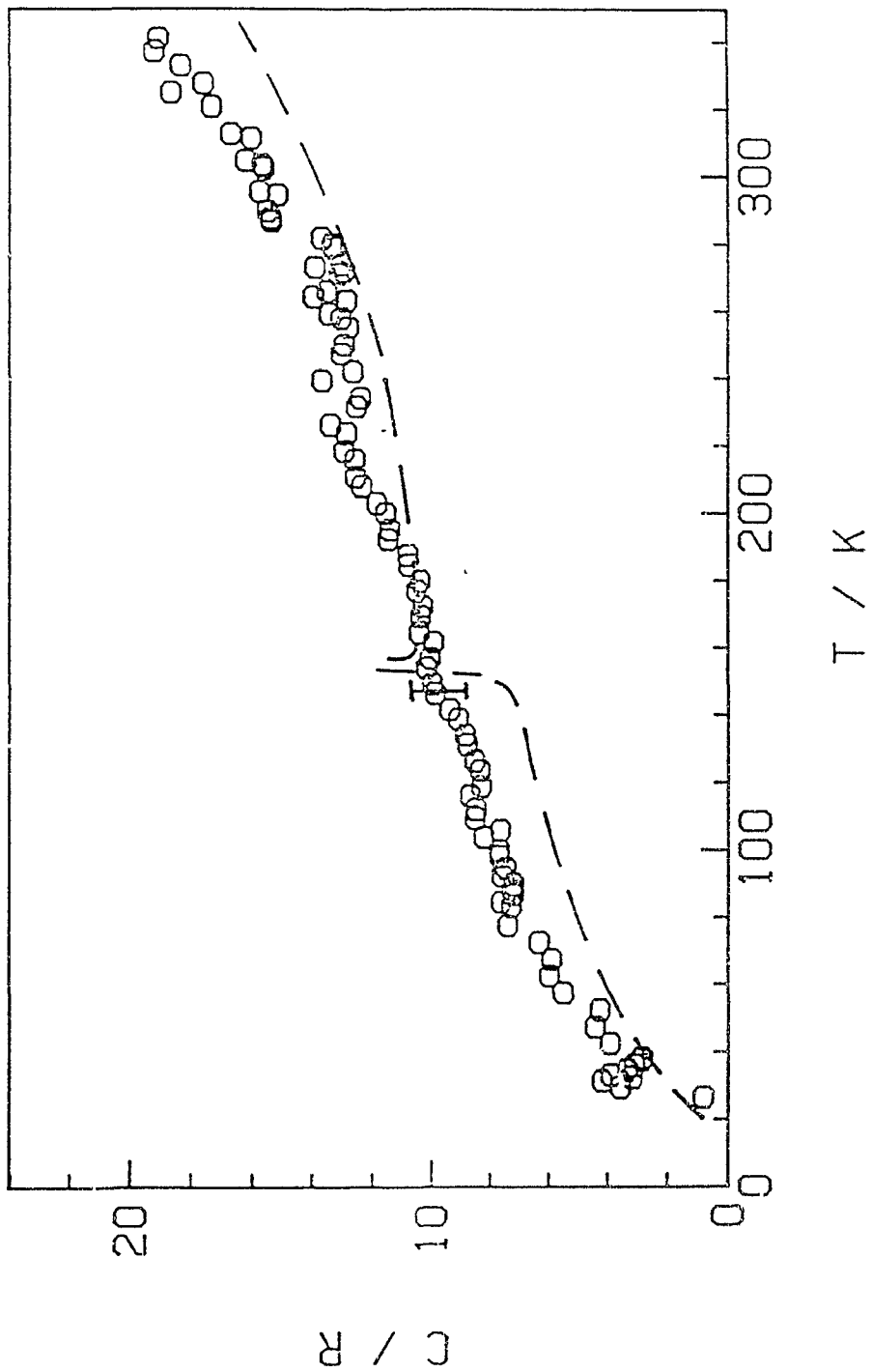

Figure 5.5

adduct of Dianin's compound deserve further attention.

Based on the simple model of guest-host heat capacity additivity, the combined investigations of the CCl_4 and ethanol adducts allow the conclusion that the number of guest molecules in the cage does not determine whether or not the properties of the guest(s) are bulk-like: the single CCl_4 is more like the bulk than is the ethanol dimer. It would be of interest to see whether placement of a second CCl_4 molecule in the cage (the thiol analogue of Dianin's compound permits this[55]) changes this result.

5.6 Contribution to The Proton Disorder

From recent ^2H nmr investigations of single crystals of the ethanol adduct of Dianin's compound it is known[89] that the phenolic hydrogen in the hydrogen-bonded ring are moving rapidly at room temperature. Within a given hexamer ring, the oxygen atoms either have their closer protons to the left or to the right, as shown schematically in Figure 5.6. Because the protons can hop at a rapid rate between the position on the left and on the right (the nmr experiment[89] showed this hopping to be concerted), there are two positional potential minima for each proton. The hexamer ring is not quite planar, which means that the minima are not quite at the same level (Figure 5.6).

The situation for these protons is then very similar to

that for protons in ice, where there are a number of positional minima that can all be experienced if there is sufficient thermal energy. In ice, at lower temperatures the protons freeze into positions randomly, giving a proton orientational glass. Warming from these low temperatures then gives rise to a glass phase transition as seen for example in heat capacity of hexagonal ice.[90]

In the case of H_2O, the glass phase transition gives rise to a step in heat capacity of about 0.3 J K^{-1} mol^{-1} at T=110 K.[90] There should be a similar effect in Dianin's compound and all its adducts at, judging from the nmr experiments,[89] a temperature near 145 K. Due to the contributions from the large Dianin's molecule, this would make the glassy transition contribution less than 0.1% of the total heat capacity for of the measured Dianin's compounds. Most unfortunately, this contribution is too small to be seen in the present results.

Figure 5.6 (a) The hexagons formed by the phenolic oxygens in Dianin's compound, in the a b plane. The oxygens sit alternately 0.143 Å above and below this plane, as indicated by "+" and "-". The deuterons jump between majority (D) and minority (D′) sites.[89]
(b) The positional potential of the phenolic hydrogens in Dianin's compound.
E_a=(33.1±1.0) kJ/mol; ΔE=(3±1) kJ/mol.[89]

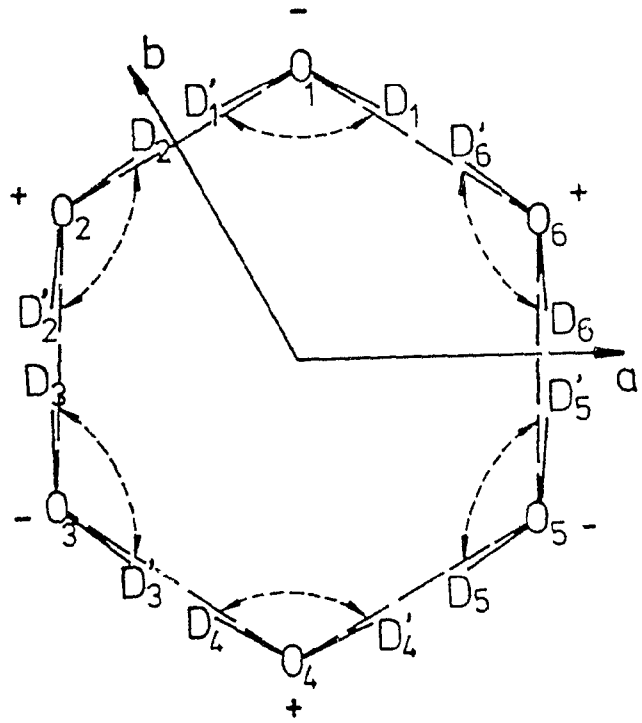
b
a
-
+
+
-
-
+
O_1
O_2
O_3
O_4
O_5
O_6
D_1
D_1'
D_2
D_2'
D_3
D_3'
D_4
D_4'
D_5
D_5'
D_6
D_6'

(a)

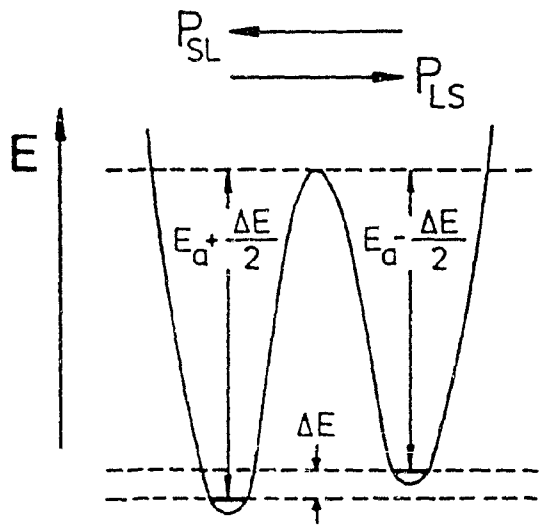
P_{SL}
P_{LS}
E
$E_a + \frac{\Delta E}{2}$
$E_a - \frac{\Delta E}{2}$
ΔE

(b)

Figure 5.6

Chapter 6: Thermal Expansion of Dianin's Adducts

6.1 Introduction and Theory

To describe heat capacity, the harmonic approximation has been used (see section 5.1). However this approximation causes certain consequences, namely: the heat capacity becomes constant at high temperatures; the specific heat measured at constant pressure and constant volume are equal; there is no thermal expansion; since there are no collisions between phonons, their mean free paths and lifetimes are infinite; consequently a perfectly harmonic crystal would have an infinite thermal conductivity; the force constants and hence the elastic constants are independent of temperature and pressure; the line width of the infrared absorption peaks and of the Raman, Brillouin and inelastic neutron scattering peaks would be zero for perfectly ordered harmonic crystals.[91]

The equations of motion for an anharmonic linear chain with nearest neighbour interaction are:

$$m\ddot{u}_\ell = f[(u_{\ell+1}-u_\ell)-(u_\ell-u_{\ell-1})]+g[(u_{\ell+1}-u_\ell)^2-(u_\ell-u_{\ell-1})^2]/2+ \\ +h[(u_{\ell+1}-u_\ell)^3-(u_\ell-u_{\ell-1})^3]/6+\ldots \qquad (6.1.1)$$

where u_ℓ is a displacement of an atom ℓ, and f, g, h, are force constants. The linear monatomic chain and interaction

energy of two neighbouring atoms are shown in Figure 6.1.[91]

For the harmonic chain the higher order force constants, g and h are exactly zero. By considering non-linear terms in equations of motion and by using quasiharmonic and higher approximations, the thermal expansion and phonon-phonon interaction can be qualitatively described. The above can be expressed by a combination of g and f force constants. Expanding the model to three dimensions produces, for an isotropic medium, the non-zero volume thermal expansion, α_v:

$$\alpha_v = \frac{1}{V}\frac{dV}{dT} \quad , \qquad (6.1.2)$$

a relationship between C_p and C_v (see equation 5.1.2) and the Grüneisen relation:

$$\alpha_v(T) = \frac{\gamma}{3VB} C_v(T) \qquad (6.1.3)$$

where B is bulk modulus ($=1/\chi^T$) and γ is the Grüneisen parameter. The mode-independent Grüneisen parameter in the Debye approximation is defined as:

$$\gamma_D = \frac{V}{\omega_D}\frac{\partial \omega_D}{\partial V} = \frac{V}{\theta_D}\frac{\partial \theta_D}{\partial V} \quad . \qquad (6.1.4)$$

Figure 6.1 a) Linear monatomic chain at T=0 with lattice spacing a_0. b) Chain at temperature T with lattice spacing a(T). c) Interaction energy of two neighbouring atoms at positions r_ℓ and $r_{\ell-1}$. $w_{0,\ell}$ and w_ℓ are the relative displacements with respect to a_0 at T=0 and a(T), respectively.[91]

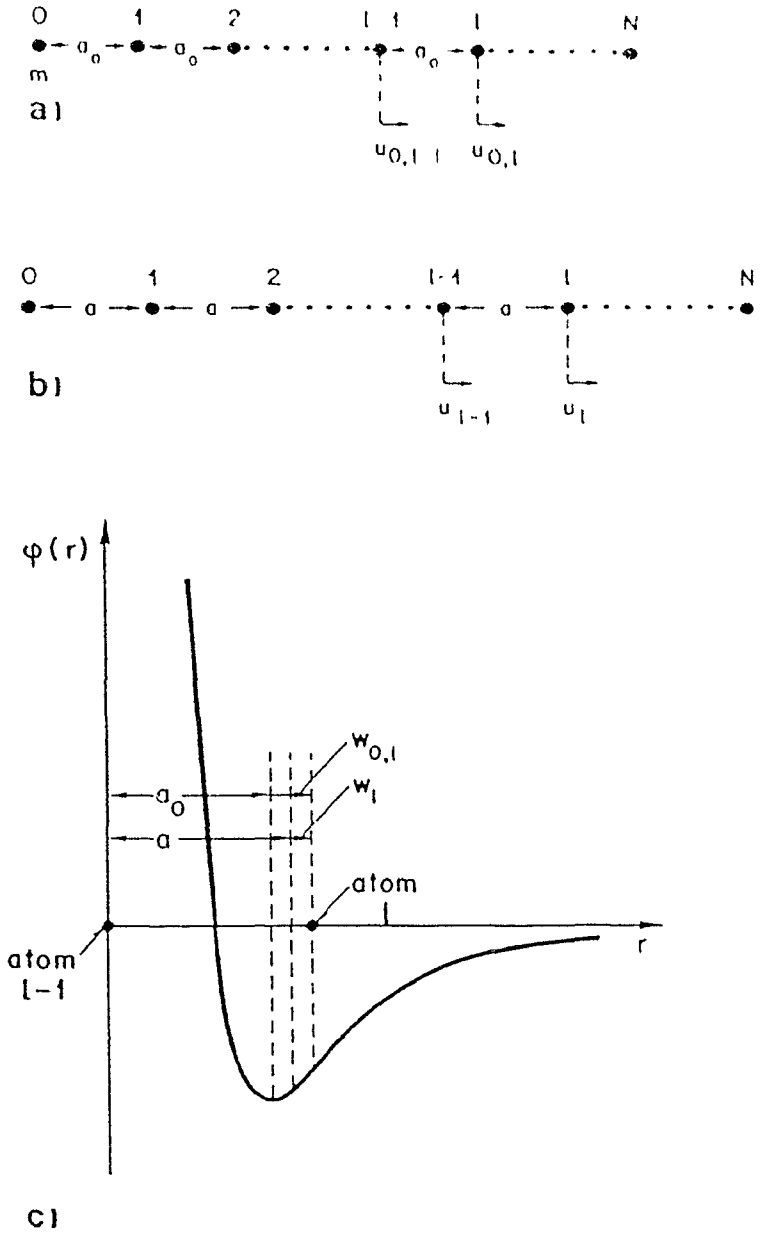

Figure 6.1

6.2 Results and Discussion

The X-ray powder diffraction pattern for unsolvated Dianin's compound and the ethanol and CCl_4 adducts were measured with the recently-developed Guinier diffractometer, using Ge-monochromatized Cu $K\alpha_1$ radiation. The temperature was varied from 10 to 300 K, and was maintained with a closed cycle helium refrigerator. The temperature was measured to ± 2 K with a silicon diode temperature sensor in intimate contact with the sample holder. The powder samples were sieved onto the silicone-moistened aluminized foil of the specimen holder. The diffractograms were recorded with a step width of 0.01° and a count time of 4 s per step in the range $4° < q < 24°$. A detailed description of the set-up is given elsewhere.[92]

Since the unit cell is trigonal ($R\bar{3}$, Z=18) for all three compounds examined, the **a**- and **c**-axes are the only independent lattice parameters considering the hexagonal setting of the unit cell. The lattice parameters were determined by least squares fit of the most intense reflections unambiguously associated with indices **hkl**. In the case of the unsolvated Dianin's compound and carbon tetrachloride adduct 11 reflections were monitored. For the ethanol adduct 10 reflections were monitored. The standard deviation of the fit was less than 0.04% for **a**, and 0.09% for **c**.

The results can be compared with the "room temperature" single crystal X-ray diffraction investigation of the ethanol adduct of Dianin's compound.[54] Assuming the temperature of that determination to be 20°C, their results and these fall within the quoted error limits (**a**: 26.969±0.002 Å,[54] 26.979±0.010 Å from present study; **c**: 10.990±0.002 Å,[54] 10.983±0.010 Å from present study; V: 6921±2 $Å^3$,[54] 6923±5 $Å^3$ from present study). Interpolation of the powder data of CCl_4 adduct to T = 293 K gives lattice parameters **a** = 27.143±0.009 Å, **c** = 10.928±0.008 Å in excellent agreement with those from the single crystal work,[57] **a** = 27.134±0.008 Å, **c** = 10.933±0.002 Å. The lattice parameters of unsolvated Dianin's compound were determined from the single crystal work[58] at 213 K and from the powder work and are in reasonable agreement (**a**: 26.874±0.003 Å from the single crystal work, 26.848±0.008 Å from the powder work; **c**: 10.897±0.003 Å from the single crystal work, 10.902±0.006 Å from the powder work).

The lattice parameters for the xenon clathrate of Dianin's compound have been determined,[93] and these are in the same general range as the present values. (However, the calculated density given[93] for the hypothetical empty clathrate based on the xenon data (1.29 g cm^{-3}) is in error; it should be 1.161 g cm^{-3} from their data. The calculated density for the empty clathrate at 20°C, based on this

determination of its lattice parameters, is 1.168±0.004 g cm^{-3}, in good agreement with 1.165±0.006 g cm^{-3} from Ref.54.)

The experimental values of the lattice parameters for the "empty", ethanol and carbon tetrachloride clathrates of Dianin's compound along the **a** and **c** directions are illustrated in Figures 6.2 and 6.3, respectively. Figure 6.4 illustrates the total volumes of the unit cells as a function of temperature. The error bars shown in the figures correspond to one standard deviation in the least squares fit to the diffractogram at that temperature.

Immediately apparent from Figure 6.3 is the expansion of the **c**-axis to accommodate the ethanol guest molecules. On the other hand, the **a**-axis is increased due to the ethanol guest molecules only above about 200 K (Figure 6.2). Xe guest causes about 0.3% increase in the **a**-axis and 0.2% reduction in the **c**-axis at room temperature.[93] CCl_4 as a guest in Dianin's compound causes about 0.6% increase in **a** and insignificant changes to **c** throughout the region from 10 to 300 K (Figures 6.2 and 6.3). One of the differences between the CCl_4 adduct and the ethanol adduct is that the latter has a dimer guest in the cage. As was shown with the single crystal work,[57] CCl_4 has only one guest per cage. The lack of expansion along the **c**-axis in the CCl_4 adduct, relative to the expansion caused by the ethanol guest dimer, may be due to "free" space in the unoccupied half the cage

Figure 6.2 The lattice rameter of the empty (open circles), ethanol (filled circles) and carbon tetrachloride (triangles) adducts of Dianin's compound along the **a**-axis as a function of temperature.

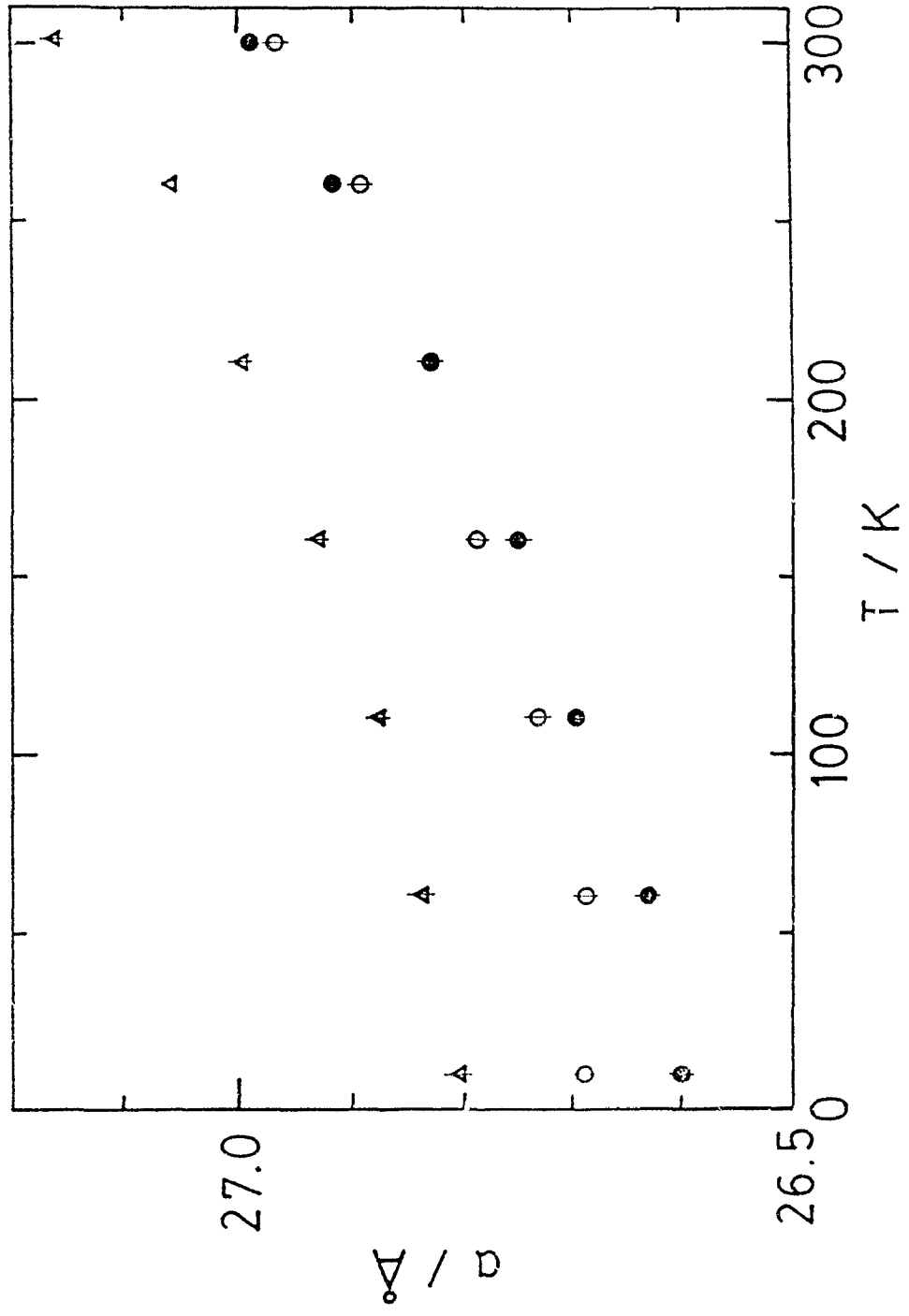

Figure 6.2

Figure 6.3 The lattice parameter of the empty (open circles), ethanol (filled circles) and carbon tetrachloride (triangles) adducts of Dianin's compound along the c-axis as a function of temperature.

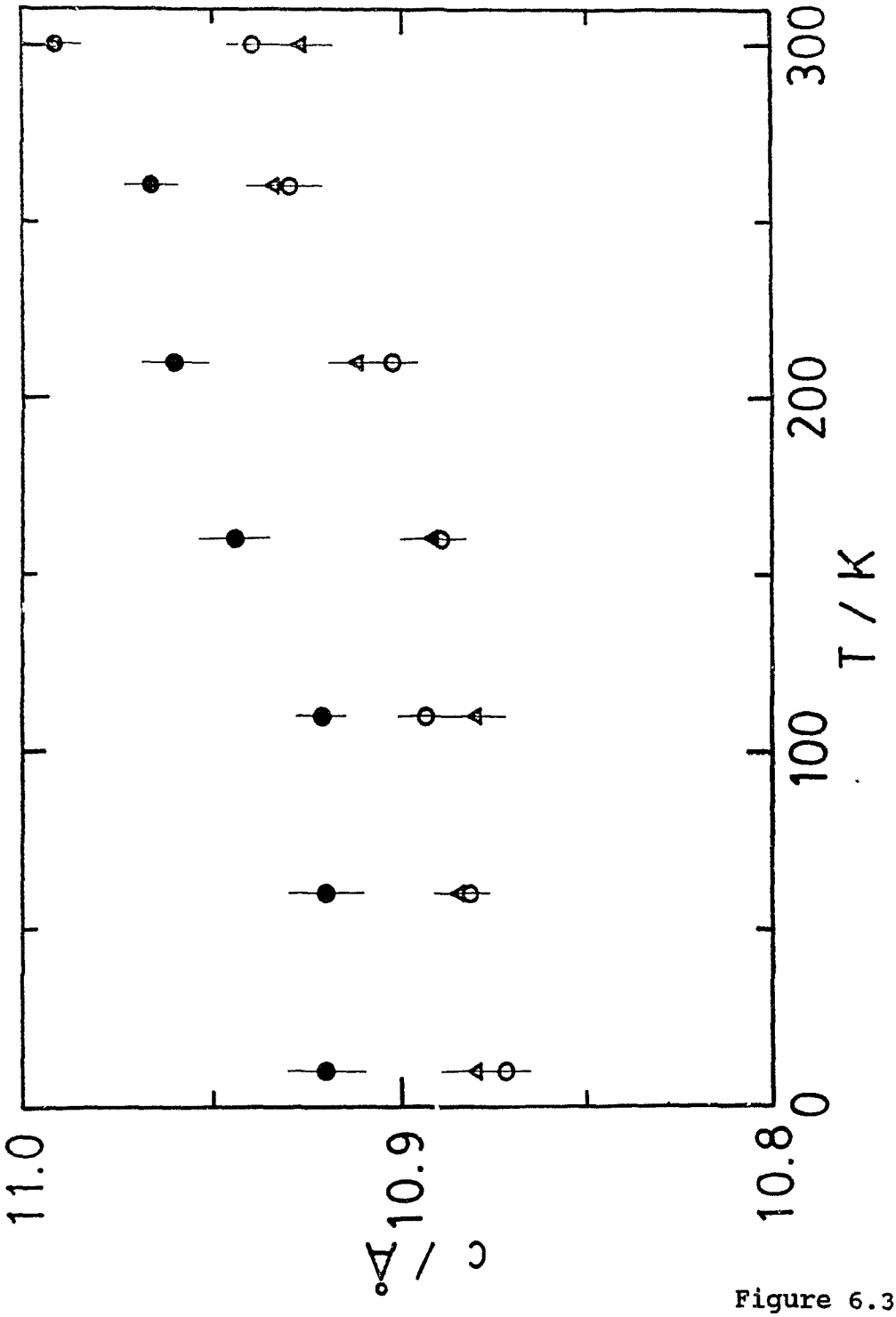

Figure 6.3

Figure 6.4 The unit cell volume of the empty (open circles), ethanol (filled circles) and carbon tetrachloride adducts (triangles) of Dianin's compound as a function of temperature.

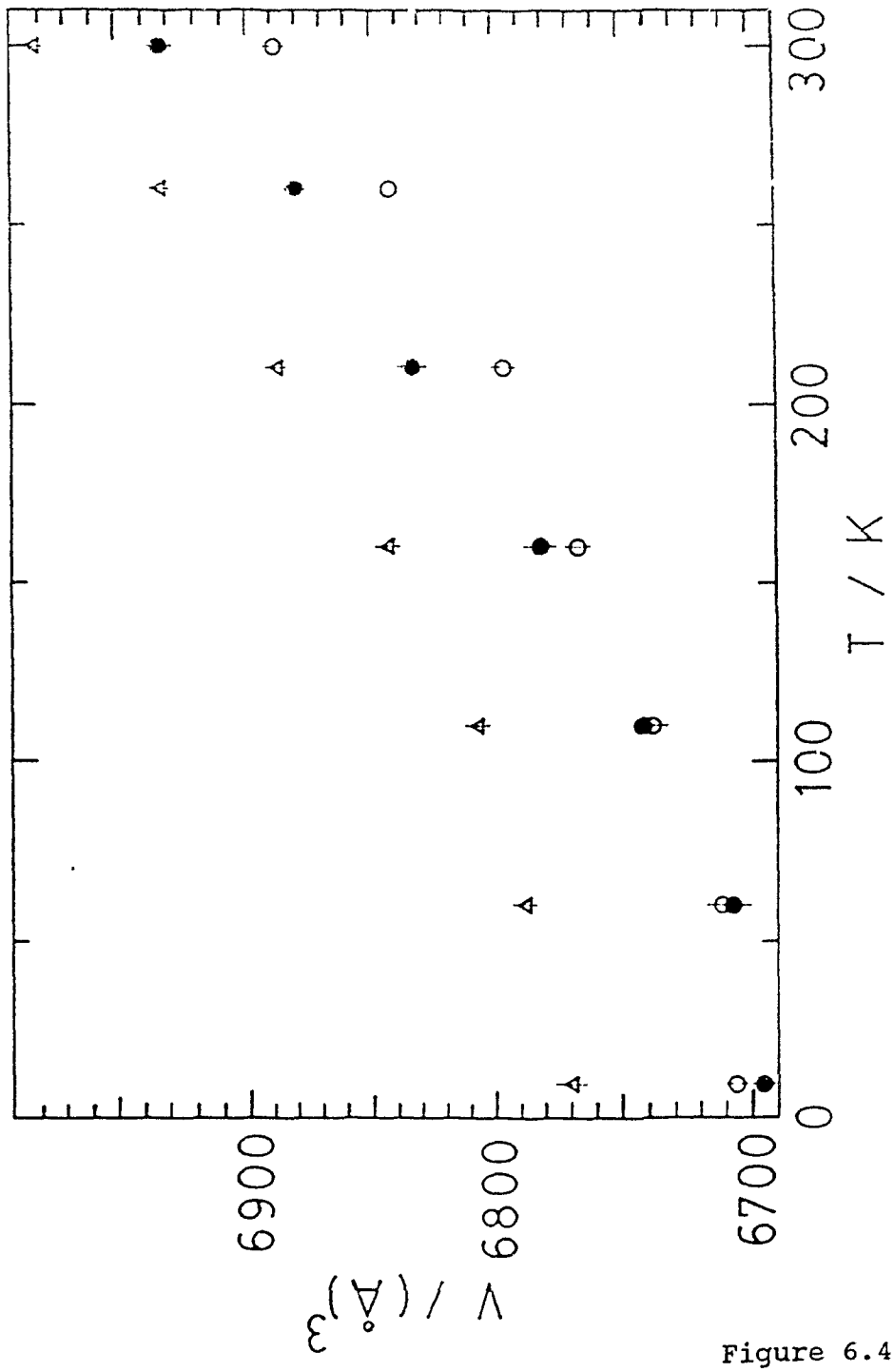

Figure 6.4

of the host lattice in the CCl_4 adduct. From this information it appears that the presence of a guest in Dianin's compound can cause anisotropic increases and decreases in the host lattice parameters, depending on the temperature range and type of guest.

Except in the ethanol adduct below about 100 K (Figure 6.4), where the volume is essentially that of the empty lattice, all the above-cited examples show increased over ll volume of the unit cell in the presence of a guest.

The lattice parameters for both the unsolvated Dianin's compound and the ethanol adduct were fitted by least squares to polynomials. For **a** and V the most physical fits were given for fourth-order polynomials, whereas for **c** a second-order polynomial was used. The coefficients of thermal expansion, α_i ($\alpha_i = i^{-1}\, di/dT$, i = **a**, **c**, V) were calculated as a function of temperature from the polynomials fitted to the lattice constants. The thermal expansion coefficients for the unsolvated clathrate and the ethanol and CCl_4 adducts along the **a**-direction (α_a) are shown in Figure 6.5. In graphical form the α_c values are not easily distinguished for the empty and ethanol adducts, so instead **c**-axis thermal expansions at selected temperatures are given Table 6.1.

Figure 6.5 Linear thermal expansion coefficients for unsolvated Dianin's compound (solid line, open circles), carbon tetrachloride (dashed dotted line, triangles) and its ethanol adduct (dashed line, closed circles) as a function of temperature in the **a**-direction, as derived from the least-squares fits to **a**. Points were obtained directly from changes in **a** at neighbouring temperatures.

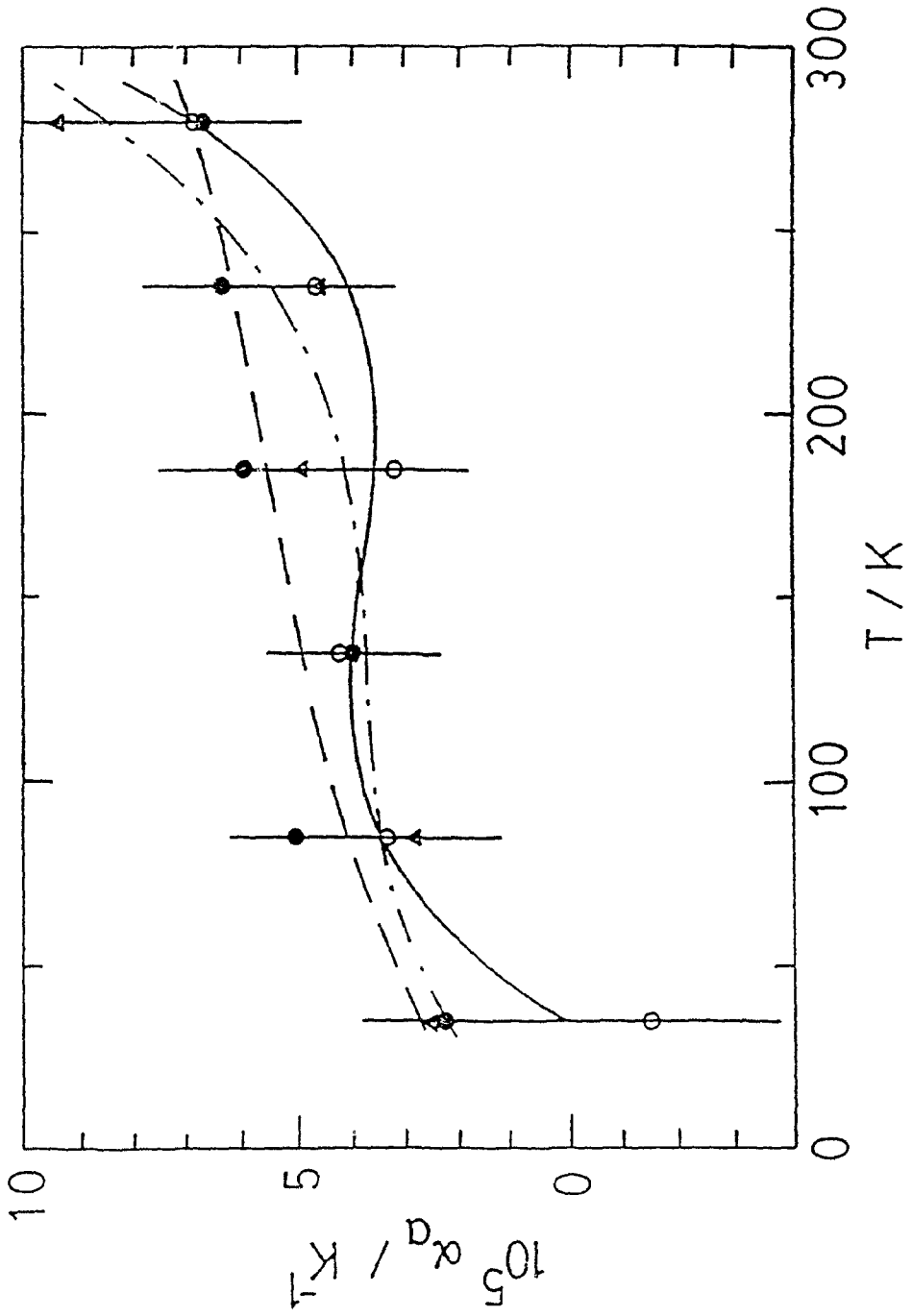

Figure 6.5

Table 6.1. The thermal expansion of the unsolvated Dianin's compound and its ethanol and carbon tetrachloride adducts along the **c**-axis at selected temperatures.

T / K	$10^5\ \alpha_c$ / K^{-1}		
	unsolvated	ethanol	CCl_4
50	0.9±0.5	0.3±0.3	0.7±0.5
100	1.4±0.3	1.5±0.5	1.2±0.5
150	2.0±0.3	2.2±0.8	1.8±0.8
200	2.6±0.8	2.3±0.6	2.3±0.8
250	3.1±0.7	3.6±0.4	2.8±0.8
300	3.7±0.6	4.3±0.6	3.3±0.8

Figure 6.6 shows the overall volume thermal expansion (α_V) for unsolvated Dianin's compound and its ethanol and CCl_4 adducts. The points in Figures 6.5 and 6.6 are calculated directly from the differences in measured lattice parameters at neighbouring temperatures. All the thermal expansion coefficients are positive, except perhaps along the **c**-axis at low temperatures (slope in Figure 6.3 *ca.* 100 K).

From Figure 6.5 and Table 6.1 it can be seen that at all temperatures investigated, the thermal expansion in all investigated clathrates of Dianin's compound along the **a**-axis is equal to or, more usually, greater than along the **c**-axis. This indicates greater anharmonicity in the **a**-direction.

Most important for the purpose of this investigation is the comparison of the magnitudes of the thermal expansion for Dianin's compound with and without its guest. Table 6.1 shows that the thermal expansion along the **c**-axis is only marginally greater in the presence of the ethanol guest than it is without the guest. The thermal expansion along **c** is slightly decreased by the presence of the CCl_4 guest. However, the thermal expansion along the **a**-axis for the ethanol adduct is appreciably greater than for the unsolvated clathrate of Dianin's compound throughout the temperature region examined (Figure 6.5). In comparison

Figure 6.6 Volume thermal expansion coefficients for unsolvated Dianin's compound (solid line, open circles), carbon tetrachloride (dashed dotted line, triangles) and its ethanol adduct (dashed line, closed circles) as a function of temperature, as derived from the least-squares fits to the volume. Points were obtained directly from changes in the volume at neighbouring temperatures.

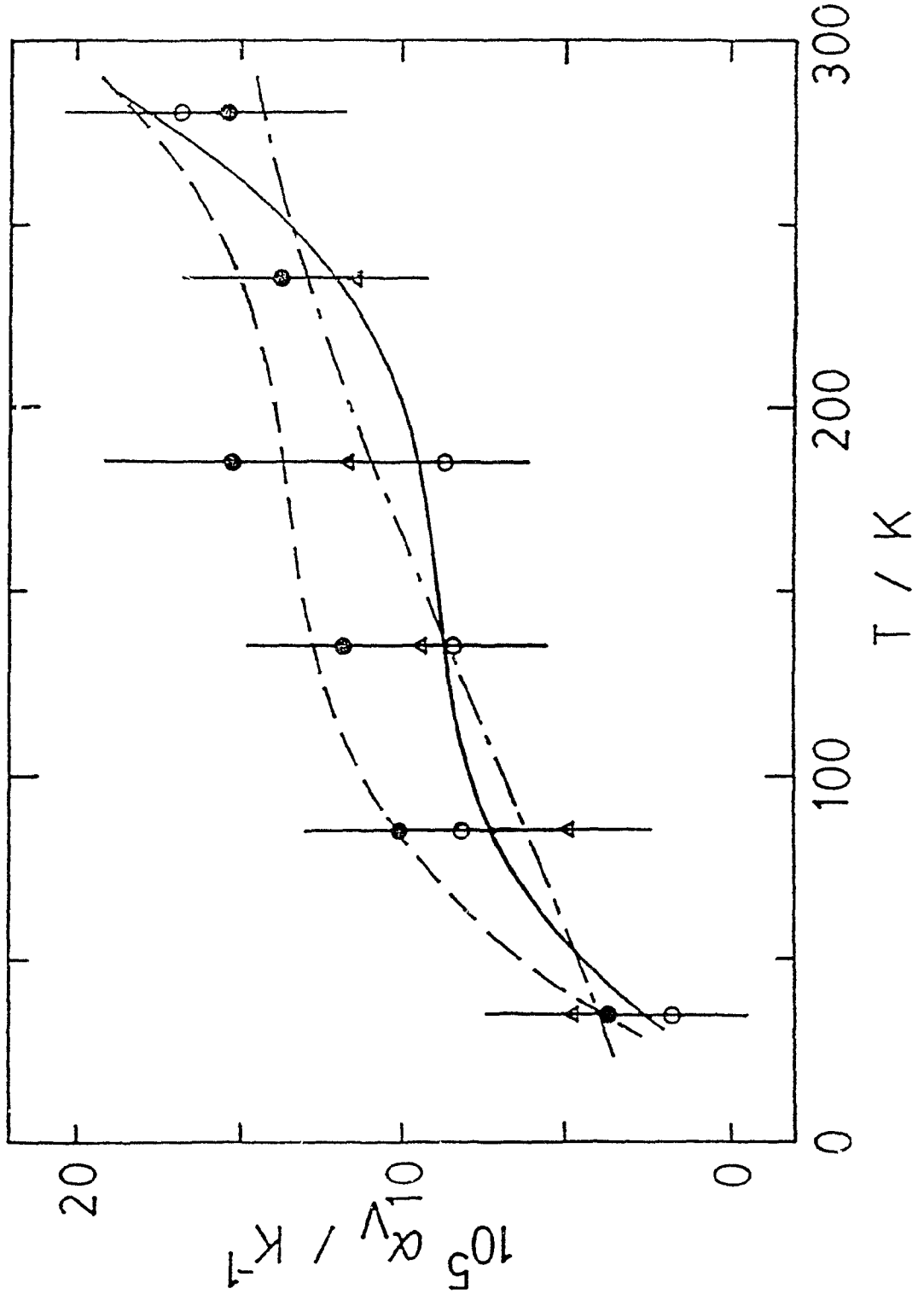

Figure 6.6

with the empty host lattice, α_a is larger for the CCl_4 adduct only for T<100 K and T>200 K; in the intermediate temperature region α_a is essentially the same with and without the CCl_4 guest. The same trends are observed in α_V (Figure 6.6) due to the dominance of the **a**-axis in the overall thermal expansion ($\alpha_V = 2\alpha_a + \alpha_c$).

It is interesting to note that, as for the clathrate hydrates,[94,95] the thermal expansion of the occupied Dianin host lattice is considerably greater than the empty lattice at low temperatures, but this difference decreases as the temperature increases. α_a and α_V for the CCl_4 adduct of Dianin's compound are smaller than for the ethanol adduct throughout the temperature region examined, *i.e.* the CCl_4 adduct is intermediate in thermal expansion between the empty host lattice and the ethanol adduct.

Since it was possible to carry out experimental investigations of lattices with the same structure, differing only in the presence or absence of guest species, it is reasonable to state that the thermal expansion results are not due to structural differences or to the openness of the lattice. As surmised from the theoretical studies of clathrate hydrates,[94,95] the observed increased thermal expansion is an experimental manifestation of increased anharmonicity due to the presence of the guest in the clathrate.

Chapter7: Brillouin Scattering

7.1 Introduction and Theory

A homogeneous stress and a homogeneous strain are each specified, in general, by a second-rank tensor. It is found that, if a general homogeneous stress, σ_{kl}, is applied to a crystal, the resulting homogeneous strain, ϵ_{ij}, is such that each component is linearly related to all the components of the stress. The generalized form of Hooke's law may be written:[96]

$$\epsilon_{ij}=s_{ijkl}\ \sigma_{kl} \qquad (7.1.1)$$

where s_{ijkl} are the compliancies of the crystal. As an alternative the above equations can be expressed in terms of strains:

$$\sigma_{ij}=c_{ijkl}\ \epsilon_{kl} \qquad (7.1.2)$$

where c_{ijkl} are the 81 stiffness constants of the crystal. c_{ijkl} and s_{ijkl} are fourth rank tensors which fulfil the following relationship:

$$s_{ijkl}=s_{jilk} \qquad (7.1.3)$$

which reduces the number of independent components from 81 to 36.

The components (u_i) of the displacement $\vec{u}$ of an elemental volume of density ρ satisfy the following differential equation: [97]

$$\rho\ddot{u}_i=c_{ijkl}\frac{\partial^2 u_l}{\partial x_j \partial x_k} \qquad (7.1.4)$$

with respect to time and Cartesian coordinates x_i. With the solution in the form of plane sinusoidal waves, equation (7.1.4) becomes:

$$\rho v^2 u_i=\Gamma_{il}u_l \qquad (7.1.5)$$

where v is the phase velocity and

$$\Gamma_{il}=c_{ijkl}\ q_j q_k \quad . \qquad (7.1.6)$$

The matrix Γ_{il} is symmetric with respect to an interchange of the subscripts and q_j, q_k are the direction cosines of the unit vector normal to the wave plane.

Using the more convenient, contracted (two-index), Voigt notation the elements of Γ_{il}, are in detail:[98]

$$\Gamma_{11}=q_1^2c_{11}+q_2^2c_{66}+q_3^2c_{55}+ \qquad (7.1.7)$$
$$2(q_1q_2c_{16}+q_1q_3c_{15}+q_2q_3c_{56})$$

$$\Gamma_{12}=q_1^2c_{16}+q_2^2c_{26}+q_3^2c_{45}+q_1q_2(c_{12}+c_{66}) \qquad (7.1.8)$$
$$+q_1q_3(c_{14}+c_{56})+q_2q_3(c_{25}+c_{46})$$

$$\Gamma_{13}=q_1^2c_{15}+q_2^2c_{46}+q_3^2c_{35}+q_1q_2(c_{14}+c_{56}) \qquad (7.1.9)$$
$$+q_1q_3(c_{13}+c_{55})+q_2q_3(c_{36}+c_{45})$$

$$\Gamma_{22}=q_1^2c_{66}+q_2^2c_{22}+q_3^2c_{44} \qquad (7.1.10)$$
$$+2(q_1q_2c_{26}+q_1q_3c_{46}+q_2q_3c_{24})$$

$$\Gamma_{23}=q_1^2c_{56}+q_2^2c_{24}+q_3^2c_{34}+q_1q_2(c_{25}+c_{46}) \qquad (7.1.11)$$
$$+q_1q_3(c_{36}+c_{45})+q_2q_3(c_{23}+c_{44})$$

$$\Gamma_{33}=q_1^2c_{55}+q_2^2c_{44}+q_3^2c_{33} \qquad (7.1.12)$$
$$+2(q_1q_2c_{45}+q_1q_3c_{35}+q_2q_3c_{34}).$$

For a non-trivial solution of equation (7.1.5) it is required that the Christoffel determinant vanishes, *i.e.*,

$$|\Gamma_{ij} - \rho v^2\delta_{ij}|=0 \qquad (7.1.13)$$

where δ_{ij} is Kronecker delta.

Brillouin scattering involves two photons, one incident and one scattered. In both Stokes (photon emission) and Anti-Stokes (photon absorption) effects a photon is scattered inelastically by a crystal, as shown in Figure 7.1. The process is called Brillouin scattering when an

Figure 7.1 Brillouin scattering of a photon with emission (Stokes process) or absorption (Anti-Stokes process) of an acoustic phonon.[43]

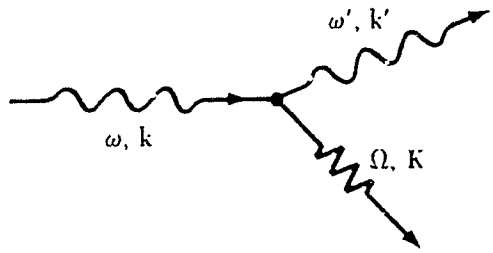

Stokes

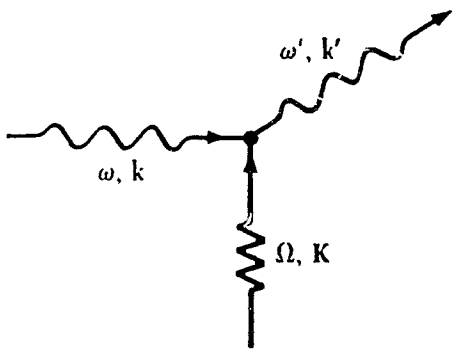

Anti-Stokes

Figure 7.1

acoustic phonon is involved. The wavevector selection rules for the first-order Brillouin effect are

$$\omega = \omega' \pm \Omega \qquad (7.1.14)$$

and

$$k = k' \pm K \qquad (7.1.15)$$

where ω and k refer to the incident photon, ω' and k′ refer to the scattered photon, and Ω and K, refer to the phonon created or destroyed in the scattering event.

Brillouin spectroscopy is a very effective and sensitive method for investigation of the elastic properties of crystals. Phonon velocities, v, can be calculated directly from the Brillouin shifts, $\Delta\nu$, using the Brillouin equation:[97]

$$\Delta\nu=\nu_0(v/c)(n_i^2+n_s^2-2n_in_s\cos\theta)^{1/2} \qquad (7.1.16)$$

where ν_0 is the frequency of the laser radiation, c is the velocity of light in vacuum, n_i and n_s are the refractive indices of the incident and scattered light respectively, and θ is the scattering angle. The elastic constants can be determined from the solution of the secular equation of motion,[99] (7.1.13), for different directions in the crystal lattice.[97]

7.2 Determination of Elastic Constants

As discussed in the previous section, the experimental Brillouin shifts can be related directly to the elastic constants of a solid through the Christoffel equation (equation (7.1.13)). The most common way to solve the Christoffel equation is to start with simple directions that give linear relationships between the elastic constants and phonon velocities; this is limited to the results of only a very few simple acoustic wave propagation directions. Subsequently results from more complex directions can be added to determine the remaining elastic constants. This method has some disadvantages, especially the requirement of simple directions in the crystal lattice. Also, experimental errors in the determination of sound velocity accumulate in the calculation of the later elastic constants.

Since Dianin's compound and its known adducts crystallize in such a low symmetry space group, $R\bar{3}$ in the trigonal system,[54,55] the elastic constant tensor in the two-suffix matrix notation reduces to seven independent components.[96] For such a system, obtaining the elastic constants directly from the phonon velocities can lead to ambiguous results or even simultaneous equations with no unique solution.

In order to solve the Christoffel equation for the

present results a proven[100,101] minimization procedure was used.[102] The algorithm consists of an iterative optimization procedure which fits all elastic constant tensor elements simultaneously to previously calculated sound velocities.[103] In each iteration the Christoffel (7.1.13) equations are solved for ρv^2_{calc}. The weighted sum of the squares of the differences between these values and the corresponding ρv^2_{obs} is calculated, and then minimized by systematically varying the elastic constants until the fit is optimized. This approach provides a superior method for determination of the complete set of elastic constants, especially since it does not rely on special directions, and it does not propagate errors. In addition the accuracy of the results improves with increasing the number of investigated directions. In the case of the $R\bar{3}$ space group of the ethanol adduct of Dianin's compound, which gives no unique analytical solution to the Christoffel equation, this method was the only tractable approach to determine the elastic constants.

7.3 Sample Preparation

Brillouin scattering was carried out for the ethanol adduct of Dianin's compound at room temperature. The experiments were limited to that material due to the size of single crystal required. The crystals were oriented using a precession camera which showed that the **c**-axis was along well-formed edges of the crystals. Weissenberg photography showed that the **a**-axis was perpendicular to two very well-formed crystal faces. Since the elastic constant tensor is defined in the Cartesian frame of reference a set of axes was assigned to the crystals using Standards on Piezoelectric Crystals.[96] The x, y, z, reference axes are shown in Figure 7.2.

Samples of five different orientations were cut out of the best crystals using a wire saw manufactured by South Bay Technology Inc. and wire blade of diameter ~.02 mm. Cutting accuracy was ±0.5°. Later the samples were polished using silicon carbide (grain sizes 600 to 1600) to produce transparent parallelepipeds. The measurements were taken on seven different crystals, of typical dimensions 5mm x 5mm x 5mm.

The refractive indices n_x, n_y and n_z (along x, y, z, reference axes) of the ethanol adduct of Dianin's compound were determined by comparison with standard liquids (Cargille Laboratories) of known refractive indices:

Figure 7.2 The hexagonal unit cell of Dianin's compound (hydrogens are excluded for clarity). The axes shown illustrate the Cartesian reference frame used for Brillouin scattering experiment. The crystallographic **c**-axis is collinear with the Cartesian z-axis and points out of the surface of the picture.

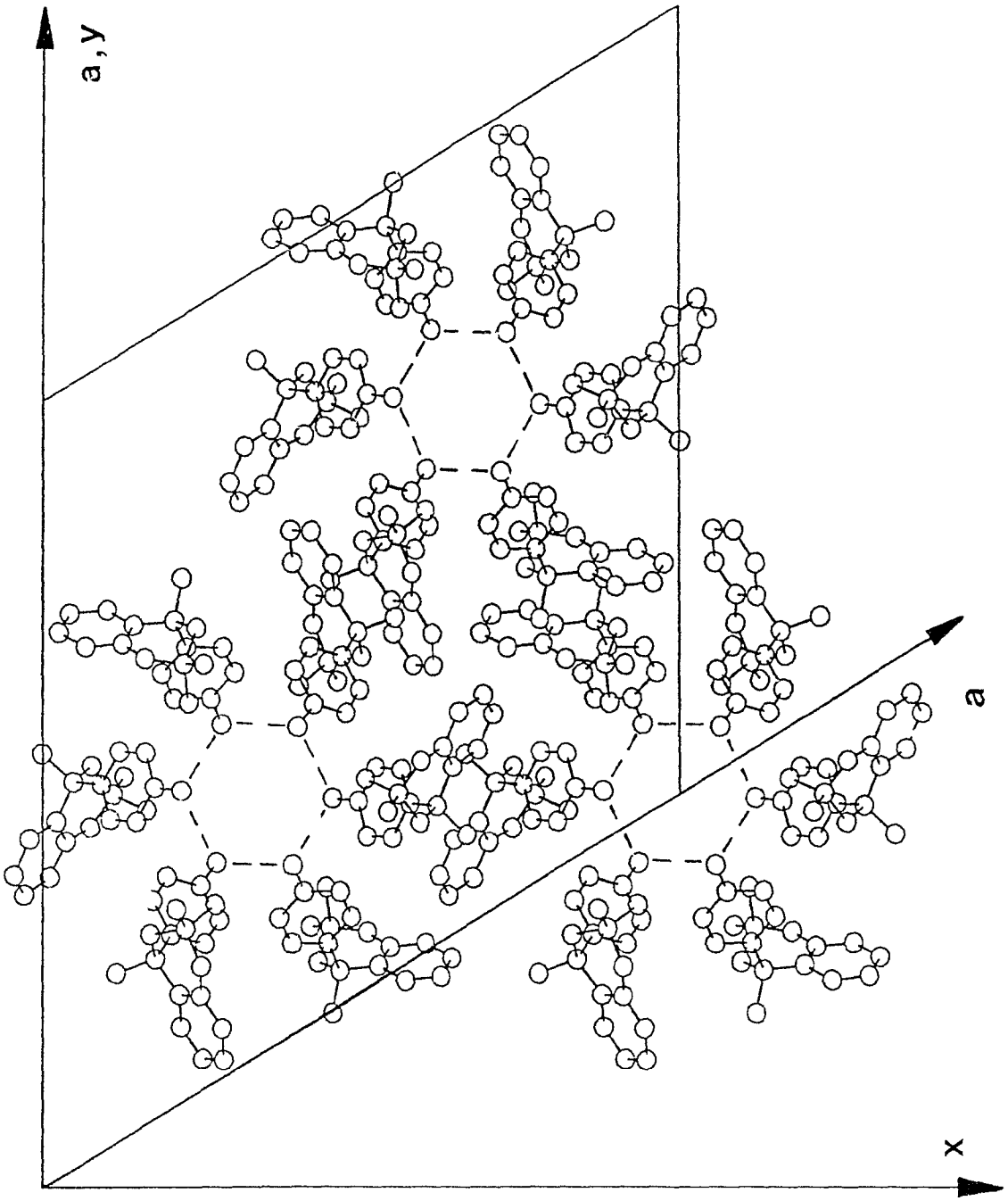

Figure 7.2

$n_x=n_y=1.640\pm0.001$ and $n_z=1.641\pm0.001$.

7.4 Apparatus

The Brillouin spectrometer used in these experiments has been described in detail elsewhere,[103] and is shown schematically in Figure 7.3. The incident light source was provided by a single-mode argon laser (Spectra Physics 2020-03) operating at a wavelength of 514.5 nm and filtered to a power of 30 or 50 mW. The scattered light was analyzed at 90° using a triple-pass piezoelectrically scanned Fabry-Perot interferometer (Burleigh RC 110) utilizing free spectral ranges (FSR) of 21.80, 26.95, and 31.66 GHz. The free spectral ranges were determined by examining a single crystal of quartz of known Brillouin shifts. The scattered light was detected by a cooled photomultiplier (ITT FW 130) which was connected to the multichannel analyzer of the data acquisition and stabilization system (Burleigh DAS-1). The spectral data was accumulated in the form of photon counts *vs.* channel number (frequency). The DAS-1 automatically compensated for drifts in the laser frequency and separation of the Fabry-Perot reflectors and optimized the finesse for indefinitely long periods of time.

A representative room-temperature Brillouin spectrum of the ethanol adduct of Dianin's compound with a central (Rayleigh) line and three Brillouin doublets (up and

Figure 7.3 Block diagram of the experimental arrangement for Brillouin scattering, CO=collimator, S=sample, SH=sample holder, A1-4=apertures, L1-4=lenses, M=mirror, FP=triple-pass Fabry-Perot interferometer, PMT=cooled photomultiplier tube, AD=amplifier-discriminator, DAS-1=data acquisition and stabilization system, REC=strip chart recorder, He-Ne laser defines the optic axis, and Ar^+ laser is the single-mode source of incident radiation.[103]

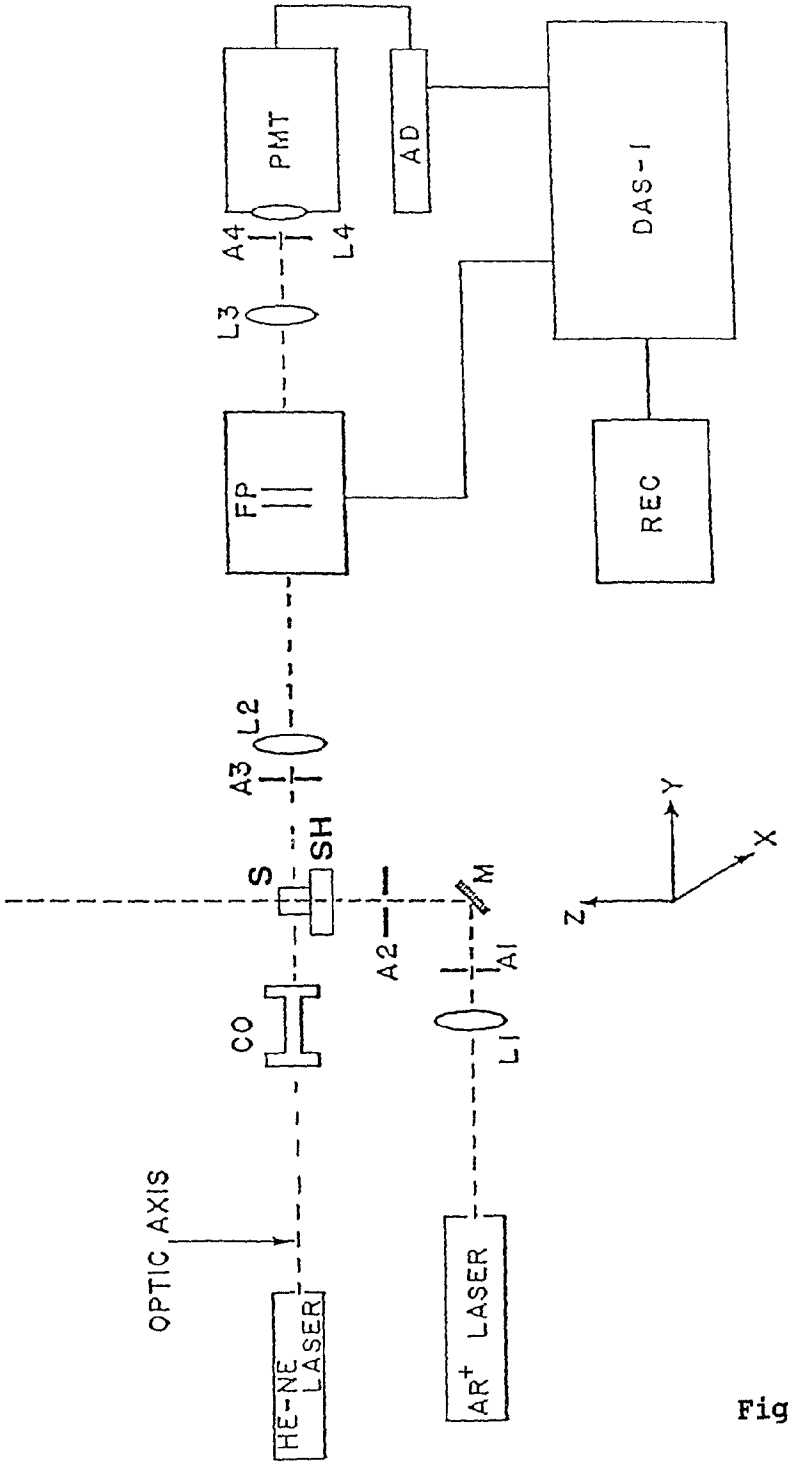
OPTIC AXIS
HE-NE LASER
CO
S
SH
A3
L2
FP
L3
A4
L4
PMT
AD
DAS-I
REC
AR+ LASER
L1
A1
A2
M
Z
Y
X

Figure 7.3

down-shifted) is shown in Figure 7.4. For these experiments, the errors in the determination of the frequency typically were of the order of 0.5 to 1%.

7.5 Results and Discussion

A total of 55 velocities were obtained investigating 22 different directions in the crystal lattice; the directions are shown in Figure 7.5.

The experimental data and the best fits are shown in Table 7.1. The goodness of the fit can be judged by the closeness of the measured and calculated values of the shifts. The average absolute values of the differences between the observed and calculated frequencies, expressed as a percentage of the observed values for the various modes, are: T1, 3.7%; T2, 3.2%; L, 1.5%. In light of the quality of the crystals, in terms of relatively poor optical clarity and the existence of cracks, and the uncertainty (few degrees) in crystal orientation after cutting and polishing and visual alignment in the experimental setup, the fit is quite good.

The Brillouin scattering results are confirmed by an independent direct determination of ultrasonic sound velocities along the **c**-axis of a single crystal of the ethanol adduct of Dianin's compound. Sound velocities were measured using a standard ultrasonic pulse method[104] applied

Figure 7.4 A representative two-hour Brillouin scattering spectrum for a single crystal of the ethanol adduct of Dianin's compound taken for the phonon direction [-0.5; -1; 0.87] at room temperature. One complete order is shown with quasilongitudinal (L) and quasitransverse (T_1 and T_2) components up- and down-shifted from the central component (R). The free spectral range of the Fabry-Perot was 28.50 GHz.

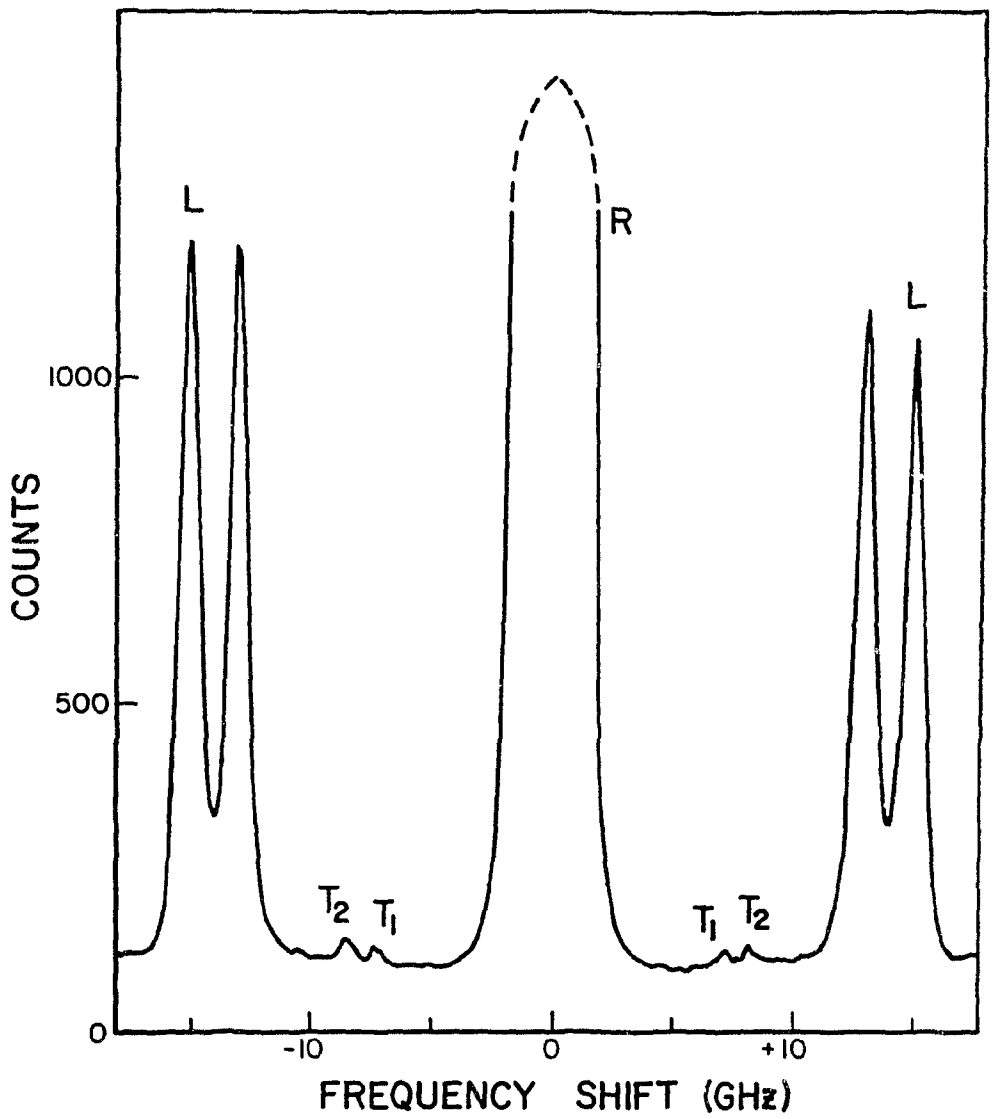

Figure 7.4

Figure 7.5 The sample orientations for the 22 different phonon directions investigated by Brillouin scattering in the single crystal of ethanol adduct of Dianin's compound.

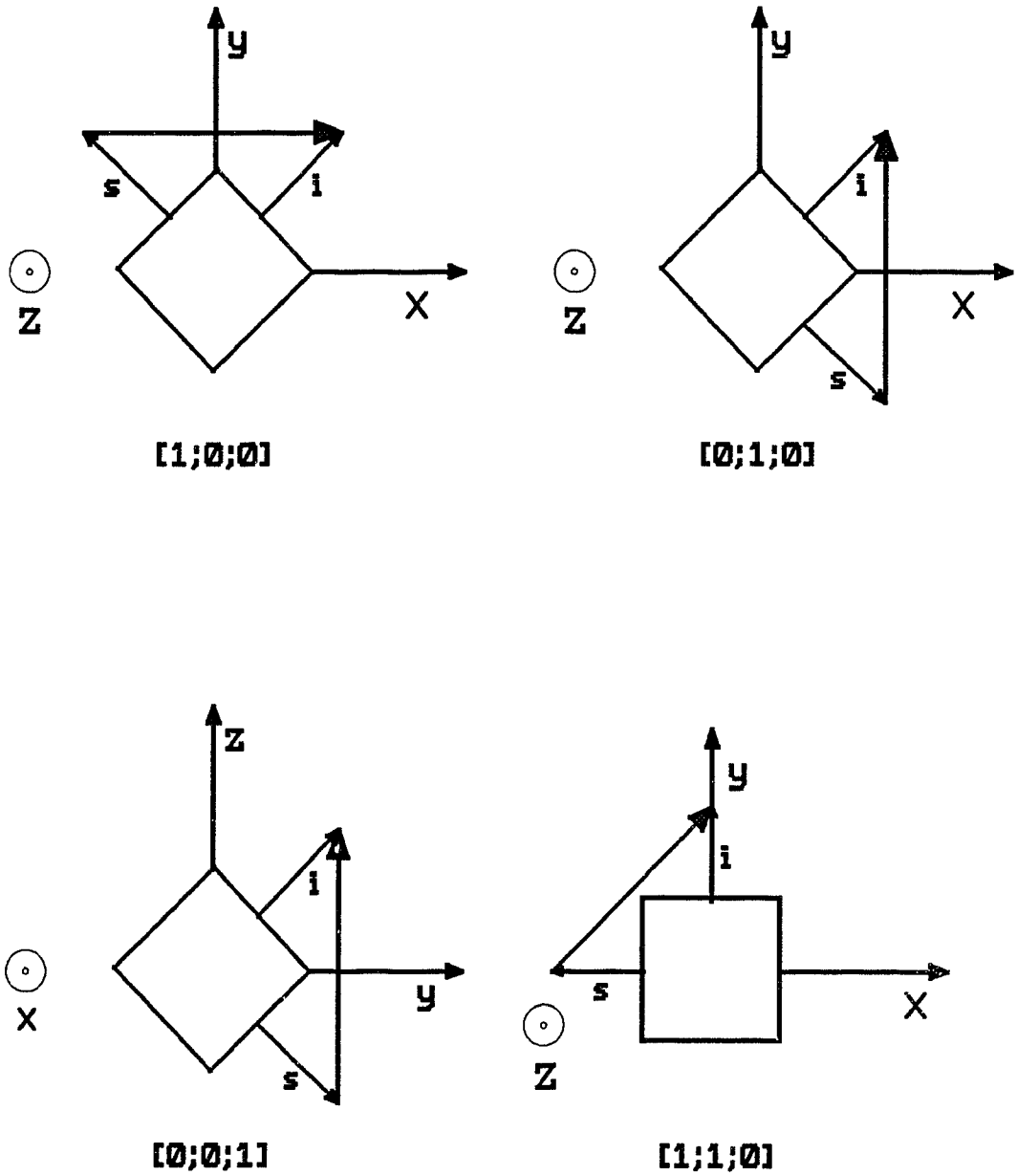

Figure 7.5 continued...

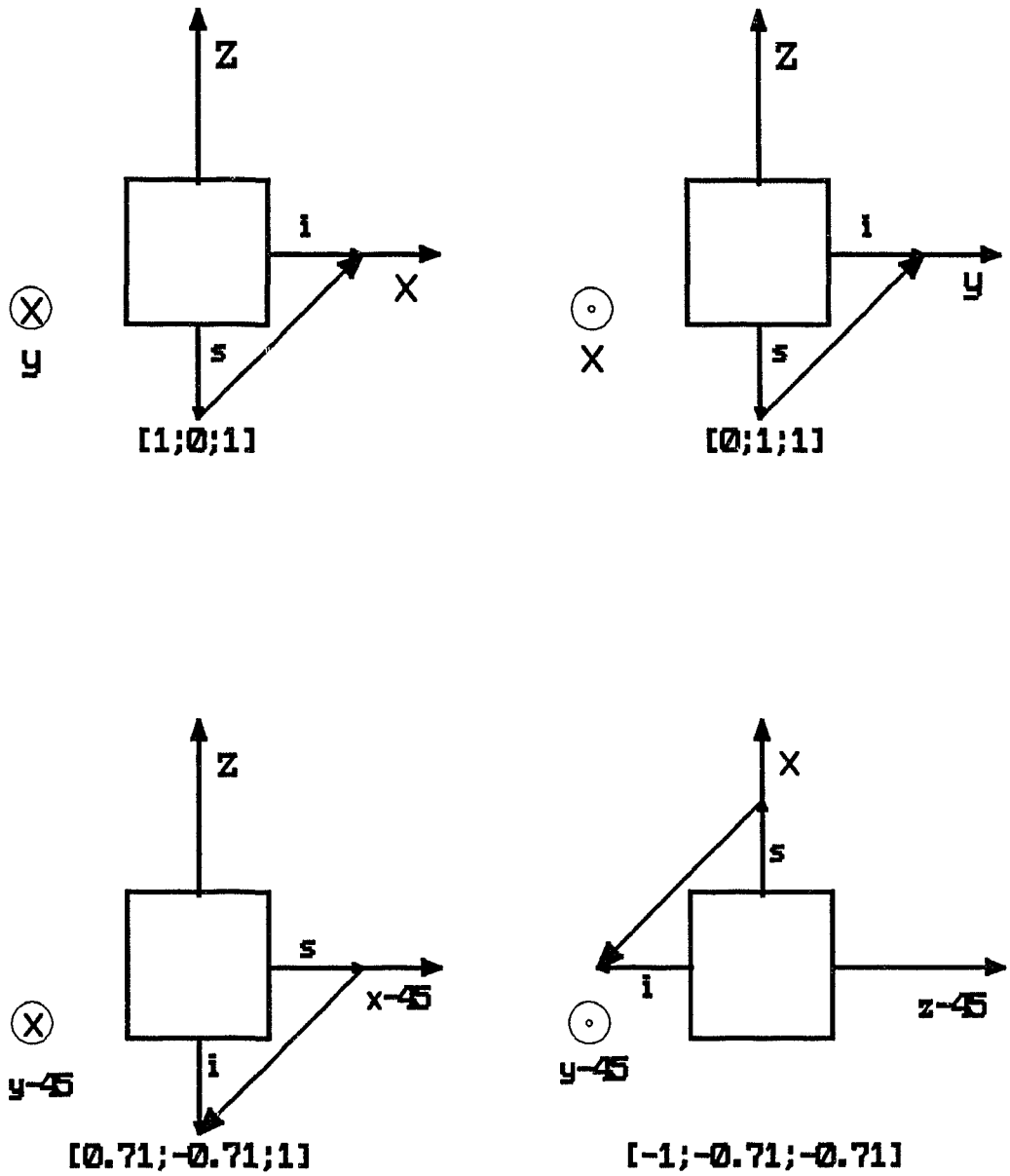

Figure 7.5 continued...

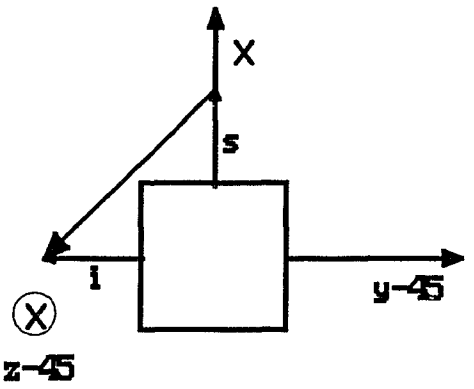

[-1;-0.71;0.71]

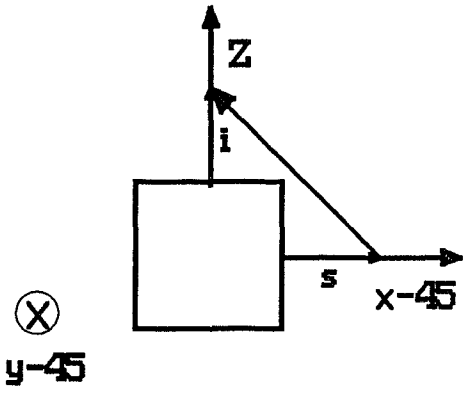

[-0.71;0.71;1]

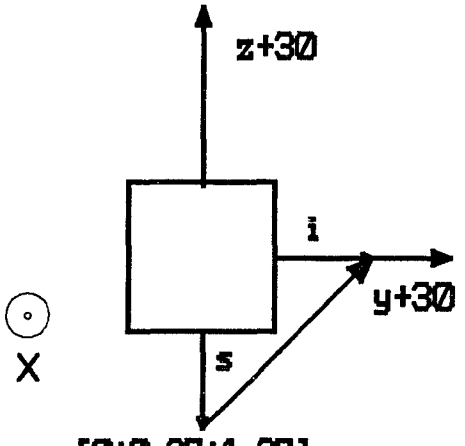

[0;0.37;1.37]

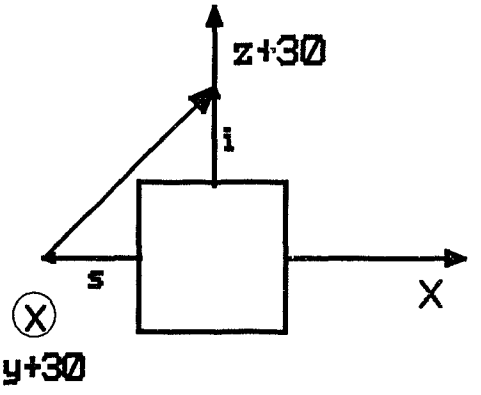

[1;-0.5;0.87]

Figure 7.5 continued...

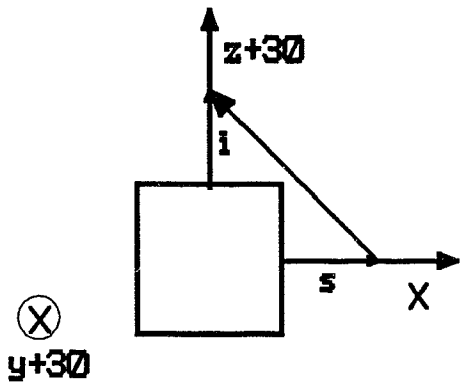

[-1;-0.5;0.87]

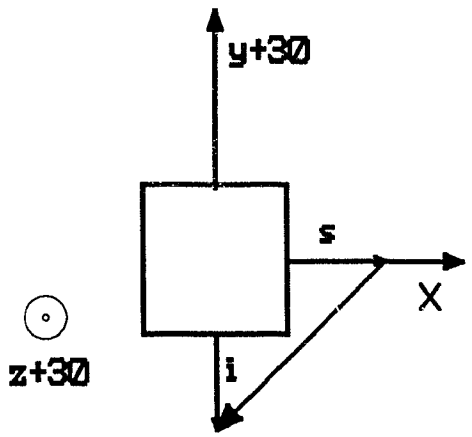

[-1;-0.87;-0.5]

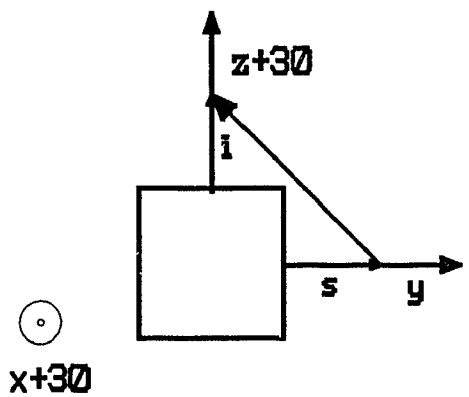

[-0.5;-1;0.87]

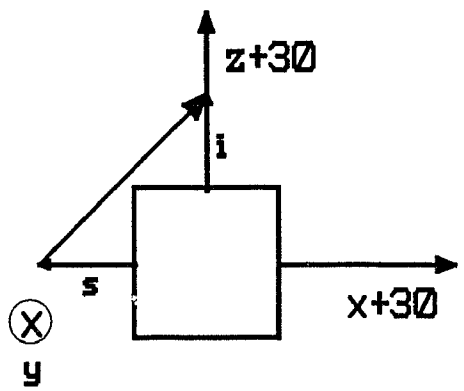

[0.37;0;1.37]

Figure 7.5 continued...

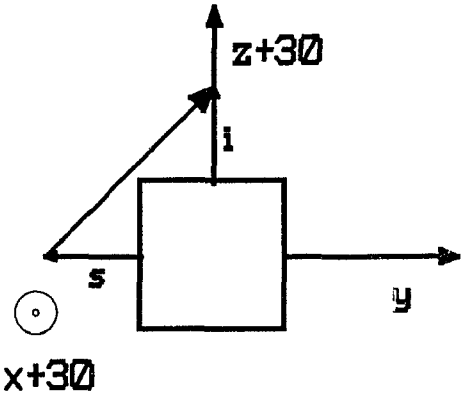

[-0.5;1;0.87]

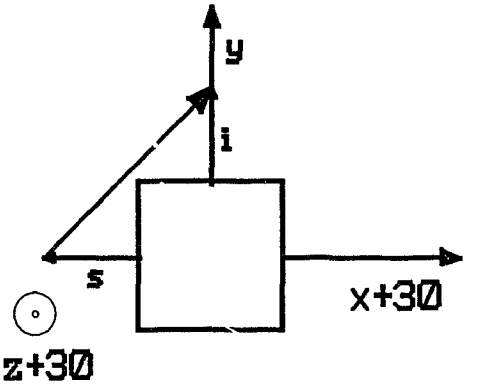

[0.87;1;0.5]

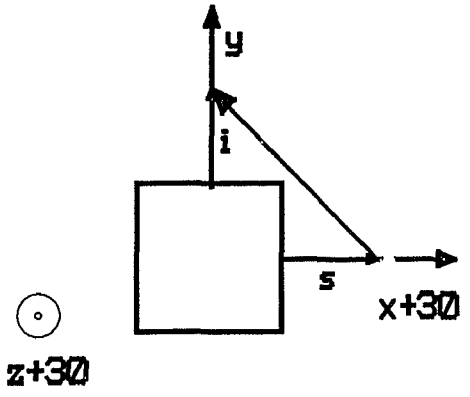

[-0.87;1;-0.5]

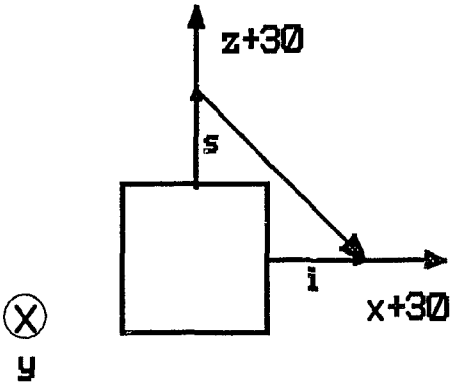

[1.37;0;-0.37]

Figure 7.5 continued...

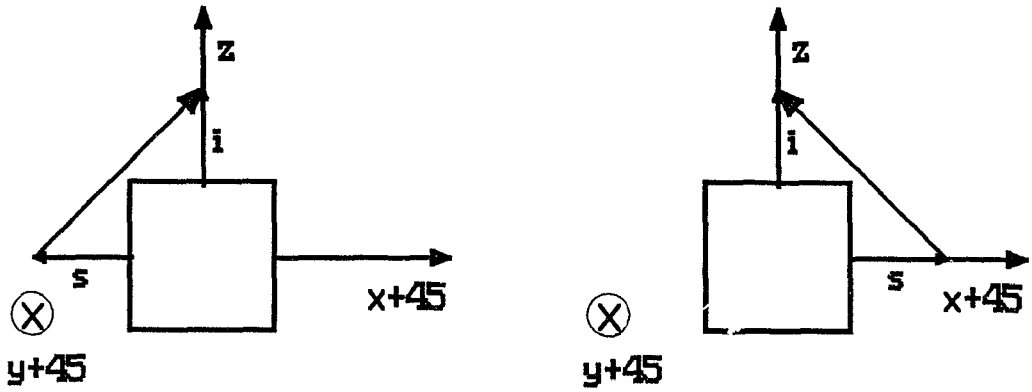

[0.71;0.71;1] [-0.71;-0.71;1]

Figure 7.5

Table 7.1. The Brillouin scattering data for single crystals of the ethanol adduct of Dianin's compound at T=293 K. T1 = slow quasitransverse mode; T2 = fast quasitransverse mode; L = quasilongitudinal mode.

Direction cosines			Observed frequency in GHz			Calculated frequency in GHz		
x	y	z	T1	T2	L	T1	T2	L
1	0	0	7.95	9.38	14.97	8.44	9.31	14.92
0	1	0	8.65	9.90	15.03	8.54	9.21	14.93
0	0	1	8.75	8.75	14.36	8.55	8.55	14.75
1	1	0	7.84	9.73	15.14	8.48	9.26	14.93
1	0	1	7.41		15.63	7.49	8.88	15.40
0	1	1	7.52		15.26	7.50	9.16	15.23
.71	-.71	1		9.21	15.52	7.49	9.08	15.28
-1	-.71	-.71	7.52		15.84	7.62	8.81	15.51
-1	-.71	.71	8.45	9.12	15.09	7.89	9.28	15.10
-.71	.71	1	7.74		15.58	7.49	8.68	15.52
0	.37	1.37	8.15	9.12	14.64	8.14	8.74	14.90
1	.5	.87	7.84	9.12	15.47	7.64	9.23	15.19
-1	-.5	.87	7.84		15.58	7.64	9.23	15.19
-1	-.87	-.5	7.29	9.02	14.87	7.94	8.98	15.33
-.5	-1	.87	7.18	8.65	15.14	7.55	8.90	15.43

continued....

Table 7.1 continued:

Direction cosines			Observed frequency in GHz			Calculated frequency in GHz		
x	y	z	T1	T2	L	T1	T2	L
.37	0	1.37		8.55	15.25	8.22	8.64	14.92
-.5	1	.87		8.45	15.47	7.58	9.00	15.36
.87	1	.5	8.26		15.14	7.98	9.04	15.27
-.87	1	-.5		8.93	14.76	8.16	9.24	15.06
1.37	0	-.37	7.74	9.02	14.64	8.22	9.21	15.07
-.71	-.71	-1	7.74		15.03	7.49	9.08	15.28
-.71	-.71	1	7.41	8.05	15.36	7.49	8.68	15.52

along the crystallographic c-axis. Lithium niobate transducers (36° Y-cut for the longitudinal mode and X-cut for the transverse mode) were used. To maintain good coupling between the transducers and sample, silicon grease and paraffin wax were used for the longitudinal and transverse modes, respectively. The pulses were generated and received by a Matec Pulse Modulator and Receiver (Model 6600, Matec Inc., Warnick, R.I.). The apparatus was tested first by measuring the velocity of sound of Harshaw NaCl crystals; the results for T = 300 K were (4.62±0.05) $x10^3$ m s^{-1} and (2.46±0.05) $x10^3$ m s^{-1} for the longitudinal and transverse modes, respectively, and can be compared with literature values[105] of $4.57x10^3$ m s^{-1} and $2.46x10^3$ m s^{-1}. For the ethanol adduct of Dianin's compound, the transverse mode velocity was determined to be 2.06 x 10^3 m s^{-1} and the longitudinal mode velocity was 3.11 x 10^3 m s^{-1}, both from the ultrasonic method; the corresponding values from the Brillouin scattering experiment were 1.94 x 10^3 m s^{-1} and 3.18 10^3 m s^{-1}.

The velocity of sound was also measured ultrasonically for unsolvated Dianin's compound, and the transverse and longitudinal mode velocities were found to be $2.01x10^3$ m s^{-1} and $3.18x10^3$ m s^{-1},respectively. The crystals of the CCl_4 adduct of Dianin's compound were too small for the measurements.

The elastic stiffness constants and elastic compliance

constants determined from the fit to the Brillouin scattering results for the ethanol adduct of Dianin's compound are shown in Tables 7.2 and 7.3, respectively. By noting the changes in calculated velocities by varying c_{ij}, it is estimated that the relative uncertainties in the elastic constants are less than 0.02×10^{10} N m^{-2}. This determination appears to be the first for all seven constants for this crystallographic symmetry.

Some of the calculated frequency shifts for different phonon directions are virtually the same. This was caused by experimentally almost indistinguishable differences between Brillouin shifts for different directions. After several hundred iterations in the fit the c_{25} elastic constant optimized at zero, causing the $R\bar{3}$ space group to look like the $R\bar{3}m$ space group, with respect to the elastic constants. The other elastic constant which is very close to zero is c_{14}. This suggests that the examined system could be closely approximated by hexagonal symmetry.[106,107] The elastic constant calculation within hexagonal symmetry was carried out and gave results (in brackets in Table 7.2) very similar to those for trigonal symmetry, verifying the close approximation of the symmetry here to hexagonal.

If hexagonal symmetry is assumed, the bulk modulus, B:

$$B = -V\left(\frac{\partial P}{\partial V}\right)_T = \frac{c_{33}(c_{11}+c_{12})-2c_{13}^{2}}{c_{11}+c_{12}+2c_{33}-4c_{13}} \qquad (7.4.1)$$

Table 7.2

The (symmetrical) elastic stiffness tensor for the ethanol adduct of Dianin's compound at 20°C, as determined by Brillouin spectroscopy. The values given in brackets are for hexagonal symmetry. All numerical values of c_{ij} are in 10^{10} N m^{-2}.

$$
\begin{matrix}
c_{11} & c_{12} & c_{13} & c_{14} & -c_{25} & 0 \\
 & c_{11} & c_{13} & -c_{14} & c_{25} & 0 \\
 & & c_{33} & 0 & 0 & 0 \\
 & & & c_{44} & 0 & c_{25} \\
 & & & & c_{44} & c_{14} \\
 & & & & & (c_{11}-c_{12})/2
\end{matrix}
$$

c_{11}=1.34 (1.34)

c_{12}=0.32 (0.30)

c_{13}=0.65 (0.64)

c_{14}=0.03 (0)

c_{25}=0 (0)

c_{33}=1.31 (1.31)

c_{44}=0.44 (0.43)

Table 7.3

They (symmetrical) elastic compliance tensor for the ethanol adduct of Dianin's compound at 20°C, as determined by Brillouin spectroscopy.

$$
\begin{matrix}
s_{11} & s_{12} & s_{13} & s_{14} & -s_{25} & 0 \\
 & s_{11} & s_{13} & -s_{14} & s_{25} & 0 \\
 & & s_{33} & 0 & 0 & 0 \\
 & & & s_{44} & 0 & 2s_{25} \\
 & & & & s_{44} & 2_{14} \\
 & & & & & 2(s_{11}-s_{12})
\end{matrix}
$$

$s_{11}=9.8 \times 10^{-11} m^2N^{-1}$

$s_{12}=-1.5 \times 10^{-13} m^2N^{-1}$

$s_{13}=-4.9 \times 10^{-11} m^2N^{-1}$

$s_{14}=6.8 \times 10^{-12} m^2N^{-1}$

$s_{25}=0\ m^2N^{-1}$

$s_{33}=1.25 \times 10^{-10} m^2N^{-1}$

$s_{44}=2.28 \times 10^{-10} m^2N^{-1}$

is 7.8 x 10^9 N m^{-2} for the ethanol adduct of Dianin's compound, and the anisotropy factor, A:

$$A = \frac{2c_{44}}{(c_{11}-c_{12})} \qquad (7.4.2)$$

is 0.83.

The elastic constants for the ethanol adduct of Dianin's compound are almost an order of magnitude larger than very soft hexagonal crystals such as β-N_2 and β-CO.[103] They are, nevertheless, much smaller (by about a factor of 5) than trigonal ferric systems such as $K_3Na(CrO_4)_2$,[108] than the trigonal layered compound $Ca(OH)_2$[106] or (by a factor of 10 to 50) than typical harder crystals such as Al_2O_3.[109] The elastic constants measured in the present experiment are, in fact, very similar to those of (hexagonal) ice Ih,[110] the exception being c_{12} which is larger by a factor of two in hexagonal ice.

Chapter 8: Derived Thermodynamic Properties

8.1. Theory

8.1.a. Heat Capacity

Equation (5.1.2) describing the relationship between C_p and C_v is strictly true only for isotropic materials. As Dianin's compound and its clathrates are trigonal, this is not the case here.

For an anisotropic crystal, C_p and C_v are related to the heat capacities at constant stress, C_σ, and at constant strain, C_ϵ, as:[111]

$$C_\sigma - C_\epsilon = C_p - C_v = VT(c_{ijkl}\ \alpha_{ij}\ \alpha_{kl}) \qquad (8.1.1)$$

where c_{ijkl} is the isothermal elastic constant tensor and α_{ij} is the thermal expansion tensor.

Clearly the usable form of equation (8.1.1) will depend on the symmetry of the crystal under consideration. It has been show in Section 7.4 that, from the perspective of the elastic properties of Dianin's compound, the symmetry may be closely approximated as hexagonal. In this case, equation (8.1.1) becomes:

$$C_p - C_v = VT\{\ 2(c_{11}+c_{12})\ \alpha_a^2 + 4c_{13}\alpha_a\alpha_c + c_{33}\alpha_c^2\} \qquad (8.1.2)$$

where the Voigt notation is used.

8.1.b. Effective Characteristic Temperatures

Although it is apparent, especially from the linear temperature-dependence of C_v, that neither Dianin's compound nor its adducts will be well-represented by the Debye model, it is nevertheless informative to calculate an effective Debye temperature, θ_D. Indeed, there is sufficient information to make this calculation from several different methods.

The value of the effective θ_D may be calculated from the C_v *vs.* T dependency according to the Debye theory described in Chapter 5.

The effective Debye temperature also can be determined from velocity of sound measurements:[112]

$$\theta_D = \frac{h}{k_B}\left(\frac{3N_o p\rho}{4\pi M}\right)^{1/3} v_m \qquad (8.1.3)$$

where h is Planck's constant, k_B is Boltzmann's constant, N_o is Avogadro's number, p is the number of "atoms" in the molecule, ρ is the density, M is the molecular weight and v_m is the average sound velocity:

$$v_m = (3)^{1/3}(2v_T^{-3}+v_L^{-3})^{-1/3} \quad . \qquad (8.1.4)$$

For the ethanol adduct of Dianin's compound, there also

is sufficient information to calculate the effective Debye temperature from the full set of elastic constants. Equation (8.1.3) can be re-written[112] as:

$$\theta_D = \frac{h}{k_B}\left(\frac{9N}{4\pi V}\right)^{1/3}\left\{\int\left[\frac{1}{v_L^3}+\frac{2}{v_T^3}\right]\frac{d\Omega}{4\pi}\right\}^{-1/3} \qquad (8.1.5)$$

where N is the number of atoms per unit cell, and V is the unit cell volume, which, applying the harmonic series method after Alers[113] becomes:

$$\theta_D = \frac{h}{k_B}\left(\frac{9N}{4\pi V}\right)^{1/3}\rho^{-1/2}J^{-1/3} \qquad (8.1.6)$$

where J can be expressed directly in terms of the elastic constants[113]:

$$5040J = 1536f_1 + 456f_2 + 1024(f_3+f_4) - 625(f_5+f_6) + 2250f_7 \qquad (8.1.7)$$

and

$$f_1 = [c_{66}]^{-3/2} + [1/2(c_{44}+c_{11}) + 1/2\{(c_{44}-c_{11})^2 + 4c_{14}^2\}^{1/2}]^{-3/2} + [1/2(c_{44}+c_{11}) - 1/2\{(c_{44}-c_{11})^2 + 4c_{14}^2\}^{1/2}]^{-3/2} \qquad (8.1.8)$$

$$f_2 = 2[c_{44}]^{-3/2} + [c_{33}]^{-3/2} \qquad (8.1.9)$$

$$f_3=[1/2(c_{66}+c_{44}-2c_{14})]^{-3/2} \tag{8.1.10}$$
$$+[1/4(c_{11}+2c_{44}+2c_{14}+c_{33})$$
$$+1/4\{(c_{11}+2c_{14}-c_{33})^2+4(c_{14}+c_{13}+c_{44})^2\}^{1/2}]^{-3/2}$$
$$+[1/4(c_{11}+2c_{44}+2c_{14}+c_{33})-1/4\{(c_{11}+2c_{14}-c_{33})^2$$
$$+4(c_{14}+c_{13}+c_{44})^2\}^{1/2}]^{-3/2}$$

$$f_4=[1/5(4c_{66}+c_{44}-4c_{14})]^{-3/2} \tag{8.1.11}$$
$$+[1/10(4c_{11}+4c_{14}+5c_{44}+c_{33})+1/10\{(4c_{11}$$
$$+4c_{14}-3c_{44}-c_{33})^2+4(4c_{14}+2c_{13}+2c_{44})^2\}^{-3/2}$$
$$+[1/10(4c_{11}+4c_{14}+5c_{44}+c_{33})-1/10\{(4c_{11}+4c_{14}-3c_{44}-c_{33})^2$$
$$+4(4c_{14}+2c_{13}+2c_{44})^2\}^{1/2}]^{-3/2}$$

$$f_5=[1/2(c_{66}+c_{44}-2c_{14})]^{-3/2} \tag{8.1.12}$$
$$+[1/4(c_{11}+2c_{44}-2c_{14}+c_{33})+1/4\{(c_{11}-2c_{14}-c_{33})^2$$
$$+4(-c_{14}+c_{13}+c_{44})^2\}^{1/2}]^{-3/2}+[1/4(c_{11}+2c_{44}-2c_{14}+c_{33})-$$
$$1/4\{(c_{11}-2c_{14}-c_{33})^2+4(-c_{14}+c_{13}+c_{44})^2\}^{1/2}]^{-3/2}$$

$$f_6=[1/5(4c_{66}+c_{44}+4c_{14})]^{-3/2} \tag{8.1.13}$$
$$+[1/10(4c_{11}-4c_{14}+5c_{44}+c_{33})+1/10\{(4c_{11}-4c_{14}-3c_{44}-c_{33})^2$$
$$+4(-4c_{14}+2c_{13}+2c_{44})^2\}^{-3/2}+[1/10(4c_{11}-4c_{14}+5c_{44}+c_{33})$$
$$-1/10\{(4c_{11}-4c_{14}-3c_{44}-c_{33})^2$$
$$+4(-4c_{14}+2c_{13}+2c_{44})^2\}^{1/2}]^{-3/2}$$

The value of f_7 is the sum of the roots of the secular

equation:

$$\begin{vmatrix} \frac{4c_{66}+c_{44}}{5} - y & \frac{-4c_{14}}{5} & \frac{-4c_{14}}{5} \\ \frac{-4c_{14}}{5} & \frac{4c_{11}+c_{44}}{5} - y & \frac{2c_{13}+2c_{44}}{5} \\ \frac{-4c_{14}}{5} & \frac{2c_{13}+2c_{44}}{5} & \frac{4c_{44}+c_{33}}{5} - y \end{vmatrix} = 0 \qquad (8.1.14)$$

8.1.c. Grüneisen Parameter

One of the main purposes of the present investigations of clathrates is to understand the role of the guest species in thermal properties. To that end, the thermal expansion of unsolvated Dianin's compound, and its ethanol and CCl_4 adducts have been examined.[57,66] Because thermal expansion directly quantifies the anharmonicity of the intermolecular forces in a solid (a perfect harmonic lattice has zero thermal expansion at all temperatures), in Chapter 6 it was concluded that the presence of the guest species increased the anharmonicity in the system, and the presence of two guests per cage (ethanol) increased the anharmonicity

relative to one guest molecule per cage (CCl_4).

Another measure of the anharmonicity in a solid is the change of frequency with change in volume. For the ith mode with frequency ω_i, the Grüneisen parameter, γ_i, is defined as[43]:

$$\gamma_i = -\frac{\partial \ln \omega_i}{\partial \ln V} \qquad (8.1.15)$$

and for the overall lattice,

$$\gamma = \frac{\sum_i \gamma_i C_{v,i}}{\sum_i C_{v,i}} \qquad (8.1.16)$$

where γ is the overall Grüneisen parameter, and $C_{v,i}$ is the contribution of the ith mode to the heat capacity, and the sum is over all normal modes. The importance of the Grüneisen parameter to the discussion here is that it is zero for a lattice with perfect harmonic interactions.

There is insufficient information to calculate the Grüneisen parameter from equation (8.1.16) for Dianin's compound and its adducts. However, for a hexagonal crystal, equation (8.1.16) can be re-written in terms of the Grüneisen parameters perpendicular and parallel to the c-axis, γ_a and γ_c , respectively:[114]

$$\gamma = \frac{(2\chi_a{}^T\gamma_a+\chi_c{}^T\gamma_c)}{\chi^T} \qquad (8.1.17)$$

where $\chi_a{}^T$ and $\chi_c{}^T$ are the isothermal compressibilities perpendicular and parallel to the c-axis, defined as:

$$\chi_a{}^T = \frac{C_{33}-C_{13}}{(C_{11}+C_{12})C_{33}-2C_{13}{}^2} \qquad (8.1.18)$$

and

$$\chi_c{}^T = \frac{C_{11}+C_{12}-2C_{13}}{(C_{11}+C_{12})C_{33}-2C_{13}{}^2} \quad , \qquad (8.1.19)$$

and γ_a and γ_c are defined as:

$$\gamma_a = \frac{V\{(C_{11}+C_{12})\alpha_a+C_{13}\alpha_c\}}{C_v} \qquad (8.1.20)$$

and

$$\gamma_c = \frac{V\{2C_{13}\alpha_a+C_{33}\alpha_c\}}{C_v} \quad . \qquad (8.1.21)$$

8.2 Results and Discussion

8.2.a. Heat capacity

Using the measured values of C_p,[62] thermal expansion[57,66] and elastic constants,[115] C_v has been calculated from equation (8.1.2) for the ethanol adduct of Dianin's compound; the results are shown in Figure 8.2. C_p is very nearly linear in temperature from about 40 K to just above room temperature; the correction for p-V work makes C_v less than C_p, up to a few per cent at room temperature. However, even C_v is quite linear in temperature. (Although full elastic constants are not known for either unsolvated Dianin's compound or its CCl_4 adduct, the similarity of the sound velocities suggests that the ethanol values for c_{ij} could be used to calculate C_v for these compounds; under that assumption, C_v for unsolvated Dianin's compound and its CCl_4 adduct both look very similar to the results for the ethanol adduct shown in Figure 8.2. These results are shown in Figures 8.1 and 8.3, respectively.)

A similar effect (linear heat capacity over a wide temperature range) was observed[116] for both the monomer and the polymer of 2,4-hexadiyne-1,6-diol-bis(*p*-toluene sulfonate). There the linear heat capacity was attributed to the dominance of the stretching vibrational modes which contribute as $C_v(\mathrm{str}) \propto T^1$. Unfortunately, the assignment

Figure 8.1 The heat capacity at constant pressure (C_p, solid line) and at constant volume (C_v, broken line) for the unsolvated Dianin's compound.

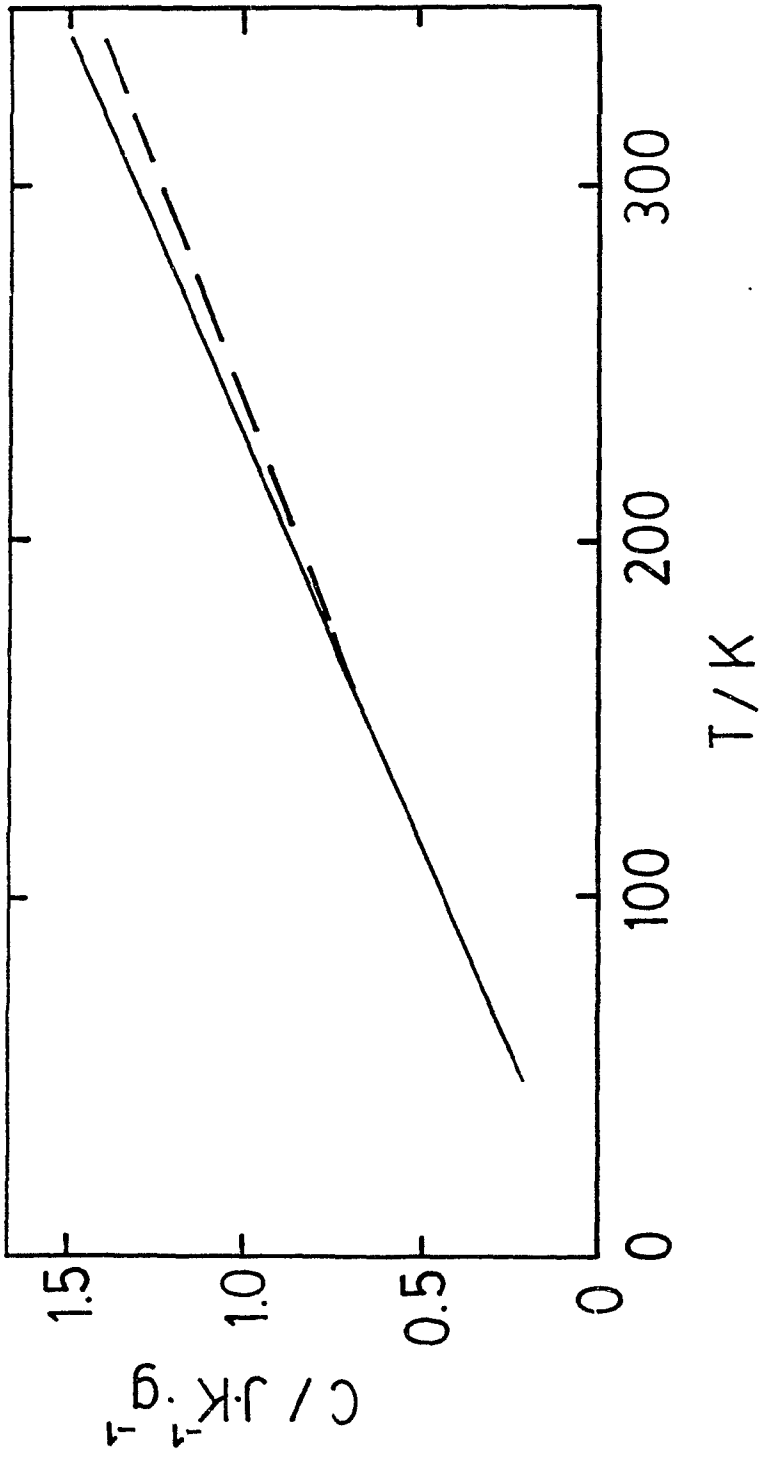

Figure 8.1

Figure 8.2 The heat capacity at constant pressure (C_p, solid line) and at constant volume (C_v, broken line) for the ethanol adduct of Dianin's compound.

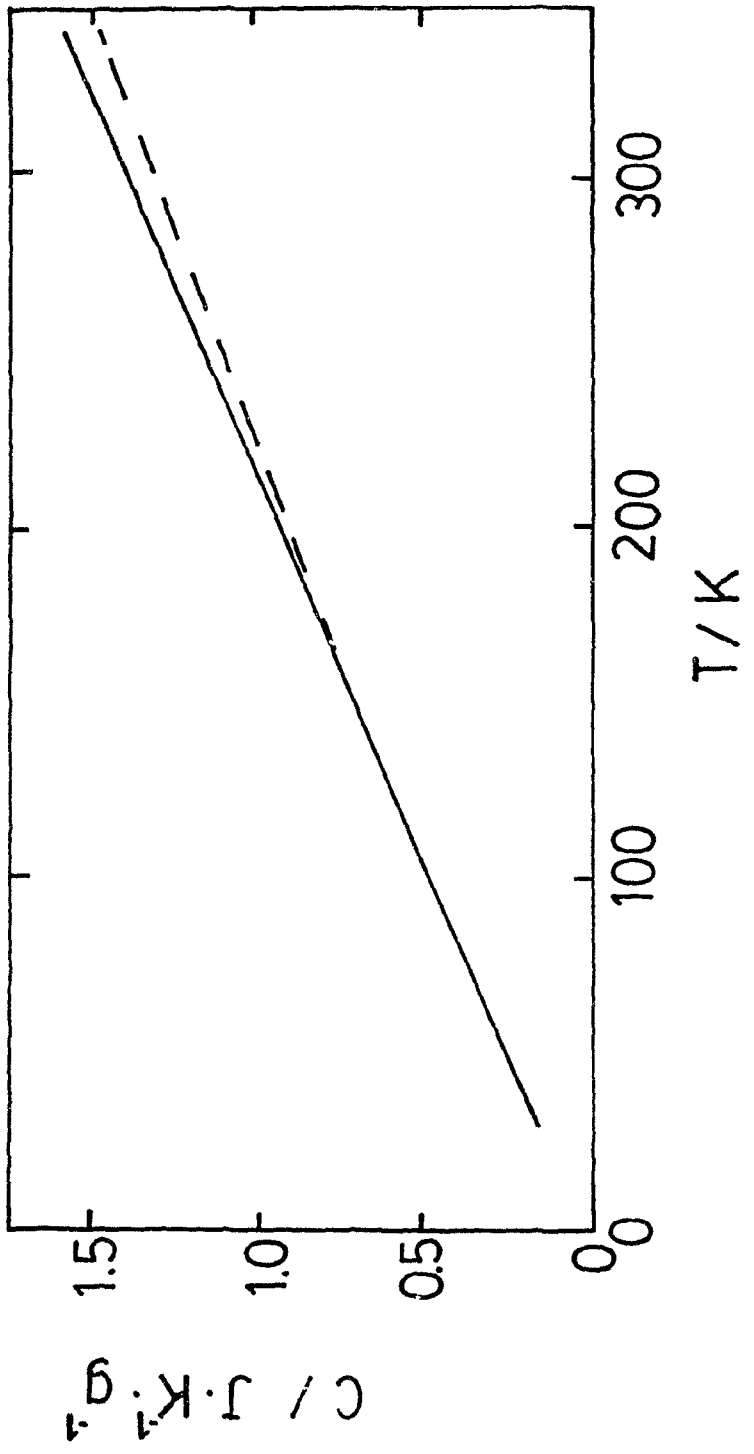

Figure 8.2

Figure 8.3 The heat capacity at constant pressure (C_p, solid line) and at constant volume (C_v, broken line) for the carbon tetrachloride adduct of Dianin's compound.

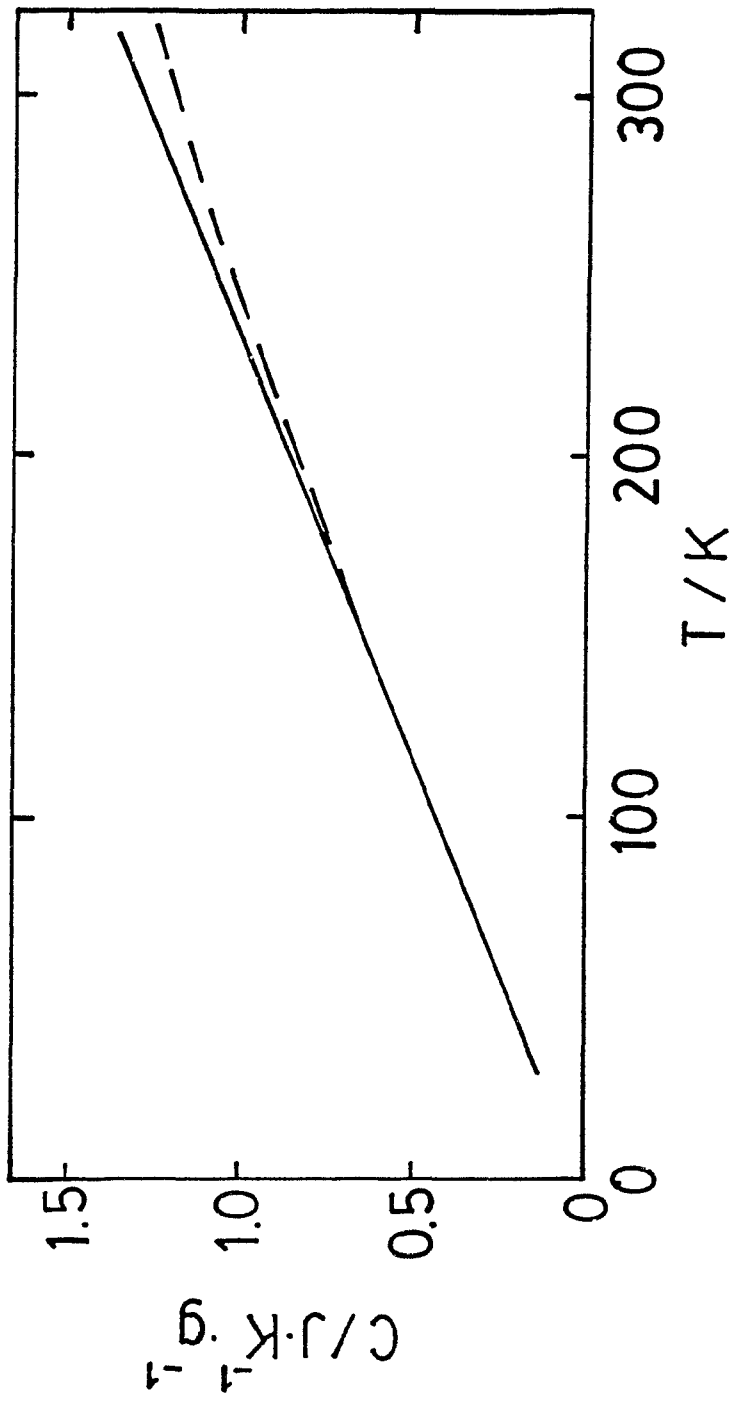

Figure 8.3

of the vibrational modes has not been carried out for the Dianin system, so it is not possible to assess the contributions of internal vibrational modes to the heat capacity. However, Dianin's compound and its adducts are molecular solids, and one could expect many contributions from internal vibrational modes to the heat capacity (for example it is known from IR[117] and Raman[63] spectroscopic studies of Dianin's clathrates that there are more than 100 distinct vibrational frequencies ranging from <40 cm^{-1} to >3000 cm^{-1}); it is likely that these are responsible for the linear temperature dependence. It is interesting to note that the polymer of 2,4-hexadiyne-1,6-diol-bis(*p*-toluene sulfonate) has an unusual temperature dependence to its thermal conductivity that has been attributed to the scattering of acoustic phonons by low-energy optic phonons;[118] the thermal conductivity of Dianin's compound and its ethanol adduct show similar behaviour (*vide infra.*). While these effects might be related, the "glass-like" thermal conductivity does not exclusively imply linear heat capacity; tetrahydrofuran clathrate hydrate is a case in point.[25,119])

8.2.b. Effective Characteristic Temperatures

Although the Debye characteristic temperature, θ_D, is

well-specified for monatomics, according to the theory presented in Chapter 5, this not the case for molecular solids. Put simply, the problem is this: How does one decide the maximum number of degrees of freedom available? Ideally, the vibrational assignment is complete, internal vibrational contributions to C_v can be subtracted and the analysis can be carried out on the remaining contribution to C_v treating the lattice as rigid units of molecules. Even if the vibrational assignment is not available (and it is not for Dianin's compound), in some molecular crystals the internal vibrations and external vibrations (translational and librational motions of molecules or molecular groups) are well-separated energetically, and can be treated separately.[120,121]

As described in the previous section, the internal and external vibrational modes of Dianin's clathrates are not well separated. However it is clear that many of the internal modes are at very high frequency and therefore contribute negligibly to the sub-ambient heat capacity. Another way to state this is that Dianin's molecule, concentrating on the unsolvated compound first, can be considered to consist of several subgroups, each of which can contribute its "external" motion. In this representation higher-frequency internal modes are ignored. Taking into account the crystal structure,[58] steric hindrance, ^{13}C nmr T_1 relaxation information,[122] recent ^{2}H

nmr data[89] and barriers to reorientation in other molecular solids,[81] it is possible to distinguish six subgroups to the Dianin's molecule: the phenolic group; three methyl groups; the chroman moiety; the phenolic phenyl ring. As there is no observable gap in the vibrational spectrum, this assignment is, of necessity, rather arbitrary, and arguments also could be put forward for five or seven subgroups, although six seems most reasonable.

For a given number of subgroups n, the high-temperature limit of C_v would be, according to Debye theory, 3nR. On this basis effective Debye characteristic temperatures, θ_D, for values of n from 5 to 10 have been calculated from C_v data for unsolvated Dianin's compound; the results are shown in Fig 8.4. All the curves show the same parabolic shape. At lower temperatures, by analogy with other solids,[114] θ_D should increase slightly.

For the ethanol adduct of Dianin's compound the heat capacity data goes to lower temperature; an analogous plot of θ_D as a function of temperature for this clathrate is given in Fig. 8.5. (Although here the guest molecules also contribute to C_v the high ratio of host-to-guest makes this contribution well within uncertainty in assignment of the number of contributing subgroups of the host lattice.) Again, all the curves show similar parabolic behaviour. The decrease at the higher temperature in Figures 8.4 and 8.5 likely is due to the increasing contribution of the

Figure 8.4 The Debye temperatures for various numbers of subgroups (n) in Dianin's compound molecule as a function of temperature derived from the heat capacity of unsolvated Dianin's compound.

———————— n=5

– – – – – – n=6

–·–·–·–·–·– n=7

—— —— —— n=8

–··–··–··–·· n=9

····· n=10

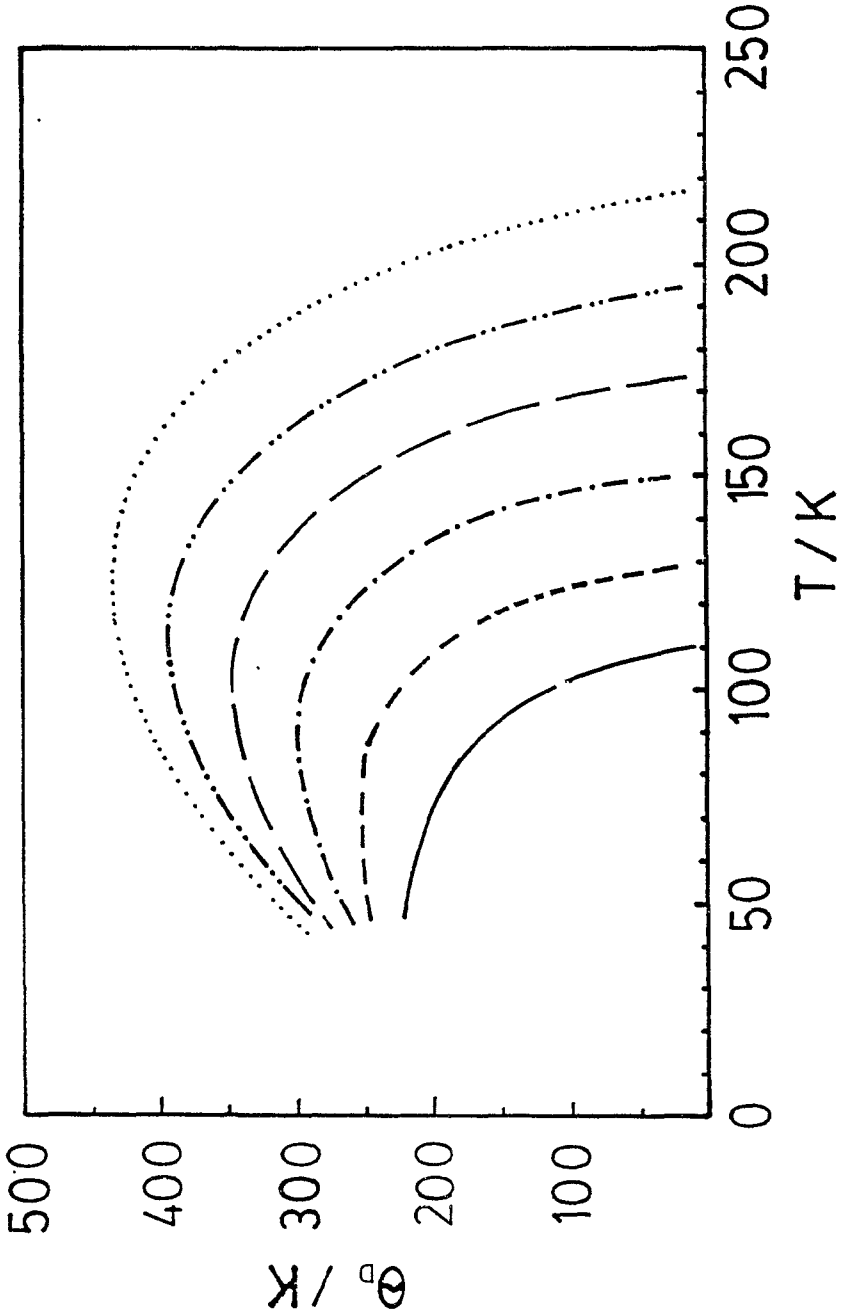

Figure 8.4

Figure 8.5 The Debye temperatures for various numbers of subgroups (n) in Dianin's compound molecule as a function of temperature derived from the heat capacity of ethanol adduct of Dianin's compound.

———————— n=5

– – – – – – n=6

–·–·–·–·–·– n=7

—— —— —— n=8

–··–··–··–·· n=9

····· n=10

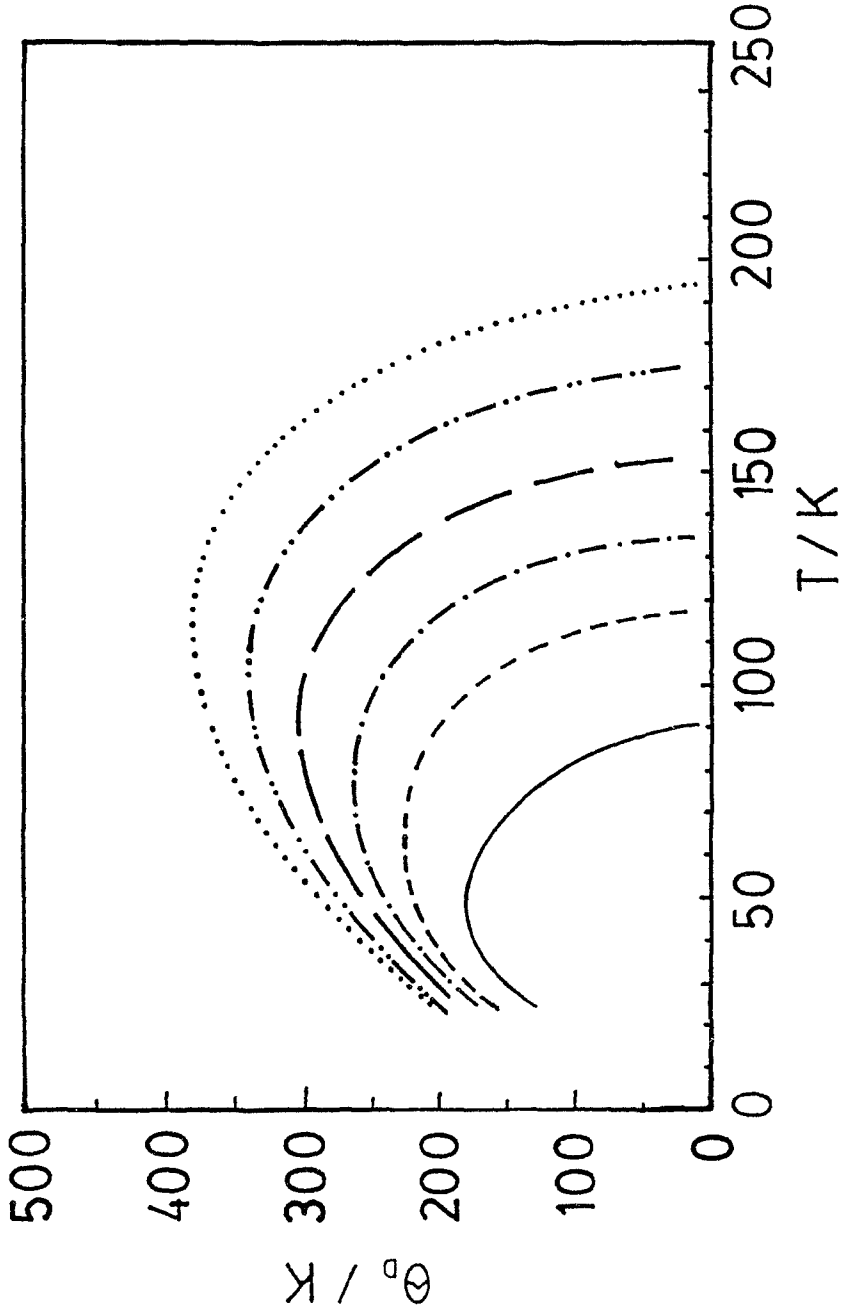

Figure 8.5

vibrational modes and anharmonic effects to the heat capacity.[121]

It is worth noting that all θ_D curves for the unsolvated Dianin's compound and its ethanol adduct (Figure 8.4 and 8.5) join in the low temperature region at values between 150 and 200 K, indicating the probable value of θ_D.

The Debye temperature also can be calculated based on sound velocity measurements by use of equation (8.1.3). Here again the division of the molecule into subgroups is crucial. With the assumption of six subgroups θ_D was found to be 167 K for ethanol adduct of Dianin's compound. Corresponding values for unsolvated Dianin's compound and its CCl_4 adduct are 164 K and 168 K respectively, assuming the velocity of sound in the CCl_4 and ethanol adducts to be the same. θ_D obtained from elastic constants, the above assumption and equation (8.1.6), was found to be 186 K for the ethanol adduct of Dianin's compound.

The differences in the values of θ_D for the ethanol adduct as calculated from different methods reflect a number of factors. The difference between the values from elastic constants and mean sound velocity likely reflect the fact that the sound velocity was measured along the c-axis. From the Brillouin scattering results (Chapter 7) it is known that for this direction the longitudinal sound velocity is the lowest observed, and the transverse sound velocity also is low, giving the (observed) lower effective Debye

temperature. Also, from the temperature-dependence of θ_D from C_v, one would expect, based on results for other solids[113], that θ_D would increase below about 25 K, making the T=0 value from C_v and velocity of sound in reasonable agreement.

8.2.c. Grüneisen Parameter

The results of the calculation of γ_a, γ_c and γ, based on equations (8.1.17) to (8.1.21), for the ethanol adduct of Dianin's compound are shown in Figure 8.6. For these calculations it was assumed that the elastic constants are independent of temperature. Although the elastic constants of unsolvated Dianin's compound are not known, from the velocity of sound results it is not unreasonable to expect them to be close to those of the ethanol adduct; under this assumption, γ for the empty Dianin's compound has been calculated, and the results are shown in Figure 8.7. Given the similarity of the sound velocities of the ethanol adduct and unsolvated Dianin's compound, one might reasonably expect that the elastic properties of the CCl_4 adduct would be similar; with this assumption, the Grüneisen parameter for CCl_4 adduct has been calculated. This result also is shown in Figure 8.7.

For non-metallic solids, the Grüneisen parameter generally is of the order of unity[114], and this is the case

Figure 8.6 The results of the calculation of γ_a (dotted line), γ_c (dashed line) and γ (solid line) for the ethanol adduct of Dianin's compound, as a function of the temperature.

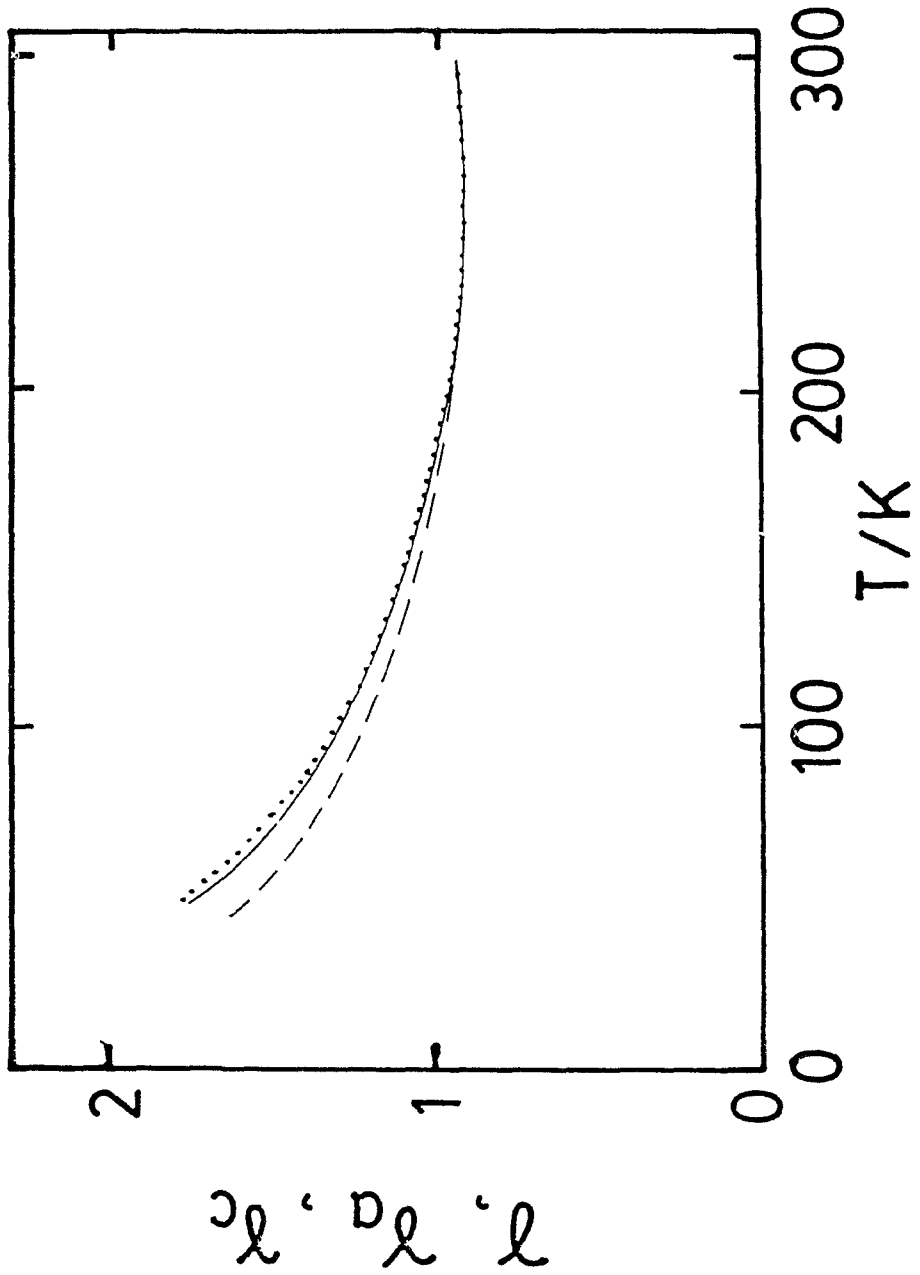

Figure 8.6

Figure 8.7 The overall Grüneisen parameters of the unsolvated (dotted line) and ethanol (solid line) and CCl_4 (dashed line) clathrates of Dianin's compound, as functions of temperature.

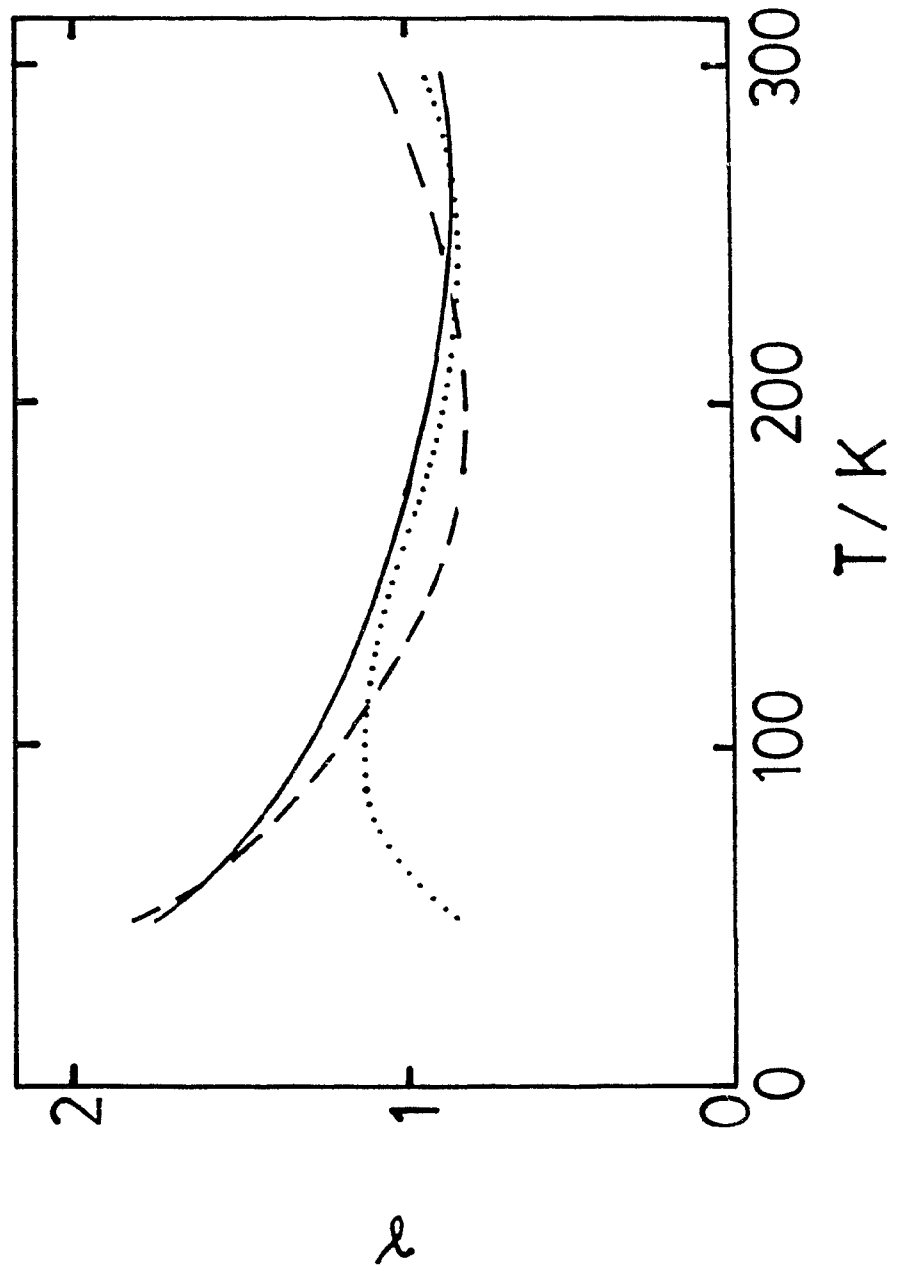

Figure 8.7

here. From Figure 8.7, it can be seen that the Grüneisen parameters for the ethanol and CCl_4 adducts are very similar to one another between 50 and 300 K. (Based on the error in the thermal expansion, γ is known to within about $\pm 30\%$.) In contrast with many solids in which γ tends to zero as the temperature decreases[114], it is found here that γ increases for both the ethanol and the CCl_4 adduct as the temperature drops. The more usual (opposite) trend is observed for the unsolvated Dianin compound. A similar effect was noted for the Grüneisen parameter of tetrahydrofuran clathrate hydrate in comparison with hexagonal ice.[123] From the present results, which give a direct comparison of a clathrate with and without its guest species, it is now clear that the presence of the guest increases the low-temperature anharmonicity of the intermolecular interactions within the solid, as manifest by the deviation of γ from zero.

Although this increase in γ at low temperatures is rare, it is not without precedence; similar behaviour has been observed[124] in CO and attributed[114] to the existence[125] of low-frequency librational modes. If, in adducts of Dianin's compound, there are low-frequency optic modes associated with motion of the guest molecules in the cages, as has been proposed in the mechanism of enhanced thermal resistance in clathrate hydrates,[29] these modes may be the source of the anharmonicity that gives rise to the unusual low-temperature dependence of γ observed here.

An increase in γ with decreasing temperature also has been observed in some amorphous materials, and attributed in part to the linear temperature dependence of the heat capacity[114]. Although this may be a factor in the Dianin clathrates, it is not the total determinant, as the heat capacity is quite linear both with and without guests in the cage, yet γ has very different temperature dependences in these different circumstances. Almost certainly, it is the enhancement of the thermal expansion due to the presence of the guest that is responsible for the increased low-temperature anharmonicity, as seen in the Grüneisen parameter in the ethanol and CCl_4 clathrates of Dianin's compound, relative to the empty lattice.

Chapter 9 : Thermal Conductivity

9.1 Theory

A true normal mode of vibration and its associated phonon (quantum energy of this vibration) are spread uniformly throughout a perfect crystal. The finite thermal conductivity of a real non-metallic crystal is caused by interactions which attenuate the vibrational energy. Therefore the atomic motions do not correspond exactly to normal modes. The thermal energy is considered as propagating by means of wave packets made up from a range of "almost normal modes". These travel with the phonon group velocity, v_g. The interactions are taken into account through the variation of the number of phonons with position: P(q) is the number of phonons which form a wave packet in a particular place with wave vector equal to q. The total heat current, h, due to all modes is given by the sum over all modes:[44]

$$h = \Sigma\ P(q)\ \hbar\omega\ v_g(q) \qquad . \qquad (9.1.1)$$

In thermal equilibrium the total heat flow is equal to zero. However in the presence of a temperature gradient in the z direction the rate of change of phonon number of mode q in some region with respect to time t is given by:[44]

$$\left(\frac{\partial P(q)}{\partial t}\right)_{drift} = -(v_g \nabla T)\ \frac{\partial P(q)}{\partial t} \quad . \qquad (9.1.2)$$

When a steady state has been established, the phonon density at all points in the crystal becomes independent of time. To make this possible there must exist opposing phonon density changes due to scattering effects. Referring to these, the Boltzmann equation for the transport phenomena can be written[44] as:

$$\left(\frac{\partial P}{\partial t}\right)_{drift} + \left(\frac{\partial P}{\partial t}\right)_{scatt} = 0 \quad . \qquad (9.1.3)$$

One of the methods of solution of equation (9.1.3) is the relaxation time method. Here it is assumed that scattering processes tend to restore a phonon distribution to the thermal equilibrium distribution. The rate of restoration is proportional to the difference from the equilibrium value (P^o):[44]

$$\left(\frac{\partial P}{\partial t}\right)_{scatt} = \left(\frac{P^o - P}{\tau}\right) \qquad (9.1.4)$$

where τ is a relaxation time which depends on wave vector and direction as well as P^o and P. Assuming further that

the distribution in the presence of a temperature gradient is close to the equilibrium distribution so it is possible to replace P by P^{o} in equation (9.1.2), Boltzmann's equation yields heat flow:[44]

$$h=-\Sigma\hbar\omega(v_g^{\,z})^2\tau\frac{\partial P^0}{\partial t}\frac{\partial T}{\partial z} \qquad (9.1.5)$$

and thermal conductivity, κ:

$$\kappa=-\frac{h}{\left(\frac{\partial T}{\partial z}\right)} \quad . \qquad (9.1.6)$$

By replacing the summation in equation (9.1.5) with an integral, using the Debye density of modes and writing the square of the phonon group velocity in the z direction, $(v_{gz})^2$, as $1/3v_g^{\,2}$ (see equation 8.1.4), the thermal conductivity is equal to:[44]

$$\kappa(T)=\frac{1}{2\pi^2 v}\int_0^{\omega_D}\tau_{total}\frac{\hbar^2\omega^4}{k_BT^2}\frac{\exp(\hbar\omega/k_BT)}{[\exp(\hbar\omega/k_BT)-1]^2}\,d\omega \quad .$$

(9.1.7)

A relaxation time can be expressed as the ratio of a mean free path to a velocity. The above and the Debye law, equation (5.1.8) in its explicit form, allow the thermal conductivity to be written as:

$$\kappa(T) = \frac{1}{3} v \int_0^{\theta/T} \ell(x)\ c(x)\ dx \qquad (9.1.8)$$

which is a logical extension of Kundsen flow, where $\ell(x)$, $C(x)$ and x are the phonon mean free path as a function of position, heat capacity as a function of position and coordinate, respectively. However it is worthwhile to point out that the relaxation time, τ, depends on many scattering mechanisms, such as lattice defects and phonon-phonon interactions. Therefore the relaxation time should be treated as a total relaxation time. If it is assumed that each scattering mechanism can be characterized by a separate relaxation time and its value, for a given mode, is independent of phonon populations of all other modes, then the total relaxation time, τ_{total}, is given by:

$$\tau_{total} = (\sum_i \tau_i^{-1})^{-1} \qquad (9.1.9)$$

where $\tau_i(x)$ are relaxation times for each mode.

9.2 Thermal conductivity apparatus

The method of measurement of thermal conductivity is particularly important in very poor thermal conductors such as clathrates.[29] The measurements were carried out on free-standing single crystals in order to preclude the thermal short-circuit correction that could be associated with a cell apparatus.

The apparatus, of the Slack design,[126] made use of the steady-state potentiometric method. This apparatus had been used previously to determine the thermal conductivity of tetrahydrofuran clathrate hydrate.[119] It had also been used to measure the thermal conductivity of a Harshaw single crystal of NaCl,[29] and the results were found to be within the range of the literature values.[127] A schematic of the apparatus is shown in Figure 9.1. The whole measuring system consists of the apparatus shown in Figure 9.1, a platinum resistance thermometer and D.C. power supply, an adiabatic shield and its heater, a digital multimeter (HP 3456A), an Artronix 5301-E shield controller, a vacuum system, the heaters for the crystal and for the heat sink, and the data acquisition system. All electrical measurements (heater resistance (four wire method), heater voltage,

Figure 9.1 Thermal conductivity apparatus.
a.to the vacuum pumps, b. vacuum, c. liquid nitrogen, d. liquid nitrogen or liquid helium, e.thermal anchor for electrical leads, f. single crystal with heater and thermocouples, g. copper heat sink, h. Pt resistance thermometer.

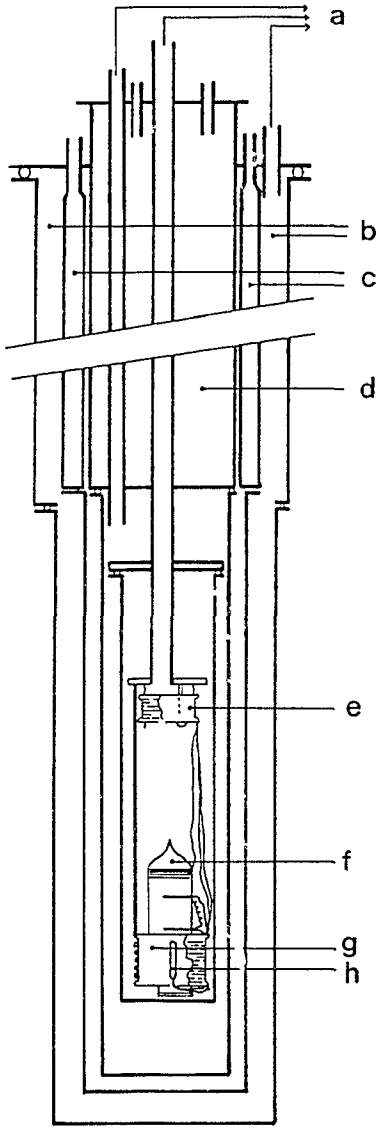

Figure 9.1

thermocouple emf, resistance ratio of Pt thermometer relative to standard resistor) were automated.

In contrast with the immersion cryostat of the adiabatic calorimeter, the cryostat used for the thermal conductivity measurements was of the aneroid type. In this design both reservoirs for liquid helium and liquid nitrogen are located on the top of the apparatus. The liquid helium reservoir is located centrally while the nitrogen reservoir surrounds the former. The sample was surrounded by four cryostat tails and an adiabatic shield. The first and second cryostat tails were sealed with indium seals. The third was in thermal contact with the liquid nitrogen reservoir and the fourth was sealed with a rubber O-ring and Apiezon-M grease.

Before cryogenic liquids were introduced to the cryostat the whole system was evacuated to avoid frozen air effects (electrical and thermal). Then the cryogenic liquids and helium exchange gas were introduced to the system to cool it. When the desired temperature was obtained the helium exchange gas was pumped away.

To maintain good insulation two vacuum pumps were connected to the system, a roughing pump and an oil diffusion pump. A low-temperature gas trap was placed between the diffusion pump and the system. The three separate inner regions of the cryostat, each of which was connected to the vacuum pumps by a separate valve, allowed regulation of the thermal condition efficiently and

provided good thermal insulation. However, the temperature range was limited at the high end by radiative heat losses, as is common for this method.[119,128] The vacuum was maintained better than 10^{-5} Torr.

The thermal anchor was made of copper. Thirty terminals were epoxied in the top and thirty in the bottom. The outside surface was varnished with GE 7031 low-temperature varnish and covered with cigarette paper for insulation and varnished again. Thirty 38 SWG Cu wires were doubly-wound around the thermal anchor, varnished in place and soldered with Leeds and Northrup thermal free solder.

The copper heat sink was varnished with low temperature varnish and covered with cigarette paper for insulation. Then 43 SWG Karma wire (230 Ohm/m) was wound around it to give a heater of 600 Ohm resistance. The platinum resistance thermometer (Pr-100B, Cryoc Inc., St. Paul, Minnesota, R (25°C ~ 100 Ohms)) was installed inside the central cavity in the heat sink and a protective cap mounted underneath it. A small detachable monel plate was installed on the top of the heat sink as a crystal platform. The heat sink was attached to a flange above the thermal anchor by support rods, as is shown in Figure 9.1.

For the same reason as was explained in Section 5.2, an adiabatic shield was introduced to the measuring system. This shield was constructed in the same way except the heater was wound more densely at the top to match the

anticipated thermal gradient of the crystal being measured; the shield was suspended by nylon filaments attached to hooks originating at the thermal anchor. A copper-constantan thermocouple junction was varnished with low temperature varnish (GE 7031) to the inside wall of the shield. The reference thermocouple junction was attached to the bottom of the crystal plate and covered with Apiezon M grease for good thermal contact. An Artronix-E shield controller worked as D.C. power supply for the shield heater.

9.3 Crystal Preparation

Because of the preferential growth direction, the crystal was oriented to measure the heat flow along the crystallographic c-axis.

The thermocouples used were 0.08-mm diameter AuFe(0.03 at.%Fe)/Chromel (Johnson Matthey; supplied and calibrated by Cryogenic Calbrations Ltd., England; accuracy ± 0.05 K in the temperature range used). This thermocouple wire was used for its high sensitivity and low thermal conductivity,[126] in order to minimize the thermal short circuit along the thermocouple. The length of the thermocouple wires between the junctions but not in contact with the crystal was 120 mm, chosen to reduce to negligible the heat flow along the thermocouple wires. The length of the chromel wires beyond the junctions but not touching the crystal was 143 mm. The

parts of thermocouple wires which were not in contact with the crystal were coiled and placed inside the shield. The thermocouple junctions were made by spark welding[129] in a helium atmosphere to reduce the thermal noise associated with using a different joining material.

43-SWG (230 Ohm/m Karma) wire was wound bifilarly, to form a heater of resistance of 77 Ohm.

The heater and the thermocouples were varnished to the crystal using low-temperature varnish (GE 7031). The solvent used for the low-temperature varnish was decanol to avoid possible problems with solvent molecules becoming guests in the clathrates. The crystal preparation process was very slow, since it had to be done incrementally and the decanol had to be evaporated under vacuum due to its high boiling point (231 °C). The crystal itself was kept in thermal contact with the heat sink by the silicon grease.

The unsolvated Dianin's compound crystal was 9.5 mm long and had a cross-sectional area of 9.04 mm^2. The lower thermocouple junction was placed 1.90 mm above the bottom of the crystal. The upper thermocouple junction was placed 2.49 mm above the lower. The heater was placed 2.00 mm above the upper thermocouple junction.

The ethanol adduct of Dianin's compound single crystal was larger, 12.5 mm long with a cross-section of 18.57 mm^2. The lower thermocouple junction was placed 2.06 mm above the bottom of the crystal. The upper thermocouple junction was

placed 2.36 mm above the lower. The heater was placed 1.10 mm above the upper thermocouple junction.

9.4 The Measurement Procedure

The thermal conductivity measurements were performed by the standard steady-state potentiometric method.[44,126,130] For the passage of power q through a single crystal of cross-section area A, the thermal conductivity, κ, is given by:

$$\kappa = \frac{q}{A}\frac{d}{\Delta T} \qquad (9.4.1)$$

where thermocouples placed a distance d apart are used to measure the temperature differential ΔT. The absolute temperature of the crystal was determined by measuring the voltage drop across the platinum resistance thermometer in the heat sink, relative to a standard resistor (as in Figure 5.3). The temperature thus measured was converted to the temperature of the crystal at the point midway between the thermocouple junctions through a knowledge of the temperature gradient along the crystal. The power to the sample heater during the measurements was chosen to give ΔT of 1 to 1.5 K, chosen to maximize accuracy[119,128] of the experiment while minimizing the relaxation time required to obtain the steady state conditions.

The sources of error in this experiment were the determination of cross-sectional area of the crystals (±10%), the thermocouple separation distance (±5%), the temperature differential (±2%), and the power input (±2%). All considered, these gave an error range for the thermal conductivity measurements of ±20%.

9.5 Results

The relaxation times following heating were about 40 to 50 min. for the empty Dianin's compound and about 40 to 60 min. for the ethanol adduct. In each case the shortest relaxation time was observed at the lowest temperature. The measured values of the thermal conductivity of Dianin's compound and its ethanol adduct are given in Tables 9.1 and 9.2 respectively.

The thermal conductivity of the ethanol adduct of Dianin's compound showed similar temperature dependence to that of tetrahydrofuran clathrate hydrate.[29] Surprisingly it was found that the thermal conductivity of unsolvated Dianin's compound behaved similarly, although it had larger magnitude. In other words, it did not show the characteristic behaviour of insulative crystals. Both the thermal conductivity of unsolvated Dianin's compound and its ethanol adduct are shown in Figure 9.2. The error bars reflect uncertainty related to the sources of error

Figure 9.2 The thermal conductivity of single crystals of Dianin's compound. The open circles stand for unsolvated Dianin's compound while the filled circles stand for its ethanol adduct. The error bars reflect the uncertainty related to the determination of cross-sectional area of the crystals, the thermocouple separation distance, the temperature differential, and the power input.

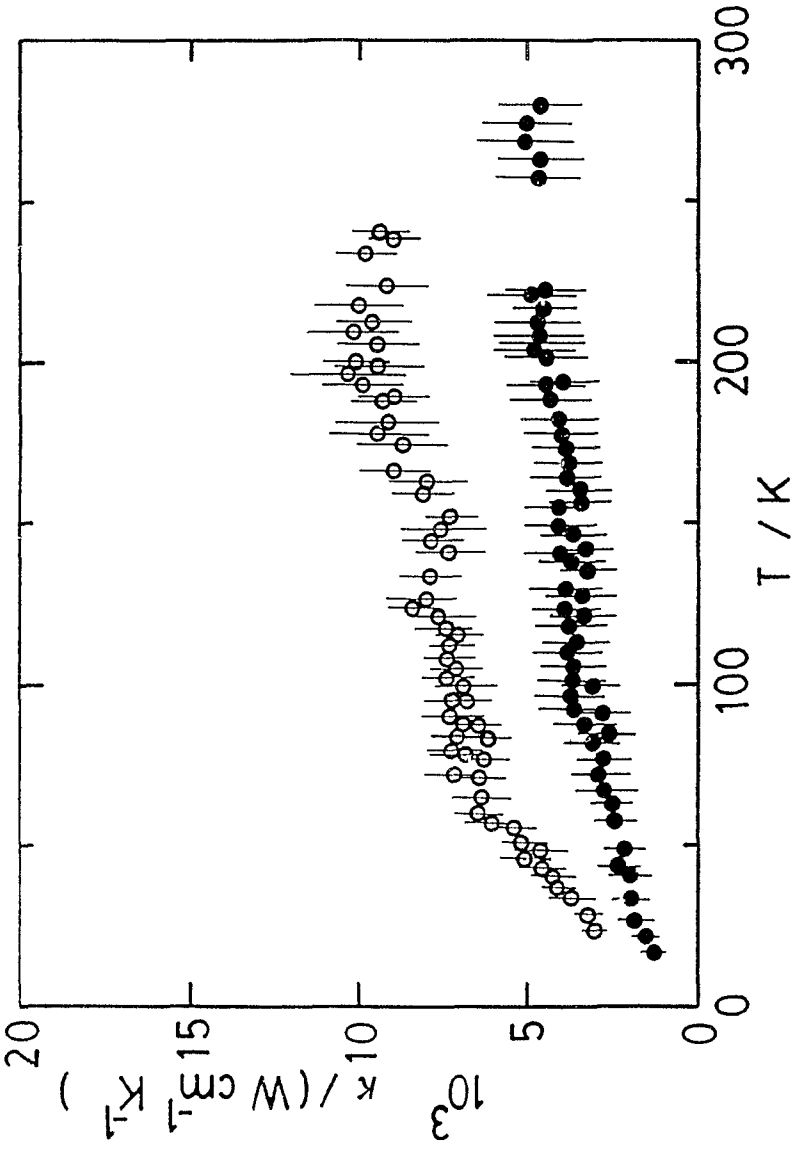

Figure 9.2

Table 9.1 The thermal conductivity κ of Dianin's compound.

T /K	κ /W m^{-1} K^{-1}	T /K	κ /W m^{-1} K^{-1}
23.73	0.31	112.29	0.73
25.87	0.31	115.45	0.70
28.77	0.32	117.03	0.74
31.19	0.36	117.72	0.73
33.93	0.37	121.21	0.76
37.05	0.41	121.78	0.81
39.23	0.41	123.67	0.84
40.39	0.42	126.31	0.79
40.90	0.43	126.57	0.83
42.53	0.46	128.80	0.80
43.41	0.45	133.41	0.78
45.96	0.50	137.33	0.72
48.39	0.46	141.06	0.72
49.38	0.52	144.75	0.78
50.92	0.51	148.42	0.75
51.40	0.53	152.06	0.72
55.48	0.53	159.33	0.80
55.53	0.54	162.91	0.79
56.97	0.60	166.32	0.89
59.35	0.60	172.92	0.89
59.92	0.64	174.26	0.86
64.77	0.65	176.11	0.89
64.95	0.63	177.80	0.94
67.08	0.64	181.27	0.91
70.92	0.63	183.98	0.93
71.96	0.71	188.08	0.92
76.76	0.62	189.26	0.89
76.98	0.65	190.02	0.97
78.30	0.67	192.40	1.01
79.68	0.71	193.26	0.98
83.19	0.61	196.29	1.03
83.90	0.70	198.65	0.94
87.27	0.64	199.89	1.00
87.47	0.69	201.84	0.94
90.16	0.72	205.44	0.94
91.30	0.67	209.24	1.01
94.72	0.67	212.47	0.96
94.97	0.71	217.55	1.00
99.17	0.68	220.87	0.90
99.62	0.69	223.67	0.91

Table 9.1 continued ..

Table 9.1 continued:

T /K	κ /W m^{-1} K^{-1}	T /K	κ /W m^{-1} K^{-1}
102.18	0.73	233.83	0.98
104.12	0.71	233.83	0.98
104.92	0.71	238.30	0.89
108.05	0.73	240.46	0.92
108.51	0.71		

Table 9.2 The thermal conductivity κ of ethanol adduct of Dianin compound.

T /K	κ /W m^{-1} K^{-1}	T /K	κ /W m^{-1} K^{-1}
16.94	0.13	109.99	0.38
19.96	0.15	113.01	0.35
20.39	0.14	114.2	0.37
22.69	0.15	116.48	0.36
22.85	0.16	118.33	0.38
25.19	0.17	121.1	0.33
25.67	0.17	121.14	0.34
26.9	0.19	122.18	0.33
28.44	0.18	122.31	0.40
29.55	0.18	122.85	0.33
30.75	0.19	123.37	0.39
31.44	0.20	123.47	0.34
33.43	0.20	127.23	0.34
33.9	0.19	127.6	0.36
36.17	0.20	129.56	0.38
36.80	0.19	131.45	0.35
38.84	0.21	135.33	0.32
40.94	0.20	138.01	0.38
43.31	0.21	140.62	0.40
43.97	0.23	141.74	0.34
44.97	0.22	141.74	0.33
47.64	0.22	142.26	0.35
48.82	0.22	145.41	0.39
49.18	0.22	146.54	0.36
51.29	0.22	148.87	0.41
51.78	0.23	151.04	0.38
53.76	0.24	151.04	0.38
57.51	0.24	151.16	0.41
58.06	0.24	154.97	0.40
61.20	0.25	156.41	0.34
63.32	0.25	160.11	0.35
65.45	0.28	162.49	0.40
67.18	0.24	164.15	0.38
67.18	0.28	168.68	0.38
70.07	0.24	173.23	0.38
70.14	0.27	177.74	0.40
72.30	0.26	182.26	0.41
72.33	0.29	186.75	0.42
76.82	0.28	188.41	0.43
76.93	0.28	192.79	0.44

continued.....

Table 9.2 continued:

T /K	κ /W m^{-1} K^{-1}	T /K	κ /W m^{-1} K^{-1}
79.17	0.29	193.83	0.39
80.58	0.29	194.83	0.45
82.11	0.31	195.86	0.43
82.77	0.29	197.22	0.44
82.83	0.27	199.19	0.43
84.08	0.28	201.53	0.44
84.44	0.25	202.64	0.44
84.65	0.26	203.57	0.48
85.10	0.30	205.69	0.45
86.30	0.27	207.94	0.47
87.22	0.33	212.16	0.47
87.87	0.33	216.57	0.45
91.05	0.28	220.54	0.47
92.22	0.36	220.90	0.49
96.53	0.37	222.38	0.45
99.58	0.31	257.10	0.47
100.74	0.36	262.92	0.46
101.40	0.36	268.55	0.51
104.74	0.33	274.16	0.50
105.74	0.36		

mentioned in the previous section.

9.6 Discussion

9.6.a. Mean Free Path

The analysis of the thermal conductivity is performed within a phenomenological mean free path model (equation 2.1) adapted from the kinetic theory of gases.[44,131,132] The phonon mean free path was calculated using equation (2.1) and the present experimental values of the density and total heat capacity (which is dominated by the accoustic modes at low temperatures) as a function of temperature, and average velocity of sound. The results for unsolvated Dianin's compound and its ethanol adduct are shown in Figure 9.3. In the case of the ethanol adduct the phonon mean free path reaches the size of the cage, 11 Å, in the low temperature region. Without guests the mean free path is about three times larger than the cavity length at low temperature and decreases to the cavity dimension in the high temperature region. In both cases the phonon mean free paths show glassy characteristics,[133,134] *i.e.* they are of the order of the cell dimensions throughout the observed temperature region.

9.6.b. Universal Thermal Conductivity

It has been demonstrated[135] by scaling thermal conductivity data to a function involving the Debye temperature, θ_D, that glassy solids exhibit universal

Figure 9.3 The phonon mean free path determined by equation (2.1).

——— unsolvated Dianin's compound

– – – ethanol adduct of Dianin's compound

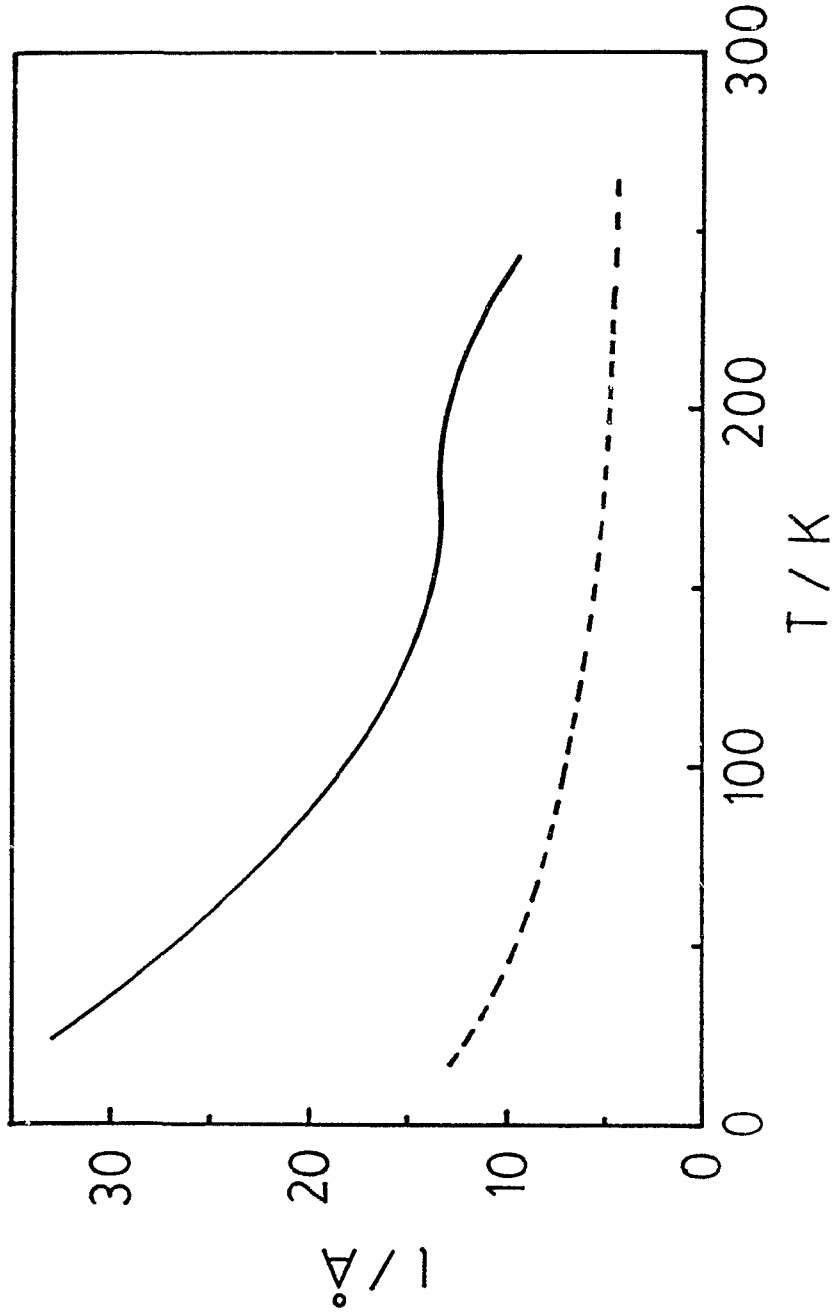

Figure 9.3

behaviour. It also has been shown[29], that by scaling the data to this same form, *viz.*:

$$\frac{\kappa(T)}{C} = \left(\frac{T}{\theta_D}\right)^3 \int_0^{\omega_D} (k_B\theta_D)\ (\tau_{total}/h) \quad \frac{\hbar^2\omega^4}{k_BT^2} \frac{\exp(\hbar\omega/k_BT)}{[\exp(\hbar\omega/k_BT)-1]^2}\, d\omega \tag{9.6.1}$$

where $C=4\pi k_B^3\,\theta_D^2/h^2v$, the THF clathrate hydrate thermal conductivity results are comparable with the results for glassy materials.

From elastic constants the Debye temperature, θ_D, for the ethanol adduct of the Dianin's compound was reported in Chapter 8 to be 186 K. The scaled thermal conductivity data for unsolvated Dianin's compound falls exactly in with glassy materials, as shown in Figure 9.4. Similarly, the results for the ethanol adduct were scaled and are shown in Figure 9.4. Considering that the thermal conductivities are of the same order of magnitude and θ_D is also virtually the same, the universal thermal conductivities of both unsolvated Dianin's compound and the ethanol clathrate of Dianin's compound are almost indistinguishable (on the logarithmic scale of Fig. 9.4) suggesting glass-like behaviour of the thermal conductivity both with and without guests in the cage.

Figure 9.4 Scaled thermal conductivi[illegible] s[8] of THF clathrate hydrate, and six amorphous solids:[135] PB-polybutadiene; PET-poly(ethylene terephthalate); PS-polystyrene; PMMA-poly(methyl methacrylate); DC- unsolvated Dianin's compound; DC-ETOH ethanol adduct of Dianin's compound.

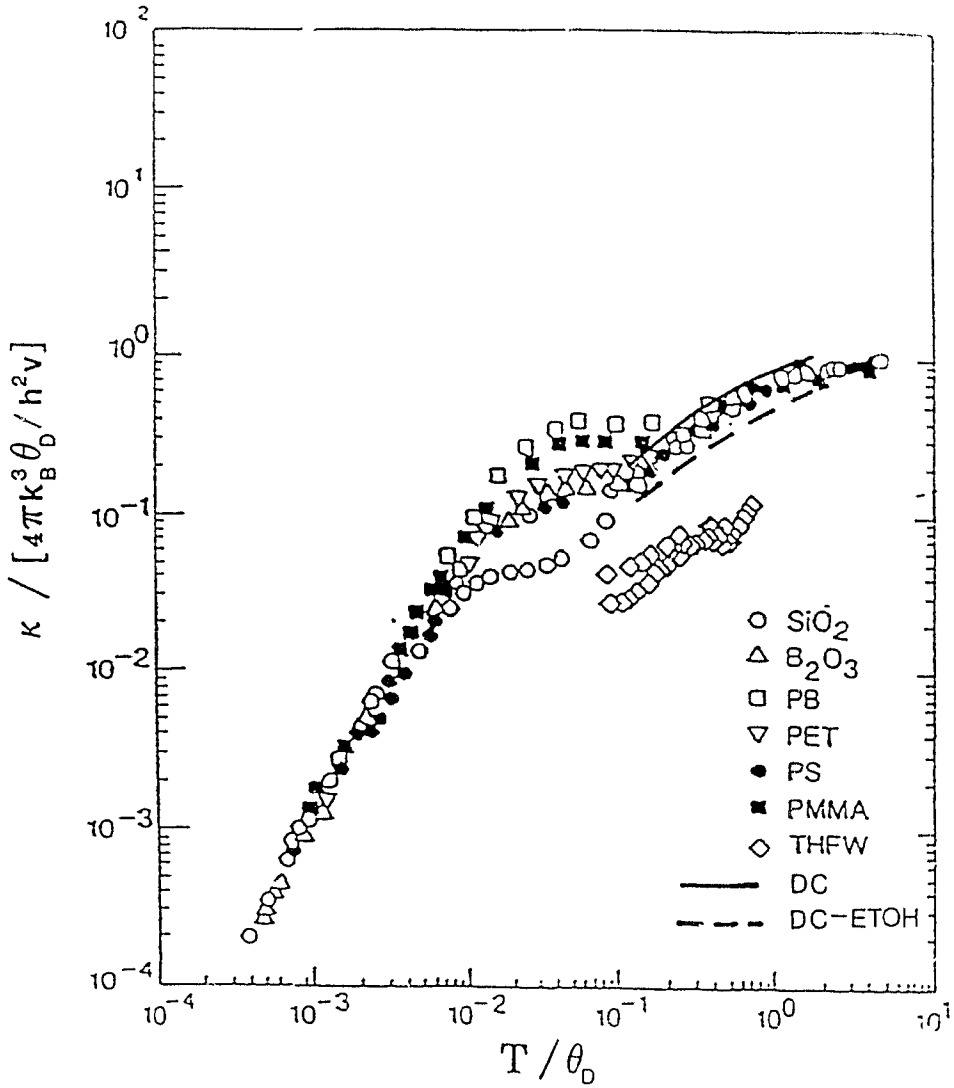
10^2
10^1
10^0
10^{-1}
10^{-2}
10^{-3}
10^{-4}
$\kappa / [4\pi k_B^3 \theta_D / h^2 v]$
10^{-4}
10^{-3}
10^{-2}
10^{-1}
10^0
10^1
T / θ_D
SiO_2
B_2O_3
PB
PET
PS
PMMA
THFW
DC
DC−ETOH

Figure 9.4

9.6.c. Einstein model

The short mean free path, see Figure 9.3., and glassy behaviour suggest the use of the Einstein model[133,136] of a random walk of localized oscillations to describe the thermal conductivity. When the oscillations are so strongly damped that they pass on their energy within half a period of oscillation, the thermal conductivity is given by:

$$\kappa_{Einst} = \frac{k_B^2 n^{1/3}}{\hbar\pi} \theta_E \frac{x^2 e^x}{(e^x-1)^2} \qquad (9.6.2)$$

where n is the density number as afunction of temperature (volume change was taken into account), θ_E is the Einstein temperature and $x=(\theta_E/T)$. The thermal velocity of the molecule then, used in equation (2.1), is $v=n^{-1/3}/\tau_E$, where τ_E is one half of a period of oscillation, and the interatomic spacing is $n^{-1/3}$.[133] The Einstein characteristic temperature was estimated, using the heat capacity results and an assumption of six subgroups per molecule, to be 160 K for Dianin's compound with or without the ethanol guest. The temperature dependence of the volume[66] was used to calculate the density number n(T). The magnitudes of κ_{Einst} in both cases are reasonably close to the experimental data (Figure 9.5). However, the model fails to distinguish between "empty" and "occupied" cages of Dianin's compound.

Figure 9.5 The thermal conductivity of Dianin's compound. The empty circles represent experimental data of unsolvated Dianin's compound, the solid line represents the Einstein model results for same crystal and the dashed line represents Slack's minimum thermal conductivity[137] obtained by applying the Debye formalism to the Einstein model. The closed circles represent experimental data of ethanol adduct of Dianin's compound.

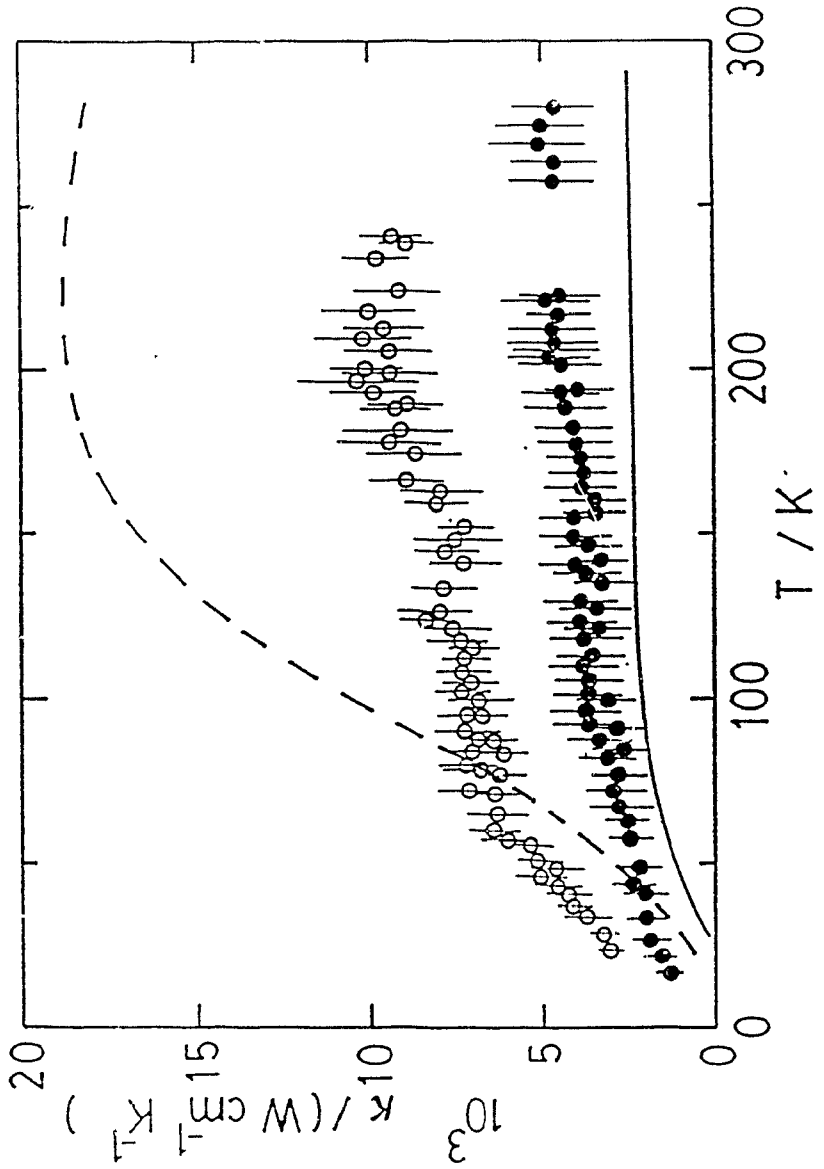

Figure 9.5

9.6.d. Minimum Thermal Conductivity

Following Cahill and Pohl[133] the Debye model was used to calculate Slack's minimum thermal conductivity[137]. This approach is advantageous because it maintains the physical picture of a random walk between Einstein oscillators and it transforms into the standard Debye model when the mean free path becomes large relative to the wavelength.

With the assumption that the frequency of oscillation of atomic groups is given by the frequency of the corresponding wave and that the separation length between atomic groups equals half the wavelength, the minimum thermal conductivity is given by:[133]

$$\kappa_{min} = \frac{1}{2.48} \; k_B n^{2/3} v_i \; 2 \left[\frac{T}{\theta_C}\right]^2 \int_0^{\theta_C/T} \frac{x^3 e^x}{(e^x-1)^2} \, dx \qquad (9.6.3)$$

for one polarization with the speed of sound v_i, where $\theta_C = \hbar/k_B \; v_i (6\pi^2 n)^{1/3}$. The total minimum thermal conductivity was calculated by adding contributions for two transverse and one longitudinal mode.[133] The resultant curves obtained by both the Einstein and the Debye-like minimum thermal conductivity models in comparison with values of the thermal conductivity of unsolvated Dianin's compound are shown in Figure 9.5. Both models maintain the $d\kappa/dT > 0$ character and

they exhibit the same relationship with each other as described by Cahill and Pohl,[133] namely the thermal conductivity from the Einstein model is much lower than from the Debye formalism. However, the experimental data fall between the model values; this appears to be the first example of thermal conductivity lower than the Slack minimum thermal conductivity.[133]

9.6.e. Guest-host Resonance Scattering Models

Having shown that the thermal conductivity of both unsolvated Dianin's compound and its ethanol adduct behave as glassy materials, the question remains as to why the "empty" clathrate behaves like that, and why the ethanol adduct has substantially lower thermal conductivity.

It has been shown[138] that the molecular ion CN^- substituted in alkali halide crystals for the halogen ion can act as a strong phonon scatterer. In a certain concentration range of CN^- the thermal conductivity becomes very like that of an amorphous material. Other studies[139,140] on crystalline KCl doped with NO_2^- and CN^-, and also on THF clathrate hydrate[29], show that resonant scattering may occur as a result of interaction between the low frequency librational motions of the guest species with the acoustic modes of the crystalline host lattice.[141,142] It is quite likely that such guest-host resonance scattering can account for the "glass-like" thermal conductivity observed in the

ethanol adduct of Dianin's compound (*vide infra*).

In the unsolvated Dianin's compound where the cages are (at least substantially) unoccupied, it is not possible to attribute the observed thermal conductivity to guest-host interaction. However, the resonance scattering mechanism is not limited to guest-host interaction: the resonance interaction of low frequency optic modes of the polymer side groups with acoustic phonons in polydiacetylene[118] is a case in point. It therefore seems likely that there are low-frequency optic modes in the Dianin's compound itself (even when the cages are empty) that can interact in a resonant manner with the lattice acoustic modes, thereby attenuating the thermal conductivity relative to a "normal" crystal. These modes may well arise from internal degrees of freedom within Dianin molecule: candidates are the three methyl groups (which maintain their motion even in the solid state[122,143]); the motion of the phenolic hydrogen[89] in the hydrogen-bonded hexamer at the roof and the bottom of the cage; the flexibility of the carbon skeleton itself to small movements into and out of the cage (especially C_{18} and C_{19} as seen by ^{13}C nmr[122]).

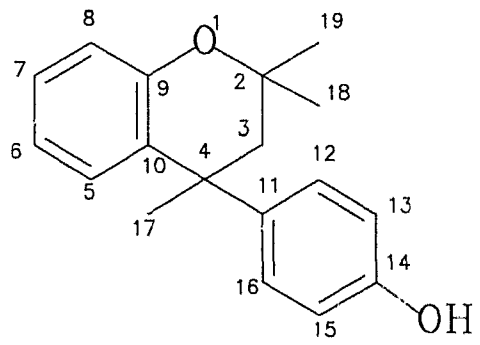

In analysing the present data the individual scattering mechanisms[29,131] and corresponding relaxation times, τ_i, were treated as separable, as shown in equation (9.1.9).

A phenomenological expression for a single resonance frequency[29,139,142,144,145] is given by:

$$\tau_s^{-1}=G_0 D \frac{\omega_0^2\omega^2}{(\omega_0^2-\omega^2)^2} \qquad (9.6.4)$$

where G_0 is the concentration of the resonant scatterer, D is a coefficient related to the strength of the acoustic-optic coupling, and ω_0 is the optical vibrational frequency involved in resonant scattering.

The dominant phonon-scattering mechanism at high temperature is likely the three-phonon Umklapp process. The theoretical expression for the relaxation time due to the Umklapp processes, τ_u, is given by:[146]

$$\tau_u^{-1}=B_u\omega^2 T \exp(-\theta_D/\alpha T) \qquad (9.6.5)$$

where B_u and α are empirical constants.

In addition to resonant and Umklapp scattering, there will be scattering from the boundaries of the sample. The relaxation time for the boundary scattering, τ_B, was evaluated using the expression for a cylindrical sample[147,148]:

$$\tau_B^{-1} = \frac{v}{1.18\ d} \qquad (9.6.6)$$

where d is the diameter of the sample.

It was shown[29] that the guest molecules do not act as "point defects" to scatter the low frequency phonons in clathrate hydrates. (Indeed this scattering gave the wrong temperature dependence.) Therefore the Rayleigh law:[149]

$$\tau_R^{-1} = F\omega^4 \qquad (9.6.7)$$

where F is related to the nature of the scatterer, was not used in the present analysis.

With the three contributions to the thermal conductivity given by equations (9.6.4), (9.6.5) and (9.6.6), the experimental data for the thermal conductivity of Dianin's compound and its ethanol adduct were fitted to equation (9.1.7) by nonlinear least squares analysis[150] using the total relaxation time from equation (9.1.9).

The use of equation (9.6.4) for resonant scattering in the case of unsolvated Dianin's compound must reflect motions of parts of the molecules relatively independent from the acoustic motions of the entire crystal lattice. The frequency of rotation of the three methyl groups was

estimated[151] to be ~10^{11} s^{-1} from ^{13}C nmr data.[122] The concentration was taken as that of methyl groups, 7.84×10^{27} m^{-3} at room temperature. The hydrogen bond flipping was reported[89] to occur at a frequency of 3.92×10^{7} s^{-1}, which is much too low to interact with the phonons in the frequency range of 10 to 120 cm^{-1} (3×10^{11} s^{-1} to 3.6×10^{12} s^{-1}) that are responsible for heat transfer.[133] Therefore this motion was not taken into account in resonant scattering.

The resulting fit to the thermal conductivity of unsolvated Dianin's compound is shown in Figure 9.6. The resonance frequency and coupling parameter extracted from the fit were 7.4×10^{11} s^{-1} (25 cm^{-1}) and 1.43×10^{-13} $m^3 s^{-1}$, respectively. The parameters B_u and α extracted from the fit were 1.4×10^{-19} s K^{-1} and 1.57 respectively.

As for unsolvated Dianin's compound three different scattering processes were taken into account for the ethanol adduct of Dianin's compound. Additionally, the motion of ethanol molecules had to be taken into the consideration. The ethanol molecules execute three different kinds of motion in the Dianin's compound cavity which could have influence on thermal conductivity. The inversion along the crystallographic c-axis happens with frequency of 8×10^{13} s^{-1}.[152] The rotation of the -OH group about the C-O bond occurs at 1×10^{14} s^{-1}.[56,152] Finally, the rotation about the crystallographic c-axis occurs at a frequency of 4×10^{12} s^{-1}.[56,152] Only the last frequency is significant for

Figure 9.6 The single resonance model fit to the experimental thermal conductivity of single a crystal of unsolvated Dianin's compound. Circles represent experimental data.

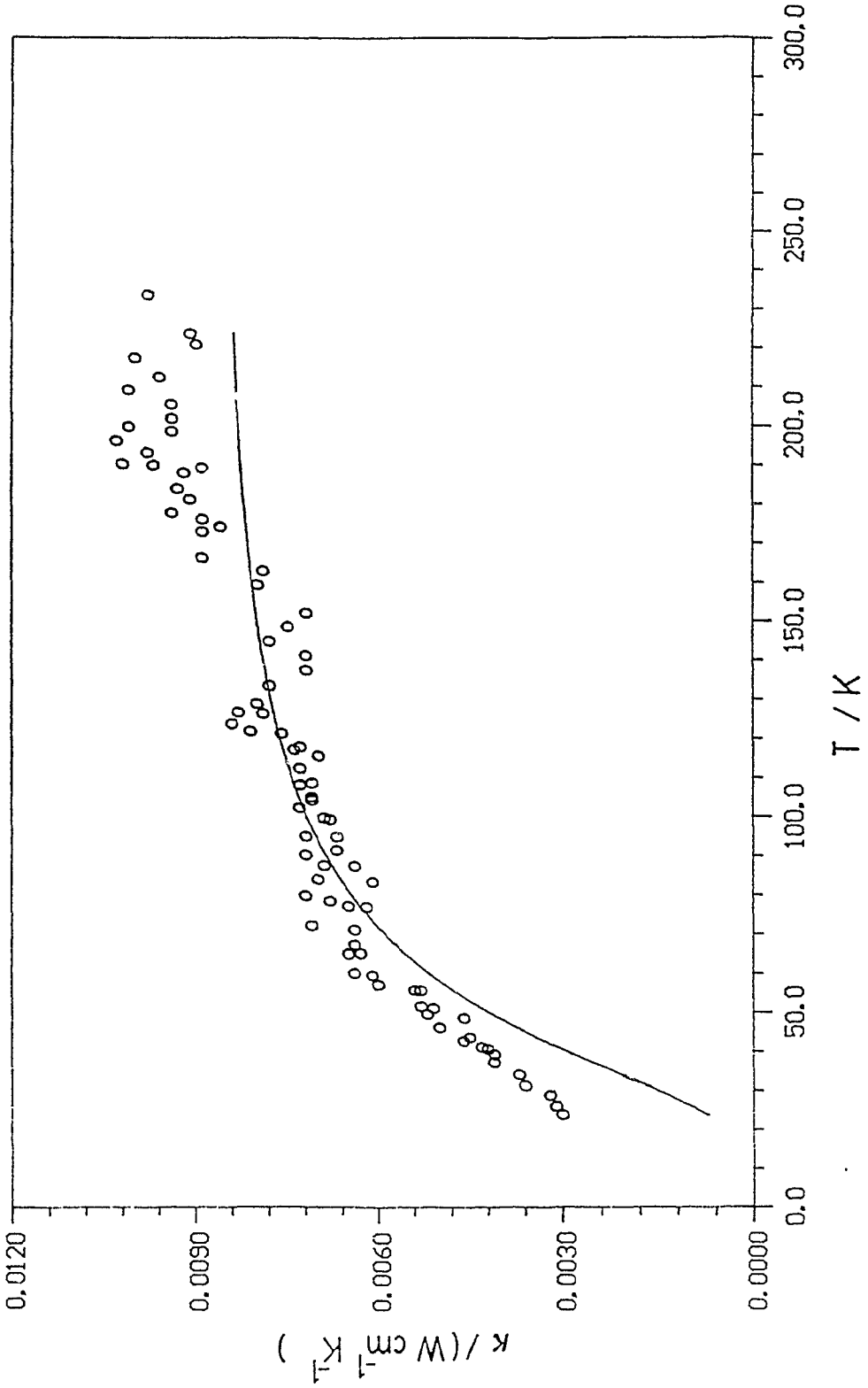
0.0120
0.0090
0.0060
0.0030
0.0000
κ /(W cm⁻¹ K⁻¹)
0.0
50.0
100.0
150.0
200.0
250.0
300.0
T / K

Figure 9.6

interaction with the phonons responsible for heat transfer.[133] Therefore two different resonators (rotation of the methyl groups and rotation of the ethanol molecules about the c-axis) were taken into account in estimating the resonant scattering relaxation time contribution. The density of ethanol scatterers was $8.7 \cdot 10^{26}$ m^{-3} and that of the methyl groups as before. The fit is shown in Figure 9.7. The resonance frequencies and coupling parameters extracted from the fit were 8.4×10^{11} s^{-1} (28 cm^{-1}) and $1.7 \times 10^{12} s^{-1}$ (58 cm^{-1}) and 1.6×10^{-13} m^3 s^{-1} and 1.6×10^{-13} m^3 s^{-1} for methyl groups and ethanol molecules respectively. The parameters B_u and α were $1.9 \cdot 10^{-19}$ s K^{-1} and 1.50, respectively.

The coupling parameters obtained here can be compared with 3.8×10^{-15} m^3 s^{-1} derived from tetrahydrofuran clathrate hydrate.[29] and 1.16×10^{-16} m^3 s^{-1} derived from a KCN^- doped KCl sample.[140] The larger values for Dianin's compound and its ethanol adduct may be a reflection of better matching of the acoustic and optic modes than in either THF clathrate hydrate or in $K(CN)_xCl_{1-x}$. The empirical constants B_u and α were similar to those for tetrahydrofuran (1.5×10^{-17} s K^{-1} and 6.55, respectively).

The thermal conductivity of carbon tetrachloride adduct of Dianin's compound was not measured since a sufficiently large single crystal was not grown. However, considering the similar behaviour of the host lattice in all three

Figure 9.7 The two-resonance model fit to the experimental data of thermal conductivity of single crystal of unsolvated Dianin's compound and its ethanol adduct. Circles represent the experimental data of unsolvated Dianin's compound and squares represent its ethanol adduct.

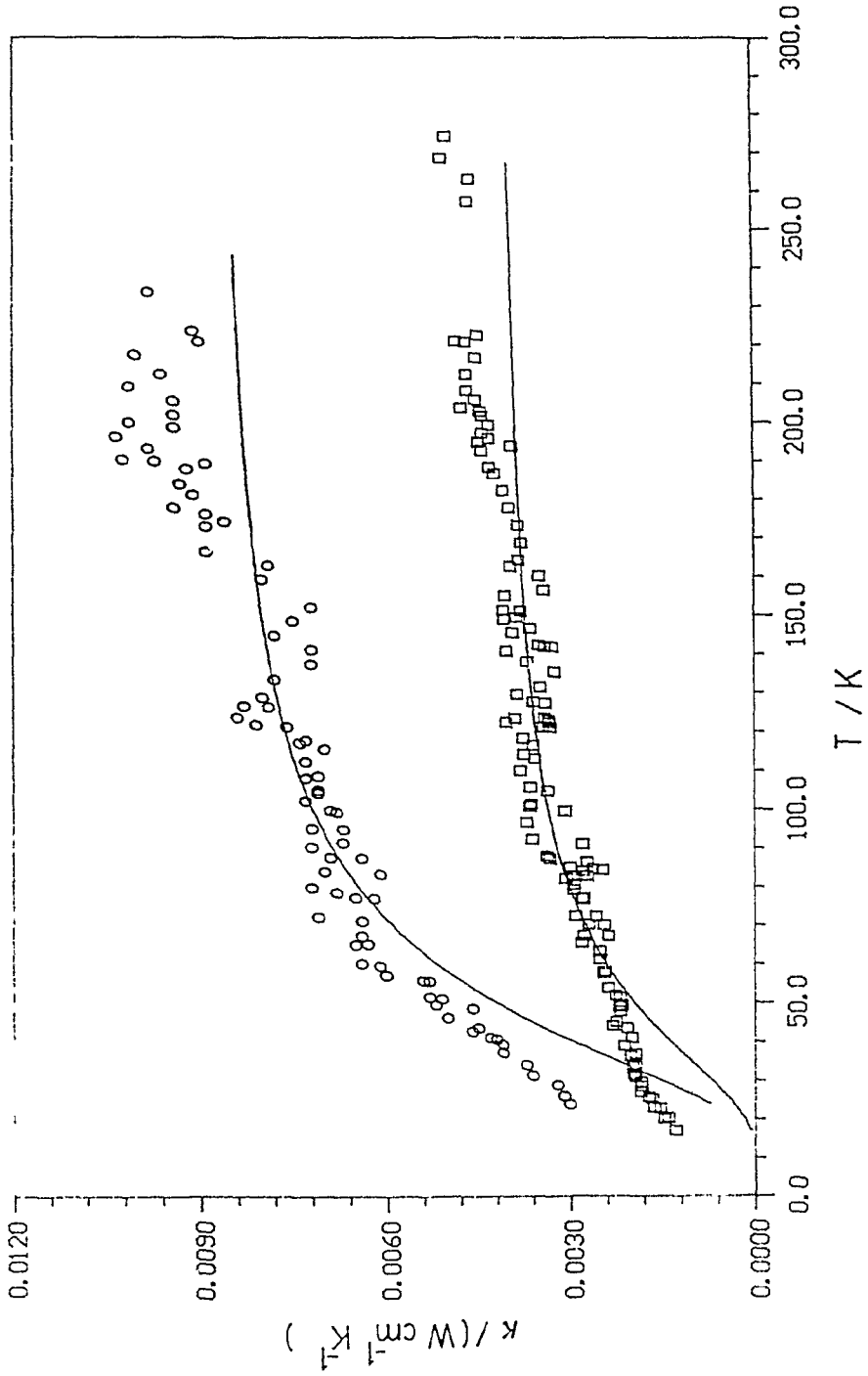
0.0120
0.0090
0.0060
0.0030
0.0000
k /(W cm-1 K-1)
0.0
50.0
100.0
150.0
200.0
250.0
300.0
T / K

Figure 9.7

adducts, as shown in previous chapters, and assuming that the last model describes properly the thermal conductivity, the thermal conductivity for the CCl_4 adduct could be calculated. The frequency of methyl group rotations, their density, average velocity of sound and parameters α and B_u were taken as the values for the ethanol adduct of Dianin's compound. The density of carbon tetrachloride molecules was 4.36×10^{26} m^{-3}. There are also two kinds of librational motion of the CCl_4 guest molecule which could influence the thermal conductivity.[87] Frequencies of these motions are 1.11×10^{12} s^{-1} (libration about the three-fold axis in Dianin's compound) and 1.41×10^{12} s^{-1} (doubly-degenerate libration). For the accuracy of this calculation these are almost indistinguishable. The frequency of libration about the c-axis has been chosen to be used in the model calculation because of two factors. First of all this is the same kind of motion which has been used in the ethanol adduct case. Secondly, the semiempirical factor which includes the temperature dependence and anharmonicity of the librational frequency, is four times larger for the axial libration then for the other suggesting stronger interaction with the lattice. The guuest-host coupling constant was taken the same as for ethanol adduct of Dianin's compound. The results are shown in Figure 9.8.

The fits to the unsolvated Dianin's compound and its ethanol adduct are in relatively good agreement with the

Figure 9.8 The thermal conductivity of single crystals of Dianin's compound and its adducts. Open circles represent experimental values of the thermal conductivity of unsolvated Dianin's compound. The solid line represents the fit obtained by use of the single resonance model. Squares show the experimental values of the thermal conductivity of the ethanol adduct of Dianin's compound. The dashed line represents the fit obtained by use of the two-resonance model. The dotted line represents thermal conductivity for the carbon tetrachloride adduct of Dianin's compound.

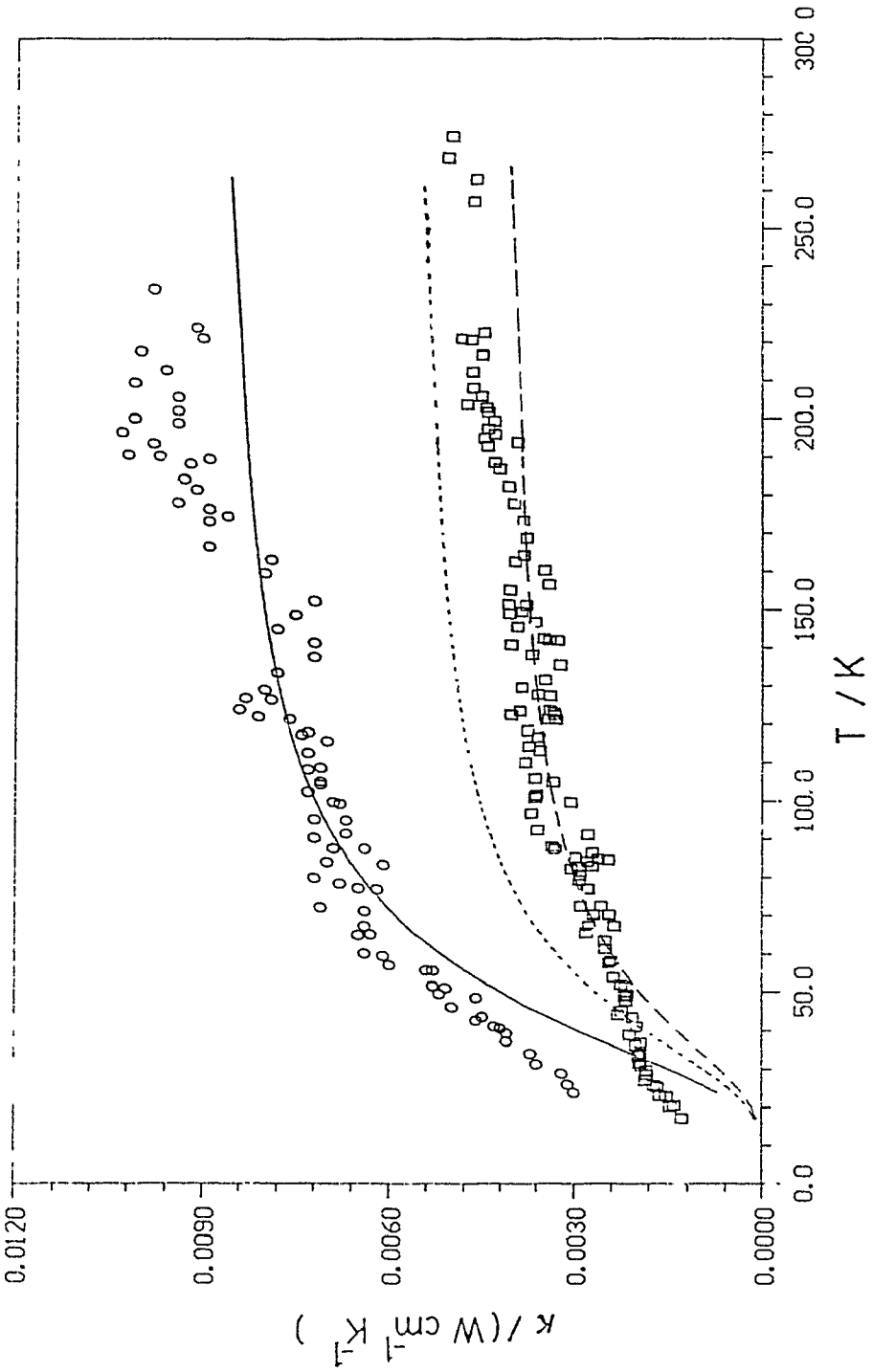
0.0120
0.0090
0.0060
0.0030
0.0000
κ / (W cm⁻¹ K⁻¹)
0.0
50.0
100.0
150.0
200.0
250.0
300.0
T / K

Figure 9.8

experimental reslts. The frequencies extracted from them are very close to the reported[56,122,152] literature values of frequencies of corresponding motions. All of the above suggest that the resonant model describes well the thermal conductivity of clathrates of Dianin's compound. This model is much more satisfactory than the simple Einstein model and even the more complex Debye model, both of which failed to explain the difference between the thermal conductivity of Dianin's compound with and without guests in the cages. Furthermore, the single resonance model predicts that the thermal conductivity of the CCl_4 adduct of Dianin's compound should fall between unsolvated Dianin's compound and its ethanol adduct which is in good logical agreement with thermal expansion and Grüneisen parameter results.

Chapter 10: Summary

The study presented here showed clearly that some properties of clathrates of Dianin's compound are affected by the guest presence. The presence of a guest causes increased anharmonicity of the interaction in the crystal lattice. The study showed the importance of host-guest interactions[55] which previously were reported to be negligible. There is also a relationship between occupancy factor and the magnitude of the anharmonicity involved: the more molecules in the cavity, the more anharmonic the lattice. The presented study showed also that even with unoccupied cavities a clathrate may exhibit glassy thermal conductivity; this is the first such report. It was also shown that Dianin's compound lattice is not as rigid as was previously believed.[55] In addition the full set of elastic constants was determined for the first time for a compound which crystallizes in the $R\bar{3}$ space group. The differences between C_p and C_v for all three investigated compounds were found and the effect of the presence of the guest on Grüneisen parameter was established.

Chapter 10: Summary

The study presented here showed clearly that some properties of clathrates of Dianin's compound are affected by the guest presence. The presence of a guest causes increased anharmonicity of the interaction in the crystal lattice the importance of host-guest interactions[55] which previously were reported to be negligible. There is also a relationship between occupancy factor and the magnitude of the anharmonicity involved: the more molecules in the cavity, the more anharmonic the lattice. The presented study showed also that even with unoccupied cavities a solid may exhibit glassy thermal conductivity; this is the first such report. It was also shown that Dianin's compound lattice is not as rigid as was previously believed.[55] In addition the full set of elastic constants was determined for the first time for a compound which crystallizes in the $R\bar{3}$ space group. The differences between C_p and C_v for all three investigated compounds were found and the effect of the presence of the guuest on Grüneisen parameter was established.

References

1. Yamaguchi, H.; Higashi, M. *J. Inclusion Phenom. Mol. Recognit. Chem.* 1990, **9**, 51.

2. Bender, M. L.; Komiyama, M. "Bioorganic Chemistry", Vol. **1**, p.19, Van Temelen, E. E. Ed.; Academic Press, New York, 1977.

3. Tanaka, Y.; Sasaki, S.; Kobayashi, A. *J. Incl. Phenom.* **2**, 851, 1984.

4. Poelma, F. G. J.; Tukker, J. J.; Hilbers, H. W.; Jansen, A. C. A. *J. Inclusion Phenom. Mol. Recognit. Chem.* 1989, **7**, 423.

5. Kurihara, M.; Fumitoshi, H.; Uekama, K. *J. Inclusion Phenom. Mol. Recognit. Chem.* 1990, **8**, 363.

6. Uekama, K.; Hirayama, F.; Yamada, Y.; Inaba, K; Ikeda, K, *J. Pharm. Sci.* 1979, **68**, 1059.

7. Uekama, K.; Hirayama, F.; Fujise, A.; Otagiri, M.; Inaba, K.; Saito, H. *J. Pharm. Sci.* 1984, **73**, 382.

8. Uekama, K.; Fujise, A.; Hirayama, F.; Otagiri, M.; Inaba, K. *Chem. Pharm. Bull.* 1984, **32**, 275.

9. Uekama, K.; Otagiri, M. *CRC Crit. Rev. Ther. Drug Carrier Systems* 1987, **3**, 1.

10. Nagai, T. *J. Incl. Phenom.* 1987, **5**, 29.

11. Szejtli, J. "Controlled Drug Bioavailability", Vol.**3**, Smolen, V. F.; Ball, L. A. Eds., Wiley, New York, 1985.

12. Uemasu, I.; Nakayama, T. *J. Inclusion Phenom. Mol. Recognit. Chem.* 1989, **7**, 327.

13. Jeffrey, G. A. "Inclusion Compounds", Vol. **1**, Chapter 5, Atwood, J.L.; Davies, J.E.D.; MacNicol, D.D. Eds.; Academic Press: London, 1984.

14. Davy, H. Philos. *Trans. R. Soc.* (London) 1811, **101**, 155.

15. Faraday, M. Quant. *J. Sci. Lit. Arts.* 1823, **15**,71.

16. Wöhler, F. *Justus Liebigs Ann. Chem.* 1849, **69**, 297.

17. Clemn, A. *Justus Liebigs Ann. Chem.* 1859, **110**, 357.

18. Mylius, F. *Ber. Bunsenges. Phys. Chem.* 1886, **19**, 999.

19. Palin, D. E.; Powell, H. M. *J. Chem. Soc.* 1947, 208.

20. von Stackelberg, M. *Naturwiss*, 1949, **36**, 327.

21. von Stackelberg, M.; Müller, H. R. *Z. Electrochem.* 1954, **58**, 25.

22. Ross, R. G.; Andersson, P.; Backström, G. *Nature*, 1981, **290**, 322.

23. Cook, J. G.; Leaist, D. *J. Geophys. Res. Lett.* 1983, **10**, 397.

24. Handa, Y. P.; Hawkins, R. E.; Murray, J. J. *J. Chem. Thermodyn.* 1984, **16**, 623.

25. White, M.A.; MacLean, M.T. *J. Phys. Chem.* 1985, **89**, 1380.

26. Kiefte, H.; Clouter, M.J.; Gagnon, R.E. *J. Phys. Chem.* 1985, **89**, 3103.

27. Ashworth, T.; Johnson, L. R.; Lai, L. P. *High Temp.-High Pressures*, 1985, **17**, 413.

28. Ahmad, N.; Philips, W. A. *Solid State Commun.*, 1987, **63**, 167.

29. Tse, J.; White, M.A. *J. Phys. Chem.* 1988, **92**, 5006.

30. Yamamuro, O.; Suga, H. *J. Therm. Anal.* 1989, **35**, 2025.

31. Yamamuro, O.; Matsuo, T.; Suga, H. *J. Inclusion Phenom. Mol. Recognit. Chem.* 1990, **8**, 33.

32. Yamamuro, O.; Kuratomi, N.; Matsuo, T.; Suga, H. *Solid State Comm.* 1990, **73**, 317.

33. Matsuo, T.; Sekii, M.; Suga, H.; Nakamura, N. Z. *Naturforsch.* 1990, **45a**, 519.

34. Kavevolden, K. A.; McMenamin, M. A. *U.S. Geol. Surv. Cire.* 1980, 825.

35. "Handbook of Gas Hydrates Properties and Occurrence" U.S. Department of Energy Publication DOE/MC/19239-1546, December 1983.

36. Ridley, I.; Dominic, K. *New Scientist*, February 1988, 25.

37. Ross, R. G.; Andersson, P. *Can. J. Chem.* 1982, **60**, 881.

38. Andersson, P.; Ross, R. G. *J. Phys. C: Solid State Phys.* 1983, **16**, 1423.

39. Andersson, P.; Ross, R. G.; Bäckström, G. *J. Phys. C: Solid St. Phys.* 1980, **13**, L73-6.

40. Freeman, J. J.; Anderson, A. C. *Phys. Rev.* 1986, **B34**, 6584.

41. Ross, R. G. *J. Inclusion Phenom. Mol. Recognit. Chem.* 1990, **8**, 227.

42. Debye, P. *Annln. Phys.* 1912, **39**, 789.

43. Ashcroft, N.W.; Mermin, N.D. "Solid State Physics" Holt, Rinehart and Winston, Philadelphia, 1976.

44. Berman, R. "Thermal Conduction In Solids" Oxford University Press, 1976.